

Photoproduction of ρ^0 -mesons and Δ -baryons in the reaction $\gamma p \rightarrow p\pi^+\pi^-$ at energies up to $\sqrt{s} = 2.6$ GeV

C. Wu¹, J. Barth¹, W. Braun¹, J. Ernst², K.-H. Glander¹, J. Hannappel¹, N. Jöpen¹, H. Kalinowsky², F.J. Klein^{1,a}, F. Klein¹, E. Klemp², R. Lawall¹, J. Link², D. Menze¹, W. Neuerburg¹, M. Ostrick¹, E. Paul¹, H. van Pee², I. Schulday¹, W.J. Schwille^{1,b}, B. Wiegers¹, F.W. Wieland¹, and J. Wißkirchen¹

¹ Physikalisches Institut, Bonn University, Bonn, Germany

² Helmholtz-Institut für Strahlen- und Kernphysik, Bonn University, Bonn, Germany

Received: 14 July 2004 / Revised version: 15 September 2004 /

Published online: 23 December 2004 – © Società Italiana di Fisica / Springer-Verlag 2004

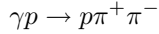
Communicated by Th. Walcher

Abstract. The photoproduction of ρ^0 -mesons and Δ -baryons at photon energies up to 2.6 GeV has been studied with the SAPHIR detector at the electron stretcher ELSA. Total and differential cross-sections were obtained. The decay angular distributions of ρ^0 -mesons show that *s*-channel helicity conservation, which is valid at high photon energies, is broken near threshold. The energy dependencies of the decay angular distributions in the helicity system as well as in the Gottfried-Jackson system hint at small *s*- or *u*-channel resonance contributions. For the reactions $\gamma p \rightarrow \Delta^{++}\pi^-$ and $\gamma p \rightarrow \Delta^0\pi^+$ new data on cross-sections are presented.

PACS. 13.60.Le Meson production – 14.40.Cs Other mesons with $S = C = 0$, mass < 2.5 GeV

1 Introduction

In this paper we report on measurements of cross-sections for the reaction



in the photon energy range $0.5 < E_\gamma < 2.6$ GeV using the SAPHIR spectrometer at ELSA.

The observed final state gives access to the subchannels



Below $E_\gamma = 1$ GeV reaction (1) dominates, mainly through a contact interaction [1,2].

In the photon energy range from $E_\gamma > 3$ GeV up to 200 GeV (recent measurements at HERA [3]) the reaction $\gamma p \rightarrow p\pi^+\pi^-$ is dominated by diffractive production of ρ^0 -mesons: $\gamma p \rightarrow pp \rightarrow p\pi^+\pi^-$. The cross-sections are characterized by a weak energy dependency, an exponential decrease with respect to the squared momentum transfer $t_\rho = (p_p - p_{p'})^2 = (p_\rho - p_\gamma)^2$, and the conservation of *s*-channel helicity.

At the typical energy scale of hadronic masses, 1–3 GeV, contributions from all three reactions (1)–(3) are expected and the production mechanisms are less clear. In case of the ρ^0 production, for instance, Friman and Soyeur pointed out the importance of meson exchange in the *t*-channel [4]. Additionally, contributions from the excitation and decay of baryon resonances are expected [5].

The paper is organised as follows. Section 2 describes the experimental setup, the kinematical reconstruction and the event selection. In sect. 3 the results for total and differential cross-sections for $\gamma p \rightarrow p\pi^+\pi^-$ are presented. The analysis procedure is described in sect. 4 and the results on ρ^0 and Δ photoproduction are discussed in sect. 5.

2 Experimental setup and data analysis

2.1 Photon beam

The electron stretcher and accelerator ELSA delivers an extracted electron beam with energies up to $E_0 = 3.4$ GeV and a duty factor up to 90%. In this experiment electron energies of $E_0 = 1.6, 2.6$ and 2.8 GeV have been used.

Quasi-monochromatic photons were produced by means of bremsstrahlung tagging. The tagging spectrometer covered the photon energy range of $E_\gamma = 0.31\text{--}0.94 \cdot E_0$

^a Now at CUA, Department of Physics, Washington D.C., USA; e-mail: klein@physik.uni-bonn.de

^b e-mail: schwille@physik.uni-bonn.de

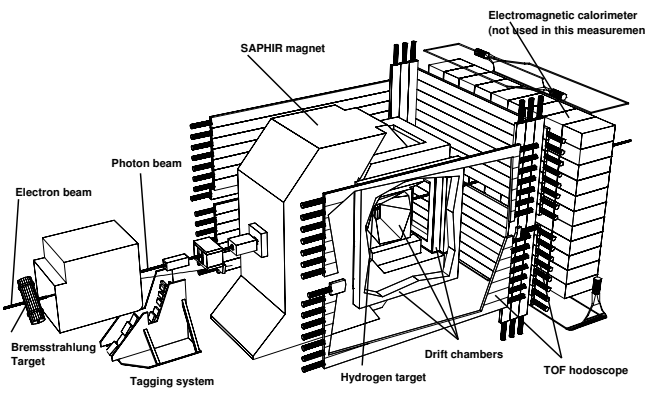


Fig. 1. Sketch of the SAPHIR detector.

at a total flux of $N_\gamma = 5 \cdot 10^5 \text{ s}^{-1}$. The effective photon flux passing through the target was continuously measured with a photon counter behind the detector (see fig. 1).

2.2 Detector setup

The SAPHIR detector [6] is shown schematically in fig. 1. It is a large acceptance magnetic spectrometer for multi-particle-final-states. The liquid hydrogen target is situated in the center between the pole pieces of a large C-shaped magnet and is surrounded by 14 cylindrical layers (partially stereo layers) of a drift chamber. An additional planar drift chamber in forward direction supports track reconstruction and improves momentum resolution.

Three surrounding plastic scintillator hodoscopes serve as trigger devices for charged particles and as a time-of-flight spectrometer.

2.3 Event selection for $\gamma p \rightarrow p\pi^+\pi^-$

The raw data (147 million events) stem from four data taking periods in 1997 and 1998. The trigger required two hits in the time-of-flight wall together with a signal in the tagging system. All events which fulfill the trigger conditions are passed through a reconstruction software which delivers momenta of the outgoing particles. Starting from (charged) three-prong events, various reaction hypotheses were tested by kinematical fits, mainly: $\gamma p \rightarrow p\pi^+\pi^-$, $\gamma p \rightarrow pK^+K^-$, $\gamma p \rightarrow p\pi^+\pi^-\pi^0$, $\gamma p \rightarrow n\pi^+\pi^+\pi^-$, $\gamma p \rightarrow pK^+\pi^-$, $\gamma p \rightarrow pK^+\pi^-\pi^0$ and $\gamma p \rightarrow pe^+e^-$. For the analysis, those with the maximum value of the χ^2 probability for the $p\pi^+\pi^-$ final state were selected. Possible contaminations mainly come from $p\pi^+\pi^-\pi^0$ and $n\pi^+\pi^+\pi^-$ final states. The crosstalk histograms (fig. 2) for the separation of $p\pi^+\pi^-$ and $p\pi^+\pi^-\pi^0$ final states demonstrate the uncritical assignment to these two processes. The majority of events with $P_{\chi^2}(p\pi^+\pi^-) > 0$ is located either at $P_{\chi^2}(p\pi^+\pi^-) \approx 0$ or $P_{\chi^2}(p\pi^+\pi^-\pi^0) \approx 0$ (fig. 2a), allowing a good separation between the two reactions. For measured data (fig. 2a) and simulated data (fig. 2b and c) a

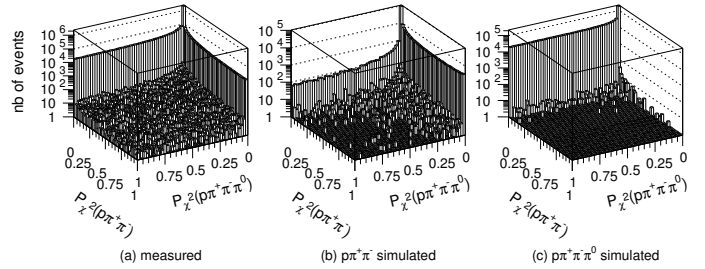


Fig. 2. Crosstalk histograms on the separation of $p\pi^+\pi^-\pi^0$ and $p\pi^+\pi^-$ final states.

rather flat χ^2 probability distribution for the $p\pi^+\pi^-$ hypothesis is visible at $P_{\chi^2} = 0$ for $p\pi^+\pi^-\pi^0$ assignment and vice versa. Figure 2c shows that virtually no $p\pi^+\pi^-\pi^0$ events are shifted into the $p\pi^+\pi^-$ channel. Figure 2b demonstrates that the loss of $p\pi^+\pi^-$ due to misidentification as $p\pi^+\pi^-\pi^0$ is $\leq 1\%$.

2.4 Acceptance and photon flux

The acceptance of the detector was determined by Monte Carlo simulation. Four mainly contributing reactions were generated:

- $\gamma p \rightarrow p\rho^0 \rightarrow p\pi^+\pi^-$,
- $\gamma p \rightarrow \Delta^{++}\pi^- \rightarrow p\pi^+\pi^-$,
- $\gamma p \rightarrow \Delta^0\pi^+ \rightarrow p\pi^+\pi^-$,
- $\gamma p \rightarrow p\pi^+\pi^-$ (phase space).

The created particles were tracked through the SAPHIR detector by an adapted version of CERN's GEANT, considering particle decays, energy losses, multiple scattering and the experimentally determined efficiencies of the detector components, *e.g.* the drift chambers and the scintillator hodoscopes. The acceptance was calculated in a five-dimensional space with respect to the photon energy E_γ , the invariant masses $M_{\pi^+\pi^-}$ and $M_{p\pi^+}$ as well as the π^+ polar and azimuthal angles, θ_{π^+} and ϕ_{π^+} , in the $\pi^+\pi^-$ helicity frame. Figure 3 illustrates the acceptance as a function of the invariant masses $M_{\pi^+\pi^-}$ and $M_{p\pi^+}$ in three different photon energy intervals. The acceptance is rather flat and about 20%.

For the photon flux normalization see ref. [7].

3 Cross-sections for $\gamma p \rightarrow p\pi^+\pi^-$

The total and differential cross-sections presented here are based on 7.68×10^6 reconstructed $p\pi^+\pi^-$ events. Figure 4 shows the result for the total cross-sections (to be found in the appendix B, tables 4 and 5) compared with previous data [8–10]. It is characterized by a steep rise at threshold, two maxima in the region $E_\gamma = 0.6$ – 1.1 GeV corresponding to center-of-mass energies of 1.4– 1.7 GeV followed by a slow decrease. The differential cross-sections $d\sigma/dt_{\pi^+\pi^-}$ and $d\sigma/dt_{p\pi^+}$ as a function of the photon energy are given in the appendices (tables 6–15) and

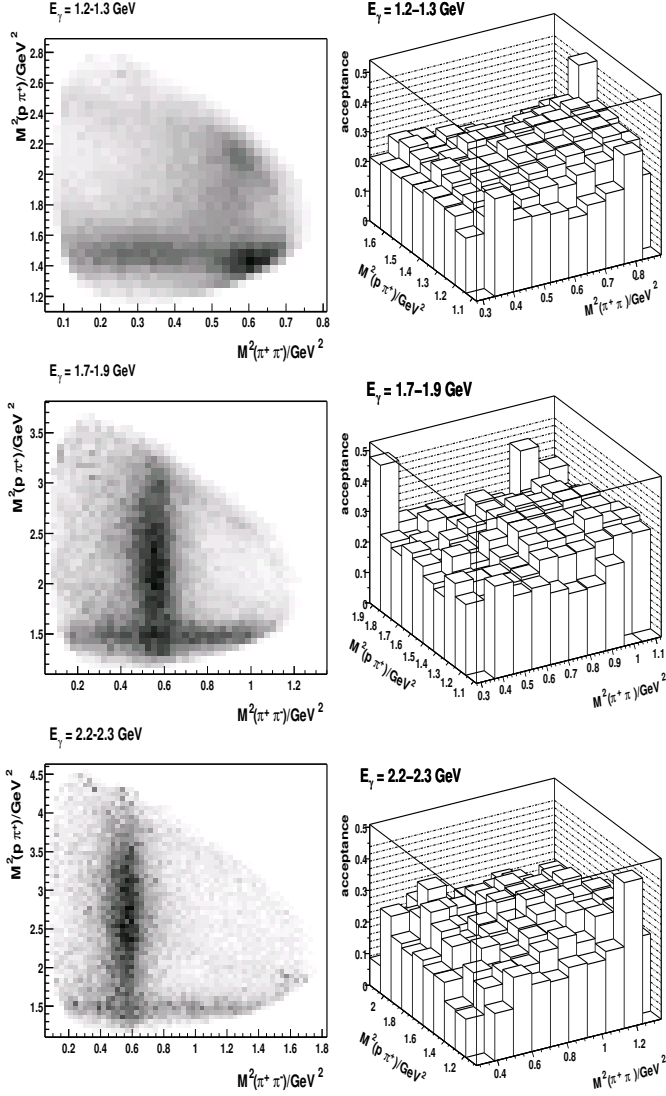


Fig. 3. Dalitz-diagrams and the corresponding detector acceptance for $\gamma p \rightarrow p\pi^+\pi^-$ showing the Δ^{++} , ρ and Δ^0 contributions for three different photon energies.

shown exemplarily for six photon energies in fig. 5. Here $t_{\pi^+\pi^-} = t_p = (p_p' - p_p)^2$ and $t_{p\pi^+} = (p_p' + p_{\pi^+} - p_p)^2$ denote the squared momentum-transfers to the $\pi^+\pi^-$ -pair or to the $p\pi^+$ -pair respectively.

A gross information about the dominant reaction dynamics is provided by the corresponding Dalitz-plots (fig. 3). One observes the ρ^0 and Δ^{++} bands and, at lower energies, the Δ^0 band along a line at 45° .

The Δ^{++} contribution, which dominates up to photon energies of 1.2 GeV, can be clearly identified in the $p\pi^+$ invariant mass. The production of ρ^0 -mesons, visible in the $\pi^+\pi^-$ mass distribution, dominates at higher energies. Quantitatively the information about the relative strengths and the energy dependences can be seen quantitatively in the projections for the three invariant mass distributions in figs. 6 and 7.

4 Channel separation method

A direct determination of the contributions from the three main exclusive channels,

$$\gamma p \rightarrow p\rho^0, \quad (4)$$

$$\gamma p \rightarrow \Delta^{++}\pi^-, \quad (5)$$

$$\gamma p \rightarrow \Delta^0\pi^+, \quad (6)$$

by fitting a parametrisation for the resonant and non-resonant part to the 1-dimensional invariant mass distributions is difficult due to the large widths of the resonances and due to the kinematical overlap in the Dalitz-diagrams. The use of detailed dynamical models (*e.g.* [2]) for a separation and interpretation is presently limited to photon energies below 1 GeV. Though some effort has been started to extend these models towards higher energies [11], we applied a phenomenological separation procedure that has already been used in the analysis of previous experiments [3, 8, 12].

4.1 Model description

In this ansatz the event distribution in the Dalitz-plot is parametrised as

$$\begin{aligned} dN = & \left(f_{ps} \frac{1}{N_{ps}} + f_\rho \frac{|T_\rho|^2 w(\cos \theta_H) e^{A_\rho t_\rho}}{N_\rho} \right. \\ & \left. + f_{\Delta^{++}} \frac{|T_{++}|^2 e^{A_{++} t_{++}}}{N_{++}} + f_{\Delta^0} \frac{|T_0|^2 e^{A_0 t_0}}{N_0} \right) \\ & \times \frac{1}{E_\gamma E_{cms}^2} dM_{p\pi^+}^2 dM_{\pi\pi}^2 h(E_\gamma) dE_\gamma \end{aligned} \quad (7)$$

Here $h(E_\gamma)$ is the photon energy spectrum, f_ρ , $f_{\Delta^{++}}$, f_{Δ^0} and f_{ps} denote the fractions of the ρ^0 , Δ^{++} , Δ^0 and phase-space contributions. The dependence on the invariant mass combinations is given by relativistic Breit-Wigner-amplitudes T_i [13]. $w(\cos \theta_H) = \frac{3}{4} [1 - \rho_{00} + (3\rho_{00} - 1) \cos^2 \theta_H]$ describes the ρ decay distribution in the helicity system. The normalization integrals N_i are given by

$$\begin{aligned} N_i = & \int |T_i|^2 w(\cos \theta_H) F(t_i) \frac{\pi^2}{4 E_{cms}^2} \\ & \times h(E_\gamma) dM_{p\pi^+}^2 dM_{\pi\pi}^2 dE_\gamma \end{aligned}$$

with $F(t_i) = 1, e^{A_\rho t_\rho}, e^{A_{++} t_{++}}$ and $e^{A_0 t_0}$ for the phase space, ρ , Δ^{++} and Δ^0 production. The weak contribution from $f_2(\gamma p \rightarrow p f_2(1270))$ is not regarded.

The interference between the Δ^0 - and Δ^{++} -amplitudes is taken into account by adding the term

$$I_{\Delta^{++}\Delta^0} = 2\alpha_{\Delta^{++}\Delta^0} \sqrt{f_{\Delta^{++}} f_{\Delta^0}} \text{Re}(T_{\Delta^{++}} \cdot T_{\Delta^0}) e^{i\phi_{++}} \quad (8)$$

to the sum in eq. (7). The parameter α describes the strength of the interference ($0 \leq \alpha \leq 1$) and ϕ_{++} is the relative phase between the amplitudes. The ρ^0 - Δ^{++} interference is treated in a similar way.

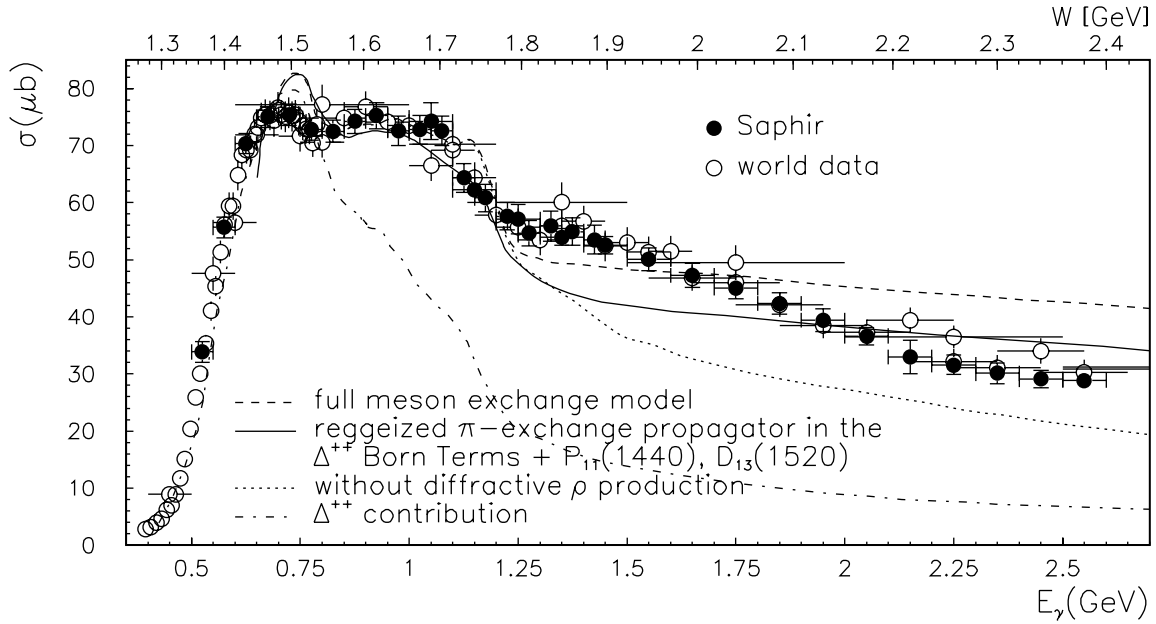


Fig. 4. Results for the total cross-section of the reaction $\gamma p \rightarrow p\pi^+\pi^-$ compared to data from [8–10]. The curves are taken from [14].

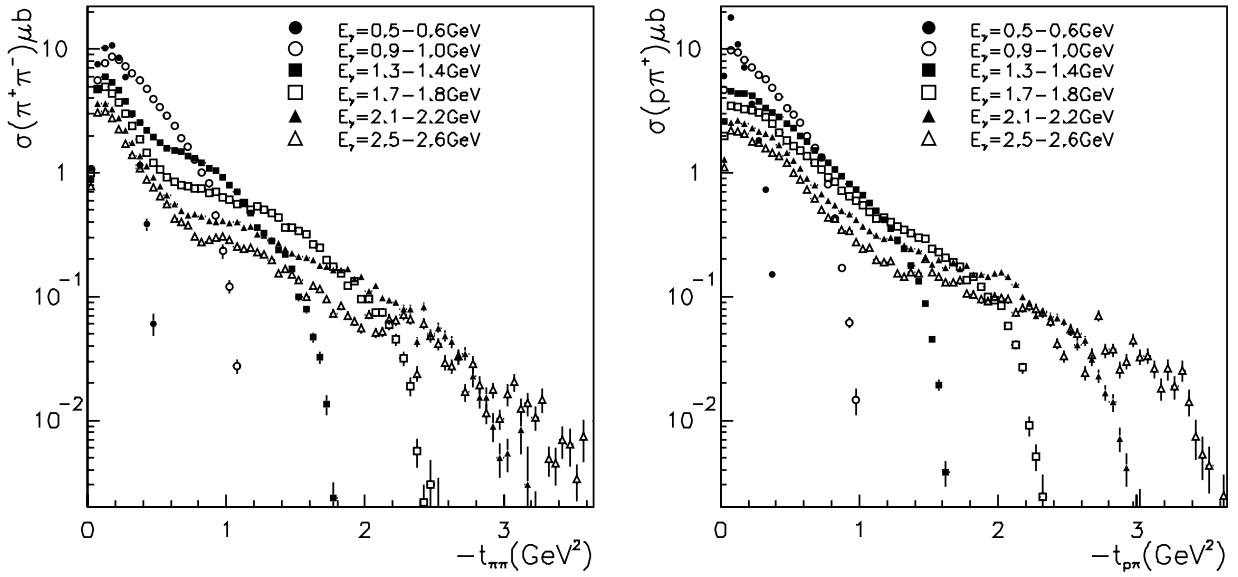


Fig. 5. Differential cross-sections $\sigma(\pi^+\pi^-) = d\sigma/dt_{\pi^+\pi^-}$ and $\sigma(p\pi^+) = d\sigma/dt_{p\pi^+}$.

It is a well-known feature of ρ^0 photoproduction that the $\pi^+\pi^-$ mass distribution resulting from the ρ^0 decay is skewed compared to a Breit-Wigner-distribution. There is an enhancement at low and a suppression at high invariant masses. Söding *et al.* attributed this behaviour to an interference of the ρ^0 production amplitude with a Drell-type background [15] which can be included by replacing the ρ^0 contribution in eq. (7) with [12]

$$\frac{f_\rho}{N_\rho} \left[|T_\rho|^2 w(\cos \theta_H) e^{A_\rho t_\rho} + 2 c T_D^* T_\rho e^{A_\rho t_\rho/2} + c^2 |T_D|^2 \right], \quad (9)$$

where $T_D = \frac{M_\rho^2 - M_{\pi\pi}^2}{M_\rho^2 - M_{\pi\pi}^2 - i M_\rho F_\rho}$ approximates the Drell-type rescattering. The free parameter c represents the strength of the Drell amplitude.

Alternatively, according to Ross and Stodolsky [16] the asymmetric shape of the mass distribution can be parametrised in the framework of a vector-meson-dominance model by multiplying the Breit-Wigner-function $|T_\rho|^2$ with the additional factor $(M_\rho/M_{\pi\pi})^4$.

Both ansatzes have been applied in our analysis (see below).

4.2 Fit procedure and determination of the cross-sections

At photon energies below 1.0 GeV the cross-section for $\gamma p \rightarrow p\pi^+\pi^-$ is dominated by Δ^{++} production. For the evaluation of the Δ^{++} and Δ^0 cross-sections eq. (7) with $|T_\rho|^2 = 0$ is applied. An interference term between Δ^{++} and Δ^0 has been introduced (see eq. (8)). To reduce the number of free parameters in the fit the mass and width of the Δ -baryons are set to $M_\Delta = 1232$ MeV and $\Gamma = 120$ MeV (see [17]). For the Δ^{++} - Δ^0 interference α and ϕ_{++} (see eq. (8)) were used in a first step as free parameters in the fits for the different photon energy bins. α was found to be around 1, so α was set to 1 for final fits. ϕ_{++} changed in a wide range, showing that the fits are insensitive to the ϕ_{++} value. For final fits an average value of $\phi_{++} = \pi$, consistent with ABBHHM [8], was used. For the higher photon energy region up to 1.4 GeV the same values were used.

For the ρ^0 analysis, the following procedure was applied. At first, mass and width of the ρ^0 -meson have been determined by fitting the measured $\pi^+\pi^-$ mass distributions using i) only Breit-Wigner-amplitudes with energy dependent width (eq. (7)), ii) the Söding-interference (eq. (9)) and iii) the Ross-Stodolsky parametrisation.

Some results for the fits of the ρ models i), ii) and iii) to the data in different photon energy ranges are shown in table 1 and figs. 6, 7 and 8.

At photon energies between 1.0 GeV and 1.4 GeV the Breit-Wigner-distribution fits, including Δ^{++} - Δ^0 and ρ^0 - Δ^{++} interferences (model i)), already gave acceptable fits to the data. The ρ^0 - Δ^{++} interference parameters were left free in the fits. For the Δ^{++} - Δ^0 interference α and ϕ_{++} were used as for the lower energies.

The additional parameters in the Söding and Ross-Stodolsky parametrisation improved the fit only slightly but yielded too large ρ masses (compare χ^2/NF and ρ masses in table 1 for the three different models in the photon energy range 1.2–1.3 GeV).

At higher energies the asymmetric shape of the mass distribution manifests itself as a shift of the ρ^0 mass to lower values extracted with Breit-Wigner-amplitudes only, indicating that a more sophisticated model has to be used. In this energy region the Söding as well as the Ross-Stodolsky parametrisation have been used to disentangle the exclusive channels. The use of these two models ii) and iii) improved the χ^2/NF of the fit by factors between 2 and 4 depending on the model and energy range, and the fitted ρ^0 mass was compatible with 0.770 GeV.

The χ^2/NF are in all cases unstatistically large. The reason for this is that the statistical error for the data points in the mass spectra are very small due to the large number of entries for each bin, but the fit of data to the theoretical curves cannot follow all data points. The large χ^2/NF therefore shows the dominance of the systematical error compared to the statistical errors. To get reliable uncertainties for the physics results (for example cross-sections) the errors for all fitted parameters in eq. (7) were rescaled in such a way that $\chi^2/\text{NF} = 1$ holds (thus increasing the error bars). The errors for the results on ρ^0

Table 1. Fit results for the mass and width of the ρ^0 -meson using Breit-Wigner-amplitudes (i), the Söding-interference (ii) and the Ross-Stodolsky parametrisation (iii). Only statistical errors are considered.

Method	E_γ (GeV)	M_ρ (GeV)	Γ_ρ (GeV)	χ^2/NF
(i)	1.2-1.3	0.766 ± 0.004	0.178 ± 0.014	13.7
	1.7-1.8	0.739 ± 0.002	0.141 ± 0.006	18.2
	2.2-2.3	0.746 ± 0.002	0.150 ± 0.007	7.58
(ii)	1.2-1.3	0.797 ± 0.007	0.158 ± 0.010	9.88
	1.7-1.8	0.770 ± 0.002	0.157 ± 0.007	6.32
	2.2-2.3	0.767 ± 0.001	0.152 ± 0.007	3.80
(iii)	1.2-1.3	0.782 ± 0.004	0.159 ± 0.009	10.8
	1.7-1.8	0.771 ± 0.002	0.152 ± 0.007	4.36
	2.2-2.3	0.769 ± 0.003	0.149 ± 0.007	3.37

and Δ production in appendices D-G (tables 16-22) declared statistical and given in brackets are already including this part of systematic error due to the error rescaling of the Likelihood-fit results.

For the determination of the total cross-sections the mass and width of the ρ^0 -meson were fixed to the PDG values ($M_\rho = 0.77$ GeV and $\Gamma_\rho = 150$ MeV) and only the relative contributions, f_ρ , $f_{\Delta^{++}}$, f_{Δ^0} and f_{ps} , in eq. (7) have been varied in the fit. At photon energies above $E_\gamma = 1.4$ GeV the kinematical overlap between Δ^{++} - and Δ^0 -contributions is relatively small (see fig. 3) and the interference can be neglected. In this energy region the observed skewness of the $\pi^+\pi^-$ mass distribution is reasonably described by the Söding and Ross-Stodolsky models.

As already mentioned, three different methods were applied to determine the cross-sections. At photon energies below 1.4 GeV the Söding parametrisation and the Breit-Wigner-distribution fits are in good agreement. However, below 2 GeV there are non-negligible differences between the results obtained with the Söding and the Ross-Stodolsky models (see fig. 12 and table 2). For a discussion see sect. 5.1.

As can be seen from eq. (7) the knowledge about the exponential decrease of the differential cross-sections, $d\sigma/dt_\rho$, $d\sigma/dt_{++}$ (Δ^{++}) and $d\sigma/dt_0$ (Δ^0), as a function of t was taken into account for the separation fitting procedure described above. For the determination of total cross-sections the parameters A_ρ , A_{++} and A_0 as a function of the photon energy were taken from fits to the measured differential cross-sections, which have been fitted in the interval $0.1 < |t| < 0.4$ GeV².

To get A_ρ , A_{++} and A_0 , one has first to determine the differential cross-sections. To determine these, for instance for the ρ^0 production, the separation procedure has to be done for events with t_ρ in a certain range. This cut for the ρ kinematics also influences the kinematics of events of, for instance, Δ^{++} and Δ^0 production. The slopes A_{++} and A_0 depend on t_ρ . For the determination of the Δ^{++} differential cross-section one has to care about the dependence of A_ρ and A_{++} from t_{++} , for the Δ^0 differential

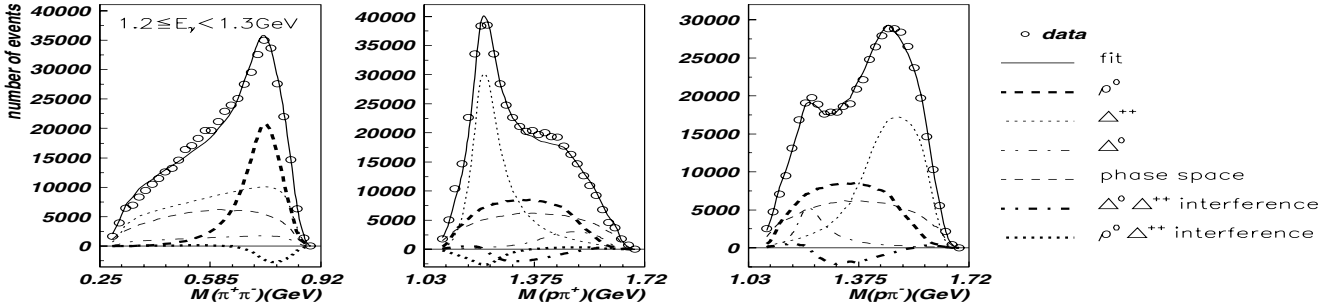


Fig. 6. Acceptance corrected mass distributions and fit results in the photon energy range of 1.2–1.3 GeV.

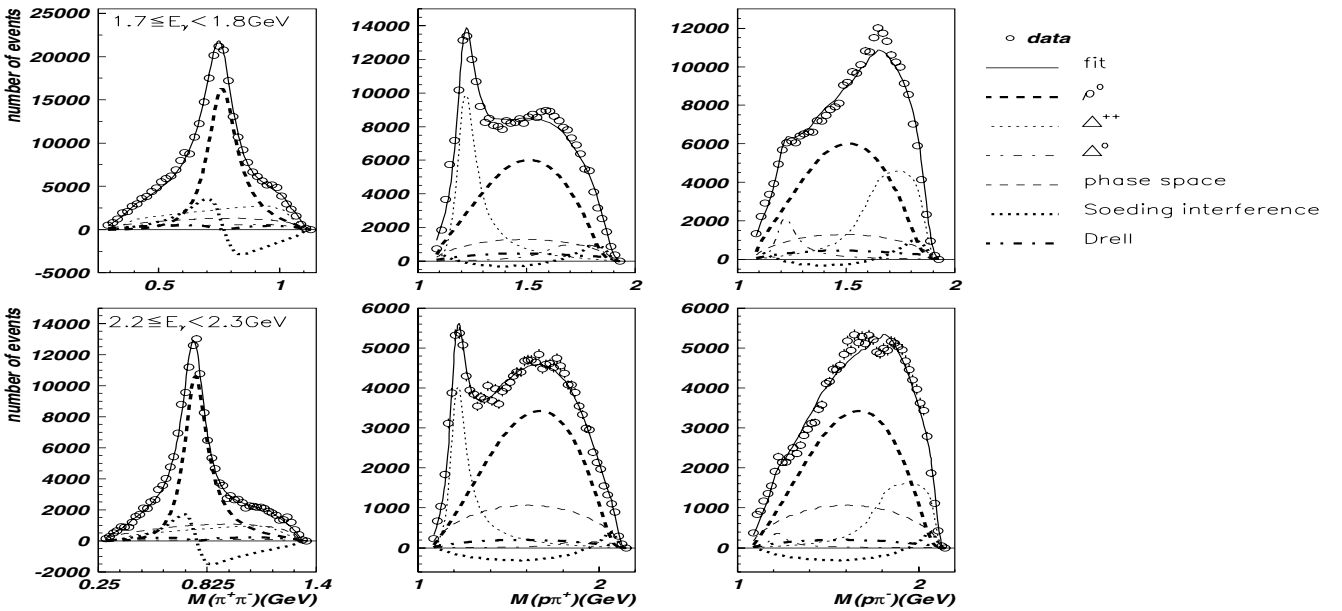


Fig. 7. Acceptance corrected mass distributions and results of the fit using the Söding-interference at two different photon energies.

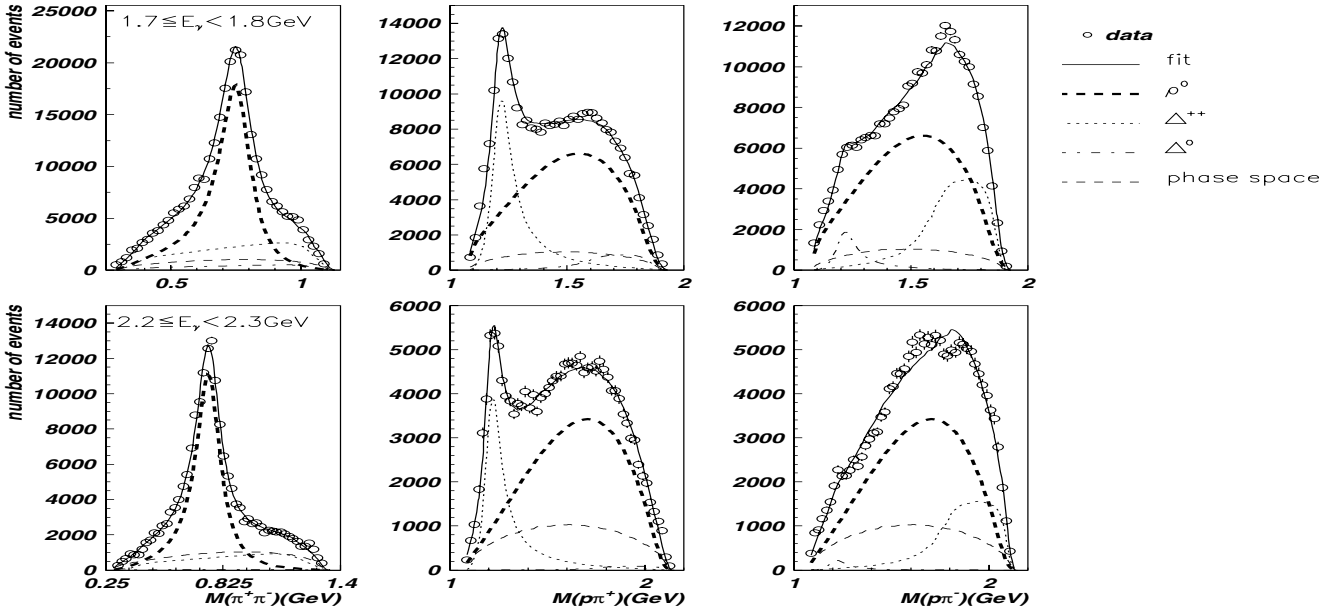


Fig. 8. Acceptance corrected mass distributions and results of the fit, Ross-Stodolsky method, at two different photon energies.

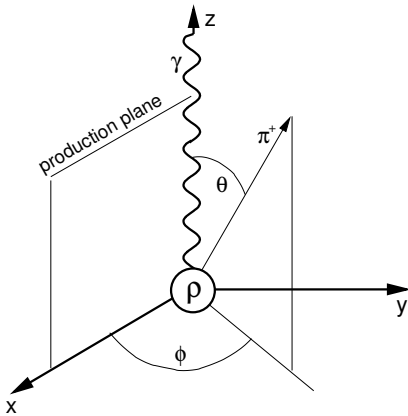


Fig. 9. Definition of angles (example Gottfried-Jackson system).

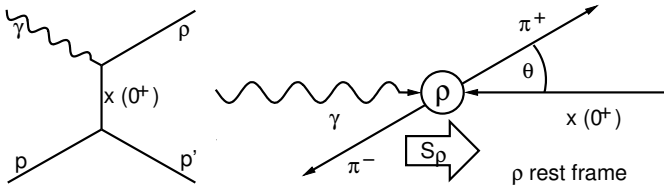


Fig. 10. GJ system.

cross-section respectively. In an iterative procedure the t distributions for ρ^0 and Δ production were measured and refixed in the Likelihood fits. The change of slopes as function of cuts on the kinematics were studied with help of Monte Carlo generated events produced with the measured slopes.

Valuable information about the ρ^0 production mechanism is contained in the spin density matrix elements. In the case of this experiment with unpolarized photons and unpolarized target three density matrix elements can be determined by measuring the ρ^0 decay angular distributions in an appropriate reference system (see eq. (10)). Two reference systems, both being ρ^0 rest frames, were applied in this analysis. In both the polar angle θ is defined between the direction of the decay π^+ and a reference frame specific z -direction. For the azimuthal angle ϕ see fig. 9. For elementary—or reggeized—particle exchange in the t -channel the Gottfried-Jackson system is used to test the t -channel helicity conservation (TCHC), which is valid if the spin of the ρ^0 is aligned along the direction of the photon (see fig. 10), which defines the z -axis.

The conservation of the s -channel helicity (SCHC) is examined in the helicity system (fig. 11), where the z -axis is chosen opposite to the direction of the outgoing proton or in the direction of the ρ^0 in the total c.m.s., respectively. The y -axis is normal to the production plane and defined by $\mathbf{p}_i \times \mathbf{p}_o$, with \mathbf{p}_i and \mathbf{p}_o the momenta of the incoming and outgoing protons.

To determine the decay density matrix elements of the ρ^0 -meson, ϱ_{ik} , the contribution $|T_\rho|^2$ in eq. (7) and the phase space contribution have been weighted by the decay angular distribution $W(\theta, \phi)$ and $W_{ps}(\theta, \phi)$. In case of photoproduction of ρ^0 -mesons with unpolarized photons

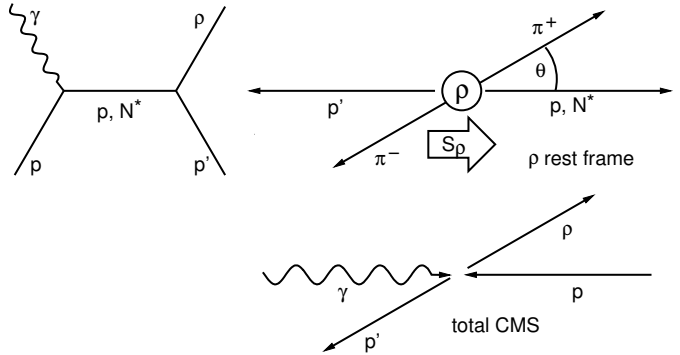


Fig. 11. Helicity system.

the angular decay distribution can be parametrised by [18]

$$W(\theta, \phi) = \frac{3}{4\pi} \left[\frac{1}{2}(1 - \varrho_{00}^0) + \frac{1}{2}(3\varrho_{00}^0 - 1) \cos^2 \theta - \varrho_{1-1}^0 \sin^2 \theta \cos 2\phi - \sqrt{2}\text{Re}\varrho_{10}^0 \sin 2\theta \cos \phi \right], \quad (10)$$

θ and ϕ are the decay angles either in the helicity or the Gottfried-Jackson system. The $W_{ps}(\theta, \phi)$ with an additional asymmetric $\cos \theta$ term can be phenomenologically written as [8]

$$W_{ps}(\theta, \phi) = \frac{3}{4\pi} \left[\frac{1}{2}(1 - \varrho'_{00}) + \frac{1}{2}(3\varrho'_{00} - 1) \cos^2 \theta - \varrho'_{1-1} \sin^2 \theta \cos 2\phi - \sqrt{2}\text{Re}\varrho'_{10} \sin 2\theta \cos \phi \right] + \frac{\sqrt{3}}{4\pi} 2\varrho'_{11} \cos \theta. \quad (11)$$

The density matrix elements ϱ_{00} , ϱ_{1-1} and $\text{Re}\varrho_{10}$ have been determined in both coordinate systems by using the same method of channel separation as described in sect. 4 with dividing the data for the fits in three energy- and eight t_ρ -intervals.

5 Results

Tables with numerical values for all measured observables are listed in appendices B-G (tables 6-22). A description of the error calculation is given in appendix A.

The error bars represent statistical errors only. For the systematic error we quote:

- arbitrary choice of the t -bins, migration effects 15%,
- flux normalisation < 2%,
- target thickness variation due to gas bubbles as well as contributions from target end caps < 3%.

5.1 The reaction $\gamma p \rightarrow p\pi^+\pi^-$

In the study of Lüke and Söding on $p\pi^+\pi^-$ photoproduction mechanisms off nucleons [1] it was shown that the dominant contribution at low energies stems from the

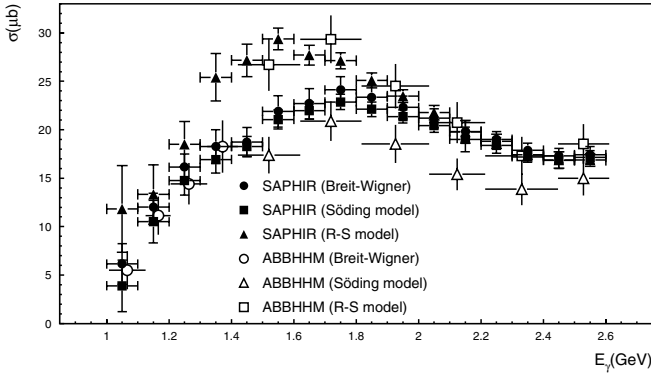


Fig. 12. Total cross-sections for the reaction $\gamma p \rightarrow pp^0$ evaluated with different methods (Söding, Ross-Stodolsky).

presence of an intermediate Δ^{++} state. By updating the Lüke-Söding model taking into account dominant baryonic resonances and improving the $\Delta\pi$ Born term contributions Murphy and Laget [14] were able to provide a reasonable description of the MAMI B (Mainz) data [9] on $p\pi^+\pi^-$ production. This model uses no free fit parameters and, additionally, gives predictions for the $p\pi^+\pi^-$ cross-sections up to $E_\gamma = 5$ GeV. Figure 4 shows our new data of the total cross-section together with the model predictions of Murphy and Laget. One observes increasing differences between data and description at energies above the ρ^0 threshold. Most likely, the reason for this is a relatively simple description of the ρ^0 production (see sect. 5.2). In addition to the total cross-section we present differential cross-sections $d\sigma/dt_{\pi^+\pi^-}$ and $d\sigma/dt_{p\pi^+}$ in 21 energy bins for $E_\gamma = 0.5$ –2.6 GeV (see tables 6–15 in the appendices and exemplary results for six photon energies in fig. 5). These differential cross-sections—together with the results for the dominant subchannels (ρ and Δ production)—provide input for tests of theoretical models and for investigations about additional production mechanisms. We see a promising starting point in this direction in [19]. The exclusive channels pp^0 and $\Delta^{++}\pi^-$ are treated separately as described in the following.

5.2 The reaction $\gamma p \rightarrow pp^0$

The total cross-section σ_{tot} was determined in 16 energy bins between threshold and $E_\gamma = 2.6$ GeV. In fig. 12 the results of both fitting methods (Söding and Ross-Stodolsky) are shown together with bubble chamber results from ABBHHM [8]. In our data the strong model dependency of the cross-sections for energies below 2 GeV calls for an explanation. Comparing the physics presuppositions for both models it is obvious that the Ross-Stodolsky model implying only diffractive ρ production in the framework of a vector-meson-dominance model might underestimate other production mechanisms at lower energies. Since the development of both models under discussion, a more detailed understanding of the ρ^0 and its coupling to the $\pi^+\pi^-$ -continuum has been reached in an effective field theory approach [20]. Based on these ideas Niesler, Piller and Weise [21] calculated the $\pi^+\pi^-$ -pair

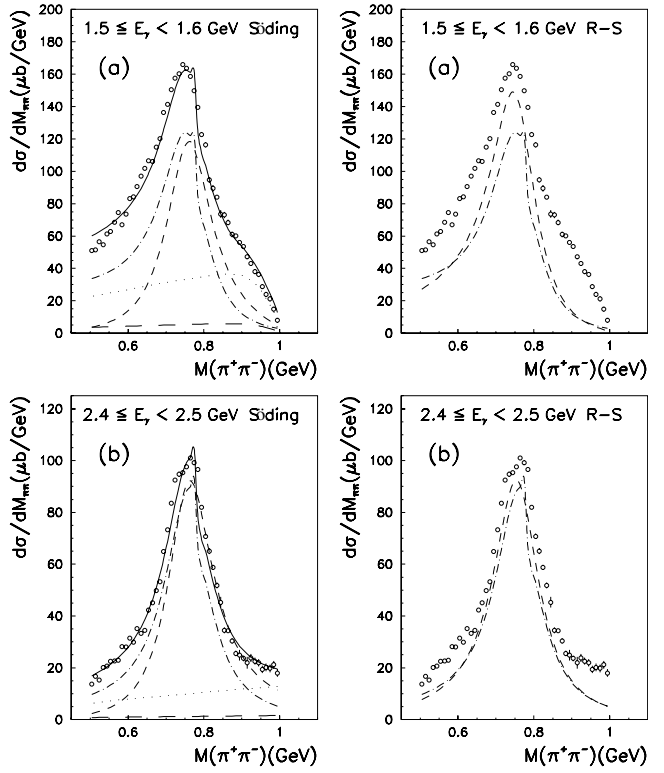


Fig. 13. Mass distributions $d\sigma/dM_{\pi\pi}$ for $1.5 \leq E_\gamma < 1.6$ GeV (a) and $2.4 \leq E_\gamma < 2.5$ GeV (b). $\cdots\cdots$: calculation according to the Niesler, Piller, Weise model (mainly from ρ^0 decay). $--$: ρ -distribution from this experiment, evaluated with the Söding or the Ross-Stodolsky model. $\circ\circ\circ$: data points from this experiment. --- : sum of Niesler, Piller, Weise calculation plus the experimental Δ^{++} and Δ^0 production background. $\cdot\cdot\cdot\cdot$: Δ^{++} contribution. $\text{---} \text{---}$: Δ^0 contribution.

mass distribution deduced from the pion formfactor in the timelike momentum region. The authors claim their predictions be valid for diffractive ρ production at high energies. To apply the model to different energies only the knowledge of the total $\pi^+\pi^-$ cross-section and the slope of the exponential decrease of the ρ^0 cross-section at small t are needed. In fig. 13b we compare the model predictions with our data for $2.4 < E_\gamma < 2.5$ GeV. The left figure shows our data on $p\pi^+\pi^-$ production together with the extracted ρ^0 distribution (Söding model) and the results of Niesler, Piller and Weise. Adding our measured $M_{\pi^+\pi^-}$ contribution from Δ production (not included in the model) to these calculations one finds a good agreement between our data and the theoretical prediction. The right figure depicts our data and the extracted ρ^0 's using the Ross-Stodolsky model together with the model prediction. Obviously, in this energy range both data evaluations (Söding, Ross-Stodolsky) are in good agreement with each other and with the theoretical prediction. At lower energies (see fig. 13a) the situation is quite different.¹ Applying the Ross-Stodolsky method for the data evaluation the ρ

¹ In the energy range $1.5 < E_\gamma < 1.6$ GeV a correction due to a possible mass dependence (see [21]) of $\sigma_{\pi\pi N}$ was applied,

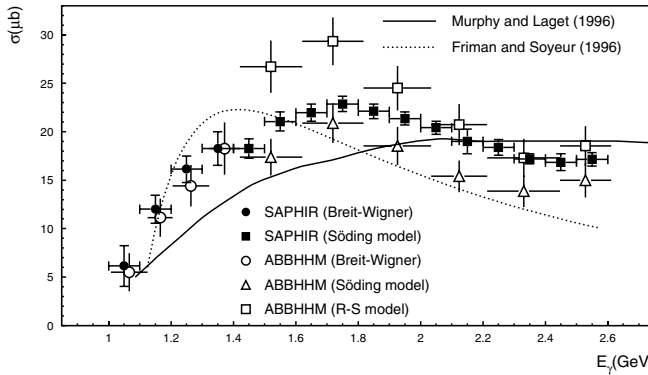


Fig. 14. Total cross-section of the reaction $\gamma p \rightarrow pp^0$ compared to the results of ABBHHM [8]. The full line shows the $\pi + \sigma$ -exchange contribution [4]. The dotted line represents the production via the exchange of the Pomeron in the model of Murphy and Laget [14].

peak in the $\pi^+\pi^-$ mass spectrum overshoots the model prediction considerably and cuts space for the Δ production. Since, according to its derivation the Niesler, Piller, Weise model should indicate rather an upper limit for the ρ cross-section, we conclude that at low energies the R-S model overestimates the cross-section and is not applicable.

Following our argumentation, we refer henceforth to the result gained via the Söding model only, as plotted in fig. 14 together with older data points from ABBHHM [8] and theoretical calculations from B. Friman, M. Soyeur [4] and L.Y. Murphy, J.-M. Laget [14].

Figures 13 and 14 indicate the model dependency of the experimental results together with the wide spread of theoretical descriptions. From the excitation curve no indication for any relatively strong s -channel resonance can be deduced.

The model of Friman and Soyeur tries to describe the ρ production for energies below 2 GeV with π^0 - and σ -exchanges in the t -channel. The data from ABBHHM served as experimental input to determine the free parameters. Compared to our data this model overshoots the points below 1.6 GeV and is below data for $E_\gamma > 1.8$ GeV. Murphy and Laget take a different point of view in their model. They simply regard a t -channel 0^+ (Pomeron) exchange and multiply the cross-section with a $(q_\rho/k)_{\text{cm}}$ phase space factor thus paying regard to the threshold behaviour. Their result is below the data for $E_\gamma < 2$ GeV and slightly above for $E_\gamma > 2.3$ GeV. This discrepancy is not astonishing since a dominant 0^+ t -channel exchange is ruled out by our data (see below).

The differential cross-sections $d\sigma/dt$ for six energy ranges are depicted in fig. 15 together with curves from [4]. Below $|t_\rho| = 0.5 \text{ GeV}^2$ they show an exponential behaviour and were fitted with

$$\frac{d\sigma}{dt_\rho} = A e^{-B|t_\rho|} \quad (12)$$

thus summarizing components with more than two pions in the photon spectral function.

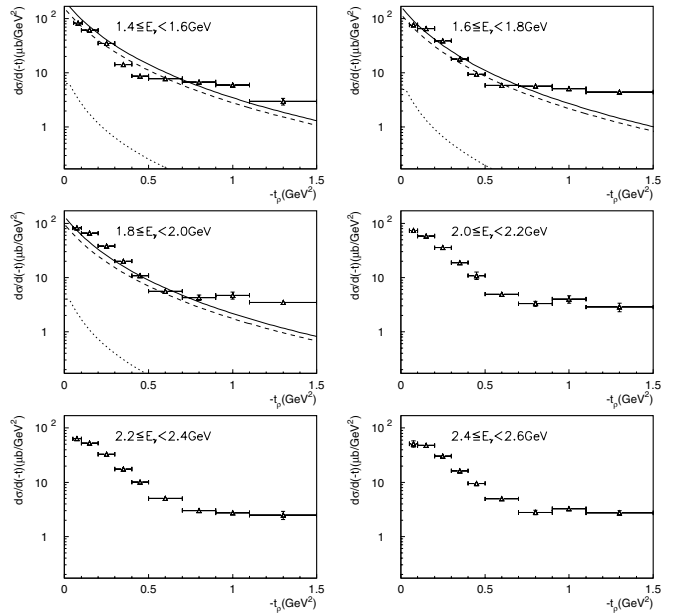


Fig. 15. Differential cross-section of the reaction $\gamma p \rightarrow pp^0$ (Söding model extraction). The curves are from [4]. Dashed lines: full model; dotted lines: π -exchange contribution; full lines: fit of this model to our data.

Table 2. The fit values of differential cross-sections of ρ production with different models.

E_γ (GeV)	A_S ($\mu\text{b}/\text{GeV}$)	B_S (GeV^{-2})	A_R ($\mu\text{b}/\text{GeV}^2$)	B_R (GeV^{-2})
1.4–1.6	170 ± 6	6.69 ± 0.17	241 ± 7	7.45 ± 0.14
1.6–1.8	175 ± 4	6.32 ± 0.10	200 ± 4	6.44 ± 0.09
1.8–2.0	164 ± 4	5.96 ± 0.09	174 ± 3	6.01 ± 0.08
2.0–2.2	136 ± 3	5.55 ± 0.08	145 ± 2	5.74 ± 0.07
2.2–2.4	121 ± 2	5.42 ± 0.08	126 ± 2	5.61 ± 0.06
2.4–2.6	108 ± 2	5.28 ± 0.08	114 ± 2	5.54 ± 0.08

in the range $0.1 \text{ GeV}^2 < |t_\rho| < 0.4 \text{ GeV}^2$. The fit results in table 2 are marked S or R corresponding to the applied model for evaluation. Figure 16 shows our data together with CLAS [22] results at higher energies. It is worth mentioning that at small t values the slope varies only slightly with energy. The t value where the slope abruptly changes towards zero increases from $|t_\rho| \approx 0.4 \text{ GeV}^2$ at 1.5 GeV to $|t_\rho| \approx 0.7 \text{ GeV}^2$ at 2.5 GeV.

The data points for $d\sigma/dt$ from fig. 16 are transformed to $d\sigma/d\cos\theta$ and shown in fig. 17. Here it becomes obvious that the SAPHIR data and the CLAS data at higher energies show a similar structure, a strong decrease (exponentially *vs.* t) at small angles and a nearly constant cross-section for $\cos\theta_\rho^{\text{cm}} < 0.3$ –0.4 (SAPHIR) or $\cos\theta_\rho^{\text{cm}} < 0.2$ (CLAS). The cross-sections for ρ production at large angles become substantially smaller with higher energies indicating the vanishing importance of s - and u -channel contributions. According to M. Battaglieri *et al.* [22] a possibility to explain the large $-t$ flat behavior around 3.3 GeV are tails of resonances having a sizeable branch in the ρ channel.

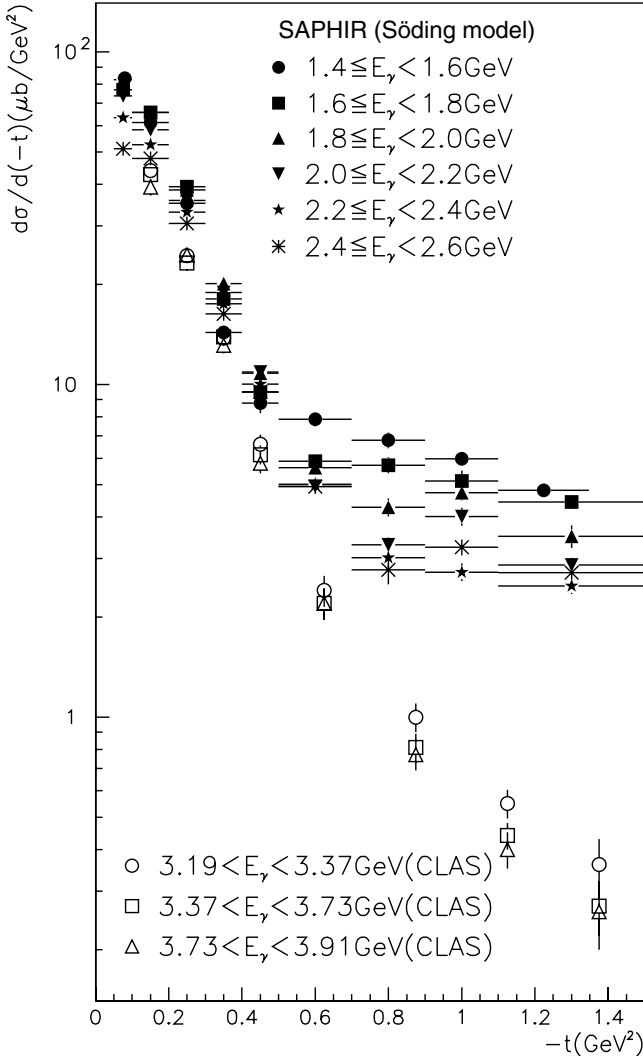


Fig. 16. Differential cross-sections (Söding model). In addition data at higher photon energies from CLAS [22] are shown.

In a recent publication Yonseok Oh and T.-S.H. Lee [23] reported on a systematic re-examination of ρ -meson photoproduction mechanism at low energies. In particular the influences of σ and f_2 exchanges are discussed. Since their published curves for the differential cross-sections start at $E_\gamma = 2.8 \text{ GeV}$, a direct comparison with our data is not possible. Anyhow, this model also shows a decrease of $d\sigma/dt$ between $-t_\rho = 0.7$ and 1.5 GeV^2 whereas our data show a virtually constant value.

As already outlined in sect. 4 the density matrix elements (see fig. 18) can provide additional information about production mechanisms. We determined the density matrix elements ρ^{00} , ρ^{1-1} and $\text{Re } \rho^{10}$ for the helicity system (testing s -channel helicity conservation, SCHC) and the Gottfried-Jackson system (testing t -channel helicity conservation, TCHC). Helicity conservation with respect to a chosen quantization axis means that all helicity flip amplitudes are zero, independent of energy or t value. In that case the angular distribution (eq. (10)) simplifies to

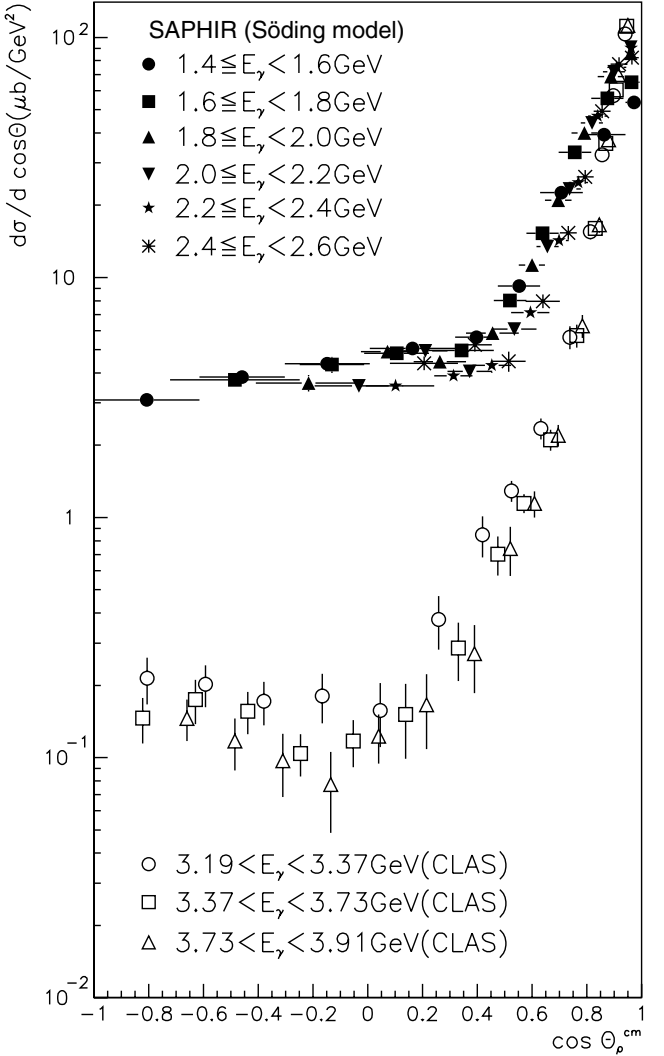


Fig. 17. Differential cross-sections (Söding model). In addition data at higher photon energies from CLAS [22] are shown.

$W(\theta, \phi) \sim \sin^2 \theta$. For our discussion in particular the ρ^{00} amplitude which contains single helicity flip contributions only, is of interest. At higher energies ($> 3 \text{ GeV}$) generally an (at least approximate) s -channel helicity conservation is observed, whereas J. Ballam *et al.* [24] show for ρ^0 production at 4.7 GeV that in the Gottfried-Jackson system the density matrix elements vary rapidly with $|t_\rho|$. This rules out t -channel helicity conservation and it consequently excludes a 0^+ t -channel exchange (Pomeron) as the dominant contribution to ρ^0 production. SCHC means that the (massive) ρ^0 behaves like a photon with the spin completely aligned along its direction of motion. For a more detailed physics discussion on s -channel and t -channel helicity conservation see Gilman *et al.* [25].

For three energy ranges we plot the $|t|$ -dependence of the density matrix elements in fig. 18. In figs. 19 and 20 we visualize the corresponding decay angular distributions for selected $|t|$ bins.

Below $E_\gamma = 1.8 \text{ GeV}$, in the helicity system the approximate $\sin^2 \theta$ form for $0.1 \text{ GeV}^2 < |t_\rho| < 0.15 \text{ GeV}^2$

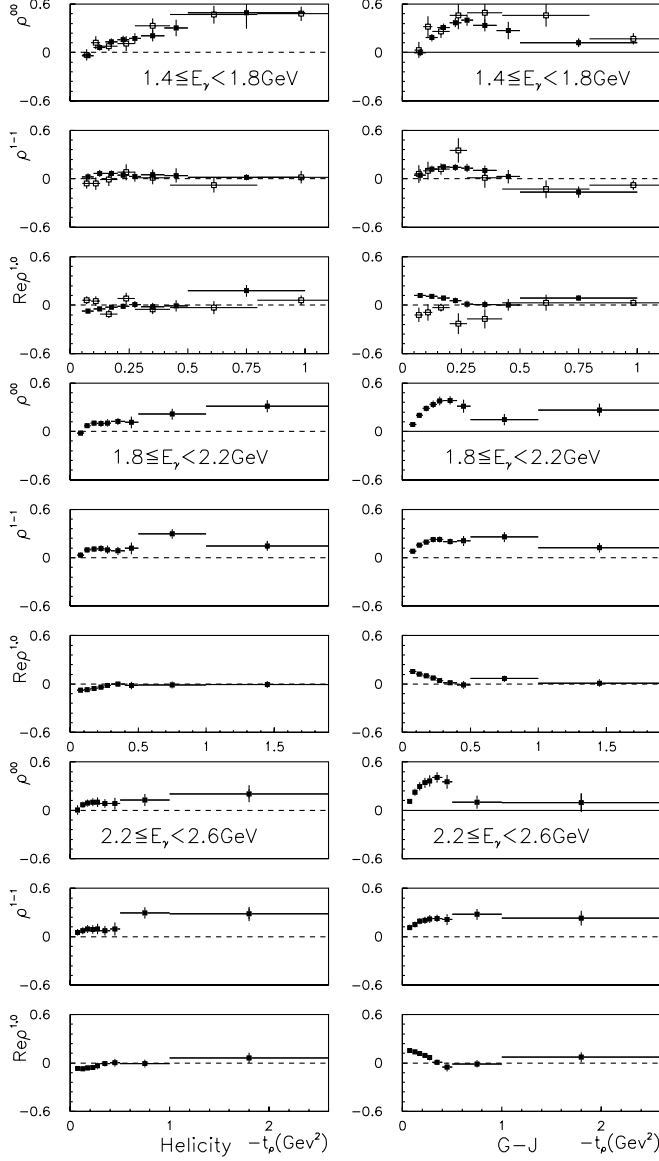


Fig. 18. $\gamma p \rightarrow pp^0$ decay density matrix elements for different energy bins in the helicity system and the Gottfried-Jackson system. \square is from [8].

is already less pure for $0.25 \text{ GeV}^2 < |t_\rho| < 0.3 \text{ GeV}^2$, for $|t|$ values $> 0.5 \text{ GeV}^2$ even the sign of the curvature changes. This is mainly reflected by the one-helicity-flip coefficient ρ^{00} which increases strongly with increasing $|t|$. For the energy ranges 1.8–2.2 and 2.2–2.6 GeV an approximate SCHC is valid for $|t_\rho| < 0.3 \text{ GeV}^2$. For $|t|$ values $> 0.5 \text{ GeV}^2$ generally non-SCHC production mechanism play a role but with decreasing importance towards higher energies. This observation is compatible with the change of the slope parameter in the $d\sigma/dt_\rho$ curves.

In the Gottfried-Jackson system the ρ^{00} matrix element increases rapidly between $|t_{\min}|$ and $|t_\rho| = 0.5 \text{ GeV}^2$ thus ruling out t -channel helicity conservation and thus a dominant 0^+ exchange.

Regarding the energy dependence for $0.5 \text{ GeV}^2 < |t| < 1 \text{ GeV}^2$ in both reference systems a strong, non-monotonic

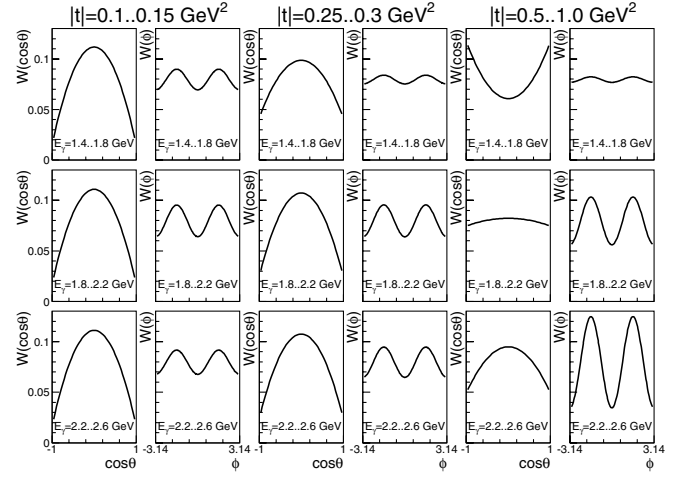


Fig. 19. ρ^0 decay angular distributions in the helicity system for three energy bins with increasing $|t|$ from left to right.

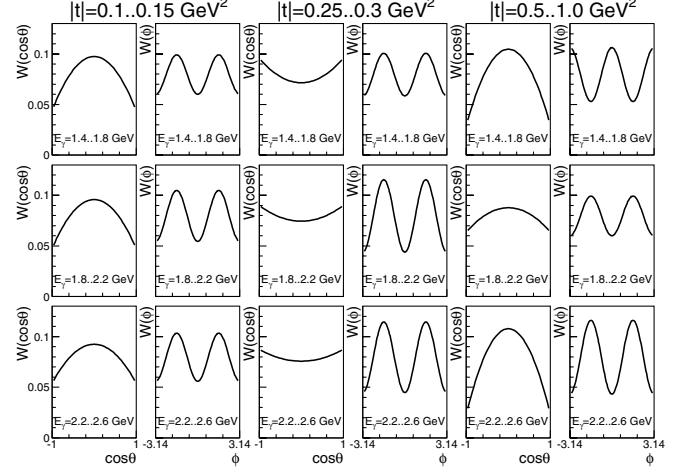


Fig. 20. ρ^0 decay angular distributions in the Gottfried-Jackson system for three energy bins with increasing $|t|$ from left to right.

variation of the angular distributions is observed. Since t -channel exchanges imply a soft energy dependence, the variation in the Gottfried-Jackson system must be induced from the s - or u -channel. We take this as an indication for resonance contribution(s).

In summary: t -channel helicity is not conserved, s -channel helicity is approximately conserved for $E_\gamma > 1.8 \text{ GeV}$ and $|t| < 0.4 \text{ GeV}^2$. In the decay angular distributions we observe an energy dependent anomaly which might be an indication for resonance contributions.

5.3 The reaction $\gamma p \rightarrow \Delta^{++}\pi^-$

The total cross-sections for the reactions $\gamma p \rightarrow \Delta^{++}\pi^-$ and $\gamma p \rightarrow \Delta^0\pi^+ \rightarrow p\pi^+\pi^-$ in the energy range $0.5 < E_\gamma < 2.5 \text{ GeV}$ together with data from other experiments is seen in fig. 21. Comparing both excitation curves a completely different structure for energies below $E_\gamma = 1.3 \text{ GeV}$ is observed, thus pointing towards influences

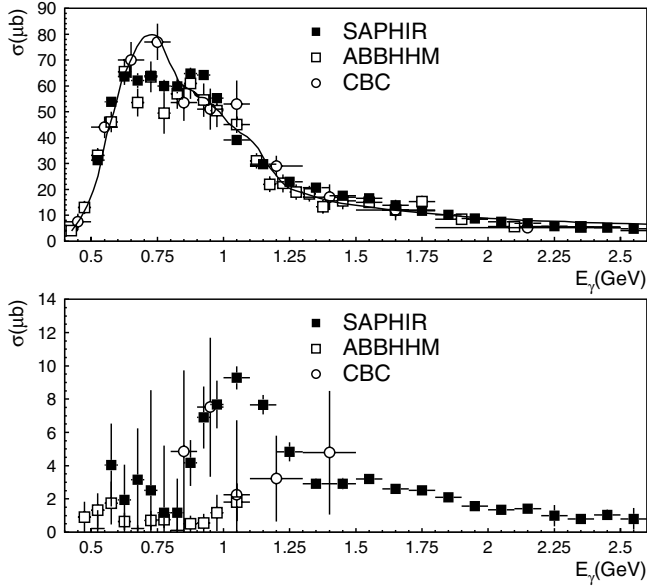


Fig. 21. Total cross-sections of Δ^{++} (above) and $\Delta^0 \rightarrow p\pi^-$ (below) production compared with [8,27]. For the separation from the ρ^0 final state the Söding model was used. The solid curve is from [14].

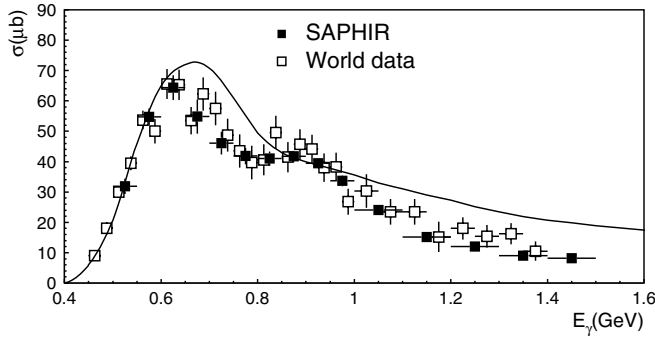


Fig. 22. Integrated Δ^{++} photoproduction cross-section for $-t < 0.3 \text{ GeV}^2$. Curve from the model of Lüke, Scheunert and Stichel [26].

from s -channel resonances with different strengths. Figure 22 shows the energy dependency of the integrated cross-section for $-t < 0.3 \text{ GeV}^2$ together with data points from ABBHHM [8] and a theoretical excitation curve [26]. The differential cross-sections $d\sigma/dt$ in four different energy bins are presented in fig. 24.

In the past different theoretical models for the description of the $\Delta^{++}\pi^-$ photoproduction were applied to describe the data. The Cambridge Bubble Chamber Group [27] used a pure isobaric model without t -channel exchange to fit their data. The gross features were described, but significant discrepancies remained. In particular, the omission of t -channel contributions leads to unrealistic resonance strengths compared with other reactions (for details see [1]). A more general description starting from the OPE model of Stichel and Scholz [28] was developed by different authors. Locher and Sandhas [29] proposed a OPE model with absorptive correc-

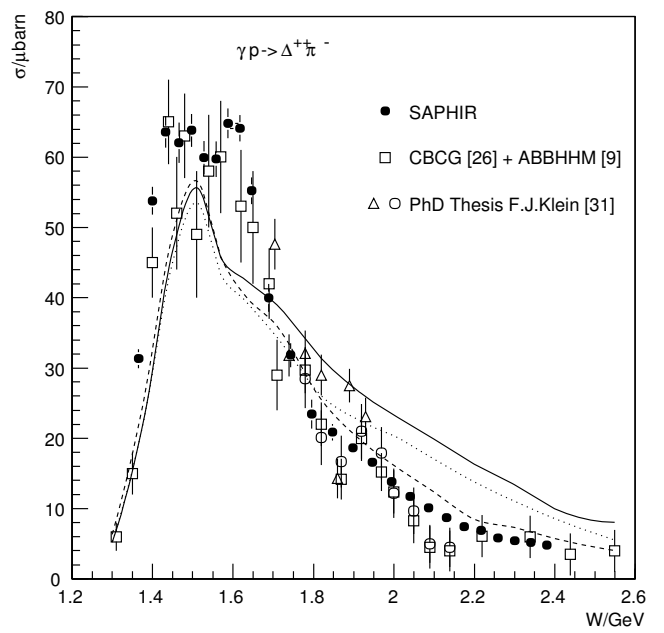


Fig. 23. Total cross-section for $\gamma p \rightarrow \Delta^{++}\pi^-$ together with theoretical calculations from Ripani *et al.* [11]. —: full model, - · - · - : model with reggeized π -exchange, - - - : as before with modified contact term (see text). The data of reference [30] stem from SAPHIR runs before 1997.

tions and gauge invariant extension; Lüke, Scheunert and Stichel [26] added small admixtures of isobaric contributions to their gauge-invariant OPE model. In 1971 Lüke and Söding [1] published an analysis for $\gamma p \rightarrow p\pi^+\pi^-$ with the subprocess $\gamma p \rightarrow \Delta^{++}\pi^-$. Following their ideas Murphy and Laget [14] presented an extension of their effective Lagrangian model. The curve in fig. 21 stems from this model showing a reasonable description of the data, but obviously the implemented resonances $D_{13}(1520)$, $D_{33}(1700)$ and $P_{11}(1440)$ are not sufficient to meet the experimental data in the region between 0.6 and 1 GeV.

M. Ripani *et al.* [11] performed a phenomenological analysis of $\Delta^{++}\pi^-$ photo- and electro-production data. Contrary to the others they implement all established N^* and Δ^* resonances between 1440 and 1950 MeV. The total reaction amplitude in this model is evaluated as coherent superposition of resonant and Born terms with absorption correction for initial and final states. According to the authors the resonance contributions and their interference terms play a non negligible role. The comparison of our data with the result of this model (fig. 23, solid curve) shows that neither in the resonance region below $W = 2 \text{ GeV}$ nor above the data are well described. In order to investigate the effects of a Reggeization, following the ideas of Guidal, Laget and Vanderhaeghen [31], they replaced the pion exchange Born term by a reggeized pion exchange propagator (fig. 23, dash-dotted line). In addition, if the contact term is accordingly modified, a remarkable lowering of the cross-section above $W = 1.8 \text{ GeV}$ is observed. The corresponding dashed curve in fig. 23 already provides a fair description of the total cross-section

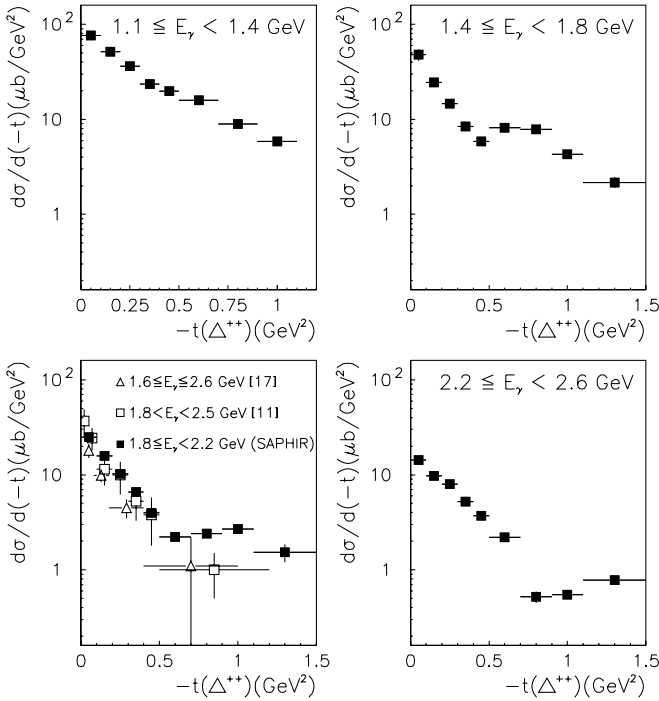


Fig. 24. Differential cross-sections of Δ^{++} photoproduction at different photon energy intervals. For the separation from the ρ^0 final state the Söding model was used.

data for $W > 1.7$ GeV. In the new SAPHIR data one observes a dip in the cross-section around $W = 1.55$ GeV. This structure is also indicated by the old CBCG [27] and ABBHHM [8] data, but is not reproduced in the model of Ripani *et al.* We take this as a hint that the $P_{33}(1600)$ isobar, not taken into account by them, might contribute.

The differential cross-sections (fig. 24) show an approximate exponential fall off at $-t$ values < 0.5 GeV^2 . Above it flattens at higher photon energies tending toward a constant value. For a photon energy of 5 GeV a similar structure but with a start of flattening at $-t = 4$ GeV^2 was measured by R.L. Anderson *et al.* [32].

6 Summary

In summary, for the reaction $\gamma p \rightarrow p\pi^+\pi^-$ total and, for the first time, differential cross-sections were measured. The data were decomposed into $p\rho^0$, $\Delta^{++}\pi^-$ and $\Delta^0\pi^+$.

Total and differential cross-sections for the reaction $\gamma p \rightarrow p\rho^0$ and ρ^0 decay spin density matrix elements were evaluated. The results show that diffraction is no longer dominant as opposed to higher energies. From the differential cross-section as well as from the decay angular distributions for $|t_\rho| > 0.5$ GeV^2 we deduce contributions from s - and u -channel resonances.

The results on Δ^{++} production confirm and improve the existing data. New total cross-section data on Δ^0 photoproduction between threshold and 2.6 GeV were also obtained.

We gratefully acknowledge the help of the technical staff of the “Physikalisches Institut” and the engagement of the ELSA accelerator group. This work is supported in part by the Deutsche Forschungsgemeinschaft (DFG) (SPP KL 980/2-3).

References

- D. Lüke, P. Söding, *Springer Tracts in Modern Physics*, Vol. **59** (Springer, Berlin, Heidelberg, 1971) p. 39.
- J.A. Gomez Tejedor, E. Oset, Nucl. Phys. A **600**, 413 (1996).
- ZEUS Collaboration (J. Breitweg *et al.*), Eur. Phys. J. C **2**, 247 (1998).
- B. Friman, M. Soyeur, Nucl. Phys. A **600**, 477 (1996).
- R. Koniuk, N. Isgur, Phys. Rev. D **21**, 1868 (1980); S. Capstick, W. Roberts, Phys. Rev. D **49**, 4570 (1994).
- W.J. Schwille *et al.*, Nucl. Instrum. Methods Phys. Res. A **344**, 470 (1994).
- J. Barth *et al.*, Eur. Phys. J. A **18**, 117 (2003).
- Aachen-Berlin-Bonn-Hamburg-Heidelberg-Munich Collaboration, Phys. Rev. **175**, 1669 (1968); **188**, 2060 (1969).
- A. Braghieri *et al.*, Phys. Lett. B **363**, 46 (1995).
- J. Ballam *et al.*, Phys. Rev. D **5**, 15 (1972).
- M. Ripani *et al.*, Nucl. Phys. A **672**, 220 (2000).
- J. Ballam *et al.*, Phys. Rev. D **5**, 545 (1972).
- J.D. Jackson, Nuovo Cimento **34**, 1644 (1964).
- L.Y. Murphy, J.-M. Laget, DAPNIA-SPHN-96-10, March 1996.
- P. Söding, Phys. Lett. **19**, 702 (1965).
- M. Ross, L. Stodolsky, Phys. Rev **149**, 1172 (1966).
- K. Hagiwara *et al.*, Phys. Rev. D **66**, 010001 (2002).
- K. Schilling, P. Seyboth, G.E. Wolf, Nucl. Phys. B **15**, 397 (1970); **18**, 332 (1970)(E).
- M. Ripani *et al.*, Phys. At. Nucl. **63**, 1943 (2000); **64**, 1292 (2001).
- F. Klingl, N. Kaiser, W. Weise, Z. Phys. A **356**, 193 (1996).
- G. Niesler, G. Piller, W. Weise, Phys. Lett. B **389**, 157 (1996).
- M. Battaglieri *et al.*, Phys. Rev. Lett. **87**, 172002 (2001).
- Y. Oh, T.-S.H. Lee, Phys. Rev. C **69**, 025201 (2004).
- J. Ballam *et al.*, Phys. Rev. Lett. **24**, 17 (1970).
- F.J. Gilman, J. Pumplin, A. Schwimmer, L. Stodolsky, Phys. Lett. B **31**, 387 (1970).
- D. Lüke, M. Scheunert, P. Stichel, DESY Report No. 68/7 (1968); Nuovo Cimento A **58**, 234 (1968).
- Cambridge Bubble Chamber Group, Phys. Rev. **163**, 1510 (1967).
- P. Stichel, M. Scholz, Nuovo Cimento **34**, 1381 (1964).
- M. Locher, W. Sandhas, Z. Phys. **195**, 461 (1966).
- F.J. Klein, Bonn University thesis BONN-IR-96-08.
- M. Guidal, J.-M. Laget, M. Vanderhaeghen, Phys. Lett. B **400**, 6 (1997).
- R.L. Anderson *et al.*, Phys. Rev. D **14**, 679 (1976).

Appendix A. Statistical and systematic errors

The physics results shown in figures and tables are based on four different SAPHIR runs (see table 3), which together cover the entire resonance region.

Table 3. SAPHIR runs in the years 1997 and 1998.

Run date	ELSA energy (GeV)	Tagging range (GeV)	Number of triggers
01/1997	2.8	0.87–2.63	29 350 000
05/1997	1.6	0.50–1.50	13 821 000
11/1997	2.6	0.81–2.44	47 028 000
02/1998	2.8	0.87–2.63	56 599 000

All runs were analyzed stand-alone using run-dependent detector simulation and reconstruction. So for each run cross-sections and spin density matrix elements with certain statistical (and in principle systematic) errors were obtained. For each photon energy bin the results x_i ($i = 1 \dots N$; N = number of runs contributing to the respective photon energy bin) were combined to one final value by building the (statistical) error-weighted mean m :

$$m = \frac{\sum_{i=1}^N \frac{x_i}{\sigma_i^2}}{\sum_{i=1}^N \frac{1}{\sigma_i^2}}, \quad \sigma_w = \sqrt{\frac{1}{\sum_{i=1}^N \frac{1}{\sigma_i^2}}}.$$

The statistical errors, σ_w , are based on the full statistics of the event samples, but do not account for uncertainties caused by differences in the run conditions. Known differences were taken into account in the simulation used for acceptance corrections. In order to take into account possible additional fluctuations and uncertainties between the runs, which were not explicitly considered in the simulations, another error σ_d has been determined as the standard deviation of the N measurements x_i to the weighted mean m given by the square root of the variance V_m :

$$\sigma_d = \sqrt{V_m} = \sqrt{\frac{1}{N(N-1)} \sum_{i=1}^N (m - x_i)^2}.$$

In cases where σ_d was smaller than σ_w , σ_d was set equal to σ_w .

In the following tables the results are given in the form $m \pm \sigma_d(\sigma_m)$. For the lower photon energies, where only the low energy run contributes, σ_d is not listed.

It is assumed that σ_d already includes the main systematic error. As described in 4.2 the error σ_m for results on ρ and Δ production (see appendices D–G) already includes some part of the systematic error which stems from the reaction channel assignment with a Likelihood-fit to the mass spectra.

Appendix B. Total cross-sections for $\gamma p \rightarrow p \pi^+ \pi^-$

Table 4. Total cross-section of the reaction $\gamma p \rightarrow p \pi^+ \pi^-$. The determination is based on one run only (May 1997), with a 1.6 GeV electron beam.

E_γ (GeV)	$\sigma_{\text{tot}}(\mu\text{b})$
0.50 … 0.55	$33.85 \pm (1.78)$
0.55 … 0.60	$55.66 \pm (1.84)$
0.60 … 0.65	$70.36 \pm (1.77)$
0.65 … 0.70	$74.98 \pm (1.84)$
0.70 … 0.75	$75.42 \pm (1.90)$
0.75 … 0.80	$72.85 \pm (1.91)$
0.80 … 0.85	$72.52 \pm (1.96)$
0.85 … 0.90	$74.22 \pm (2.09)$
0.90 … 0.95	$75.23 \pm (2.30)$
0.95 … 1.00	$72.60 \pm (2.55)$
1.00 … 1.05	$72.79 \pm (2.53)$
1.05 … 1.10	$72.59 \pm (2.56)$
1.10 … 1.15	$64.33 \pm (2.56)$
1.15 … 1.20	$60.81 \pm (2.40)$
1.20 … 1.25	$57.63 \pm (2.39)$
1.25 … 1.30	$54.62 \pm (2.21)$
1.30 … 1.35	$55.88 \pm (2.68)$
1.35 … 1.40	$54.94 \pm (2.39)$
1.40 … 1.45	$53.49 \pm (2.53)$

Table 5. Total cross-section of the reaction $\gamma p \rightarrow p \pi^+ \pi^-$. The determination is based on four runs, three of which with a 2.8 GeV electron beam, one with 2.6 GeV electrons. As for the 1.6 GeV run a different energy binning was used (see table 4), the results of this low-energy run are not included in the values of this table.

E_γ (GeV)	$\sigma_{\text{tot}}(\mu\text{b})$
1.00 … 1.10	$74.23 \pm 3.24 (0.23)$
1.10 … 1.20	$62.24 \pm 2.17 (0.18)$
1.20 … 1.30	$57.09 \pm 2.54 (0.18)$
1.30 … 1.40	$54.00 \pm 1.50 (0.18)$
1.40 … 1.50	$52.56 \pm 1.52 (0.19)$
1.50 … 1.60	$50.06 \pm 2.03 (0.21)$
1.60 … 1.70	$47.27 \pm 2.12 (0.20)$
1.70 … 1.80	$45.08 \pm 1.92 (0.21)$
1.80 … 1.90	$42.33 \pm 1.90 (0.22)$
1.90 … 2.00	$39.41 \pm 2.01 (0.20)$
2.00 … 2.10	$36.63 \pm 1.54 (0.21)$
2.10 … 2.20	$32.98 \pm 2.98 (0.25)$
2.20 … 2.30	$31.62 \pm 1.74 (0.19)$
2.30 … 2.40	$30.14 \pm 1.83 (0.19)$
2.40 … 2.50	$29.08 \pm 1.49 (0.24)$
2.50 … 2.60	$28.90 \pm 0.29 (0.29)$

Appendix C. Differential cross-sections for $\gamma p \rightarrow p\pi^+\pi^-$

Table 6. Differential cross-section $d\sigma/dt_{\pi\pi}$ ($\mu\text{b}/\text{GeV}^2$) of the reaction $\gamma p \rightarrow p\pi^+\pi^-$.

$-t_{\pi\pi}$ (GeV^2)	$E_\gamma = 0.5\text{--}0.6 \text{ GeV}$	$E_\gamma = 0.6\text{--}0.7 \text{ GeV}$	$E_\gamma = 0.7\text{--}0.8 \text{ GeV}$	$E_\gamma = 0.8\text{--}0.9 \text{ GeV}$
1.00 ... 0.95	0.000 ± 0.000 (0.000)			
0.95 ... 0.90	0.000 ± 0.000 (0.000)	0.000 ± 0.000 (0.000)	0.000 ± 0.000 (0.000)	0.057 ± 0.017 (0.017)
0.90 ... 0.85	0.000 ± 0.000 (0.000)	0.000 ± 0.000 (0.000)	0.000 ± 0.000 (0.000)	0.165 ± 0.030 (0.030)
0.85 ... 0.80	0.000 ± 0.000 (0.000)	0.000 ± 0.000 (0.000)	0.000 ± 0.000 (0.000)	0.356 ± 0.039 (0.039)
0.80 ... 0.75	0.000 ± 0.000 (0.000)	0.000 ± 0.000 (0.000)	0.026 ± 0.010 (0.010)	0.642 ± 0.046 (0.046)
0.75 ... 0.70	0.000 ± 0.000 (0.000)	0.000 ± 0.000 (0.000)	0.213 ± 0.041 (0.032)	1.001 ± 0.057 (0.055)
0.70 ... 0.65	0.000 ± 0.000 (0.000)	0.000 ± 0.000 (0.000)	0.382 ± 0.035 (0.035)	1.284 ± 0.055 (0.055)
0.65 ... 0.60	0.000 ± 0.000 (0.000)	0.030 ± 0.011 (0.011)	0.875 ± 0.050 (0.050)	1.772 ± 0.060 (0.060)
0.60 ... 0.55	0.000 ± 0.000 (0.000)	0.207 ± 0.027 (0.027)	1.753 ± 0.066 (0.066)	2.566 ± 0.071 (0.071)
0.55 ... 0.50	0.000 ± 0.000 (0.000)	0.689 ± 0.049 (0.049)	2.466 ± 0.071 (0.071)	3.094 ± 0.075 (0.075)
0.50 ... 0.45	0.061 ± 0.025 (0.025)	1.655 ± 0.065 (0.065)	3.618 ± 0.080 (0.080)	4.118 ± 0.084 (0.084)
0.45 ... 0.40	0.387 ± 0.054 (0.054)	3.310 ± 0.084 (0.084)	4.708 ± 0.086 (0.086)	4.931 ± 0.089 (0.089)
0.40 ... 0.35	1.157 ± 0.097 (0.067)	5.157 ± 0.094 (0.094)	6.183 ± 0.095 (0.095)	6.149 ± 0.099 (0.099)
0.35 ... 0.30	2.927 ± 0.113 (0.085)	7.806 ± 0.125 (0.109)	8.301 ± 0.110 (0.110)	7.314 ± 0.106 (0.106)
0.30 ... 0.25	6.023 ± 0.166 (0.117)	10.211 ± 0.122 (0.122)	9.327 ± 0.114 (0.114)	7.968 ± 0.108 (0.108)
0.25 ... 0.20	8.443 ± 0.139 (0.127)	12.300 ± 0.131 (0.131)	9.844 ± 0.114 (0.114)	8.782 ± 0.115 (0.115)
0.20 ... 0.15	10.643 ± 0.140 (0.140)	12.553 ± 0.129 (0.129)	10.095 ± 0.121 (0.121)	8.968 ± 0.122 (0.122)
0.15 ... 0.10	10.172 ± 0.131 (0.131)	11.800 ± 0.131 (0.131)	9.844 ± 0.128 (0.128)	8.327 ± 0.124 (0.124)
0.10 ... 0.05	7.479 ± 0.118 (0.118)	8.406 ± 0.118 (0.118)	6.512 ± 0.109 (0.109)	5.796 ± 0.106 (0.106)
0.05 ... 0.00	1.087 ± 0.045 (0.045)	1.327 ± 0.047 (0.047)	1.288 ± 0.050 (0.050)	1.205 ± 0.049 (0.049)
$-t_{\pi\pi}$ (GeV^2)	$E_\gamma = 0.9\text{--}1.0 \text{ GeV}$	$E_\gamma = 1.0\text{--}1.1 \text{ GeV}$	$E_\gamma = 1.1\text{--}1.2 \text{ GeV}$	$E_\gamma = 1.2\text{--}1.3 \text{ GeV}$
1.70 ... 1.65	0.000 ± 0.000 (0.000)			
1.65 ... 1.60	0.000 ± 0.000 (0.000)	0.000 ± 0.000 (0.000)	0.000 ± 0.000 (0.000)	0.002 ± 0.001 (0.001)
1.60 ... 1.55	0.000 ± 0.000 (0.000)	0.000 ± 0.000 (0.000)	0.000 ± 0.000 (0.000)	0.009 ± 0.002 (0.002)
1.55 ... 1.50	0.000 ± 0.000 (0.000)	0.000 ± 0.000 (0.000)	0.000 ± 0.000 (0.000)	0.025 ± 0.013 (0.013)
1.50 ... 1.45	0.000 ± 0.000 (0.000)	0.000 ± 0.000 (0.000)	0.002 ± 0.001 (0.001)	0.056 ± 0.005 (0.003)
1.45 ... 1.40	0.000 ± 0.000 (0.000)	0.000 ± 0.000 (0.000)	0.010 ± 0.003 (0.003)	0.088 ± 0.006 (0.004)
1.40 ... 1.35	0.000 ± 0.000 (0.000)	0.000 ± 0.000 (0.000)	0.027 ± 0.003 (0.003)	0.141 ± 0.017 (0.017)
1.35 ... 1.30	0.000 ± 0.000 (0.000)	0.002 ± 0.001 (0.001)	0.076 ± 0.006 (0.002)	0.201 ± 0.012 (0.012)
1.30 ... 1.25	0.000 ± 0.000 (0.000)	0.010 ± 0.002 (0.001)	0.148 ± 0.009 (0.009)	0.270 ± 0.014 (0.014)
1.25 ... 1.20	0.000 ± 0.000 (0.000)	0.053 ± 0.010 (0.010)	0.235 ± 0.011 (0.011)	0.312 ± 0.009 (0.006)
1.20 ... 1.15	0.000 ± 0.000 (0.000)	0.117 ± 0.007 (0.004)	0.367 ± 0.012 (0.012)	0.381 ± 0.012 (0.012)
1.15 ... 1.10	0.000 ± 0.000 (0.000)	0.248 ± 0.013 (0.013)	0.484 ± 0.026 (0.026)	0.443 ± 0.016 (0.016)
1.10 ... 1.05	0.028 ± 0.010 (0.010)	0.415 ± 0.013 (0.002)	0.566 ± 0.016 (0.016)	0.512 ± 0.020 (0.020)
1.05 ... 1.00	0.121 ± 0.022 (0.022)	0.617 ± 0.016 (0.016)	0.615 ± 0.019 (0.019)	0.610 ± 0.011 (0.008)
1.00 ... 0.95	0.232 ± 0.032 (0.032)	0.737 ± 0.046 (0.046)	0.755 ± 0.015 (0.015)	0.765 ± 0.017 (0.017)
0.95 ... 0.90	0.454 ± 0.044 (0.042)	0.889 ± 0.063 (0.063)	0.886 ± 0.015 (0.015)	0.922 ± 0.031 (0.031)
0.90 ... 0.85	0.827 ± 0.061 (0.055)	1.070 ± 0.060 (0.060)	1.113 ± 0.015 (0.013)	1.069 ± 0.031 (0.031)
0.85 ... 0.80	0.999 ± 0.063 (0.056)	1.314 ± 0.050 (0.050)	1.298 ± 0.025 (0.025)	1.196 ± 0.035 (0.035)
0.80 ... 0.75	1.273 ± 0.057 (0.057)	1.577 ± 0.032 (0.032)	1.507 ± 0.021 (0.021)	1.259 ± 0.031 (0.031)
0.75 ... 0.70	1.604 ± 0.063 (0.061)	1.916 ± 0.040 (0.040)	1.606 ± 0.053 (0.053)	1.422 ± 0.063 (0.063)
0.70 ... 0.65	1.915 ± 0.065 (0.065)	2.208 ± 0.090 (0.090)	1.809 ± 0.067 (0.067)	1.573 ± 0.053 (0.053)
0.65 ... 0.60	2.408 ± 0.072 (0.072)	2.405 ± 0.088 (0.088)	2.114 ± 0.069 (0.069)	1.786 ± 0.087 (0.087)
0.60 ... 0.55	2.889 ± 0.076 (0.076)	2.789 ± 0.105 (0.105)	2.433 ± 0.083 (0.083)	1.940 ± 0.066 (0.066)
0.55 ... 0.50	3.384 ± 0.080 (0.080)	3.249 ± 0.177 (0.177)	2.728 ± 0.069 (0.069)	2.070 ± 0.082 (0.082)
0.50 ... 0.45	3.961 ± 0.085 (0.085)	3.817 ± 0.199 (0.199)	2.887 ± 0.101 (0.101)	2.264 ± 0.060 (0.060)
0.45 ... 0.40	4.789 ± 0.091 (0.091)	4.209 ± 0.207 (0.207)	3.197 ± 0.097 (0.097)	2.630 ± 0.104 (0.104)
0.40 ... 0.35	5.666 ± 0.096 (0.096)	4.678 ± 0.201 (0.201)	3.648 ± 0.151 (0.151)	3.028 ± 0.143 (0.143)
0.35 ... 0.30	6.405 ± 0.100 (0.100)	5.457 ± 0.262 (0.262)	4.214 ± 0.152 (0.152)	3.492 ± 0.152 (0.152)
0.30 ... 0.25	7.250 ± 0.108 (0.108)	6.196 ± 0.218 (0.218)	4.833 ± 0.137 (0.137)	4.242 ± 0.173 (0.173)
0.25 ... 0.20	8.106 ± 0.115 (0.115)	7.138 ± 0.263 (0.263)	5.725 ± 0.118 (0.118)	5.369 ± 0.232 (0.232)
0.20 ... 0.15	8.685 ± 0.128 (0.128)	7.534 ± 0.300 (0.300)	6.311 ± 0.163 (0.163)	6.024 ± 0.313 (0.313)
0.15 ... 0.10	7.595 ± 0.122 (0.122)	6.977 ± 0.250 (0.250)	6.072 ± 0.208 (0.208)	6.277 ± 0.334 (0.334)
0.10 ... 0.05	5.603 ± 0.108 (0.108)	5.382 ± 0.189 (0.189)	4.662 ± 0.204 (0.204)	4.769 ± 0.255 (0.255)
0.05 ... 0.00	1.063 ± 0.048 (0.048)	1.169 ± 0.083 (0.083)	0.986 ± 0.072 (0.072)	0.953 ± 0.049 (0.049)

Table 7. Differential cross-section $d\sigma/dt_{\pi\pi}$ ($\mu\text{b}/\text{GeV}^2$) of the reaction $\gamma p \rightarrow p\pi^+\pi^-$.

$-t_{\pi\pi}$ (GeV 2)	$E_\gamma = 1.3\text{--}1.4$ GeV	$E_\gamma = 1.4\text{--}1.5$ GeV	$E_\gamma = 1.5\text{--}1.6$ GeV	$E_\gamma = 1.6\text{--}1.7$ GeV
2.40 ... 2.35	0.000 ± 0.000 (0.000)			
2.35 ... 2.30	0.000 ± 0.000 (0.000)	0.000 ± 0.000 (0.000)	0.000 ± 0.000 (0.000)	0.002 ± 0.001 (0.001)
2.30 ... 2.25	0.000 ± 0.000 (0.000)	0.000 ± 0.000 (0.000)	0.000 ± 0.000 (0.000)	0.002 ± 0.002 (0.002)
2.25 ... 2.20	0.000 ± 0.000 (0.000)	0.000 ± 0.000 (0.000)	0.000 ± 0.000 (0.000)	0.007 ± 0.003 (0.003)
2.20 ... 2.15	0.000 ± 0.000 (0.000)	0.000 ± 0.000 (0.000)	0.002 ± 0.002 (0.001)	0.019 ± 0.005 (0.005)
2.15 ... 2.10	0.000 ± 0.000 (0.000)	0.000 ± 0.000 (0.000)	0.006 ± 0.002 (0.001)	0.024 ± 0.008 (0.008)
2.10 ... 2.05	0.000 ± 0.000 (0.000)	0.000 ± 0.000 (0.000)	0.006 ± 0.002 (0.002)	0.034 ± 0.012 (0.012)
2.05 ... 2.00	0.000 ± 0.000 (0.000)	0.000 ± 0.000 (0.000)	0.019 ± 0.003 (0.002)	0.062 ± 0.006 (0.005)
2.00 ... 1.95	0.000 ± 0.000 (0.000)	0.002 ± 0.002 (0.002)	0.024 ± 0.003 (0.002)	0.072 ± 0.006 (0.006)
1.95 ... 1.90	0.000 ± 0.000 (0.000)	0.009 ± 0.002 (0.000)	0.044 ± 0.005 (0.005)	0.079 ± 0.017 (0.017)
1.90 ... 1.85	0.000 ± 0.000 (0.000)	0.015 ± 0.005 (0.005)	0.063 ± 0.006 (0.006)	0.091 ± 0.011 (0.011)
1.85 ... 1.80	0.001 ± 0.000 (0.000)	0.035 ± 0.004 (0.003)	0.066 ± 0.010 (0.010)	0.102 ± 0.008 (0.008)
1.80 ... 1.75	0.002 ± 0.001 (0.001)	0.045 ± 0.005 (0.003)	0.091 ± 0.006 (0.005)	0.119 ± 0.013 (0.013)
1.75 ... 1.70	0.013 ± 0.004 (0.004)	0.075 ± 0.006 (0.003)	0.136 ± 0.007 (0.006)	0.146 ± 0.008 (0.008)
1.70 ... 1.65	0.032 ± 0.004 (0.001)	0.096 ± 0.006 (0.005)	0.158 ± 0.023 (0.023)	0.175 ± 0.007 (0.005)
1.65 ... 1.60	0.047 ± 0.005 (0.005)	0.119 ± 0.012 (0.012)	0.171 ± 0.010 (0.010)	0.208 ± 0.014 (0.014)
1.60 ... 1.55	0.079 ± 0.006 (0.006)	0.145 ± 0.007 (0.007)	0.193 ± 0.008 (0.007)	0.256 ± 0.009 (0.007)
1.55 ... 1.50	0.099 ± 0.007 (0.007)	0.164 ± 0.013 (0.013)	0.229 ± 0.017 (0.017)	0.298 ± 0.011 (0.011)
1.50 ... 1.45	0.168 ± 0.008 (0.007)	0.213 ± 0.019 (0.019)	0.285 ± 0.015 (0.015)	0.348 ± 0.033 (0.033)
1.45 ... 1.40	0.218 ± 0.011 (0.011)	0.239 ± 0.008 (0.005)	0.338 ± 0.022 (0.022)	0.433 ± 0.018 (0.018)
1.40 ... 1.35	0.241 ± 0.022 (0.022)	0.302 ± 0.018 (0.018)	0.429 ± 0.011 (0.009)	0.451 ± 0.019 (0.019)
1.35 ... 1.30	0.280 ± 0.024 (0.024)	0.357 ± 0.016 (0.016)	0.497 ± 0.021 (0.021)	0.523 ± 0.012 (0.006)
1.30 ... 1.25	0.323 ± 0.018 (0.018)	0.451 ± 0.019 (0.019)	0.577 ± 0.013 (0.013)	0.521 ± 0.012 (0.006)
1.25 ... 1.20	0.364 ± 0.011 (0.011)	0.549 ± 0.019 (0.019)	0.664 ± 0.022 (0.022)	0.606 ± 0.015 (0.015)
1.20 ... 1.15	0.474 ± 0.016 (0.016)	0.686 ± 0.034 (0.034)	0.743 ± 0.014 (0.014)	0.637 ± 0.017 (0.017)
1.15 ... 1.10	0.572 ± 0.011 (0.004)	0.748 ± 0.019 (0.019)	0.795 ± 0.028 (0.028)	0.683 ± 0.020 (0.020)
1.10 ... 1.05	0.708 ± 0.013 (0.007)	0.854 ± 0.022 (0.022)	0.798 ± 0.019 (0.019)	0.708 ± 0.013 (0.007)
1.05 ... 1.00	0.799 ± 0.013 (0.013)	0.903 ± 0.014 (0.008)	0.880 ± 0.039 (0.039)	0.726 ± 0.019 (0.019)
1.00 ... 0.95	0.926 ± 0.018 (0.018)	1.004 ± 0.015 (0.005)	0.916 ± 0.028 (0.028)	0.759 ± 0.013 (0.010)
0.95 ... 0.90	1.049 ± 0.016 (0.016)	1.058 ± 0.037 (0.037)	0.933 ± 0.014 (0.005)	0.827 ± 0.013 (0.011)
0.90 ... 0.85	1.094 ± 0.024 (0.024)	1.140 ± 0.022 (0.022)	1.027 ± 0.023 (0.023)	0.860 ± 0.041 (0.041)
0.85 ... 0.80	1.202 ± 0.037 (0.037)	1.201 ± 0.016 (0.016)	1.035 ± 0.015 (0.015)	0.888 ± 0.031 (0.031)
0.80 ... 0.75	1.318 ± 0.036 (0.036)	1.271 ± 0.044 (0.044)	1.034 ± 0.014 (0.012)	0.890 ± 0.034 (0.034)
0.75 ... 0.70	1.376 ± 0.035 (0.035)	1.299 ± 0.017 (0.017)	1.043 ± 0.020 (0.020)	0.933 ± 0.023 (0.023)
0.70 ... 0.65	1.493 ± 0.016 (0.007)	1.312 ± 0.036 (0.036)	1.111 ± 0.039 (0.039)	0.943 ± 0.072 (0.072)
0.65 ... 0.60	1.517 ± 0.062 (0.062)	1.373 ± 0.037 (0.037)	1.119 ± 0.035 (0.035)	0.975 ± 0.045 (0.045)
0.60 ... 0.55	1.589 ± 0.025 (0.025)	1.412 ± 0.030 (0.030)	1.197 ± 0.053 (0.053)	1.081 ± 0.021 (0.021)
0.55 ... 0.50	1.761 ± 0.049 (0.049)	1.540 ± 0.041 (0.041)	1.277 ± 0.040 (0.040)	1.134 ± 0.018 (0.018)
0.50 ... 0.45	1.947 ± 0.064 (0.064)	1.671 ± 0.063 (0.063)	1.425 ± 0.048 (0.048)	1.286 ± 0.029 (0.029)
0.45 ... 0.40	2.200 ± 0.086 (0.086)	1.909 ± 0.035 (0.035)	1.625 ± 0.047 (0.047)	1.561 ± 0.031 (0.031)
0.40 ... 0.35	2.525 ± 0.101 (0.101)	2.214 ± 0.086 (0.086)	1.987 ± 0.062 (0.062)	1.902 ± 0.039 (0.039)
0.35 ... 0.30	2.990 ± 0.072 (0.072)	2.673 ± 0.126 (0.126)	2.535 ± 0.066 (0.066)	2.438 ± 0.043 (0.043)
0.30 ... 0.25	3.765 ± 0.092 (0.092)	3.477 ± 0.091 (0.091)	3.212 ± 0.111 (0.111)	3.041 ± 0.060 (0.060)
0.25 ... 0.20	4.660 ± 0.122 (0.122)	4.277 ± 0.136 (0.136)	4.040 ± 0.101 (0.101)	3.870 ± 0.058 (0.058)
0.20 ... 0.15	5.402 ± 0.141 (0.141)	5.100 ± 0.149 (0.149)	4.840 ± 0.098 (0.098)	4.591 ± 0.075 (0.075)
0.15 ... 0.10	5.949 ± 0.246 (0.246)	5.762 ± 0.206 (0.206)	5.546 ± 0.123 (0.123)	5.152 ± 0.100 (0.100)
0.10 ... 0.05	4.778 ± 0.238 (0.238)	4.951 ± 0.195 (0.195)	5.036 ± 0.163 (0.163)	4.857 ± 0.182 (0.182)
0.05 ... 0.00	0.886 ± 0.084 (0.084)	0.901 ± 0.053 (0.053)	0.980 ± 0.084 (0.084)	1.018 ± 0.061 (0.061)

Table 8. Differential cross-section $d\sigma/dt_{\pi\pi}$ ($\mu\text{b}/\text{GeV}^2$) of the reaction $\gamma p \rightarrow p\pi^+\pi^-$.

$-t_{\pi\pi}$ (GeV 2)	$E_\gamma = 1.7\text{--}1.8$ GeV	$E_\gamma = 1.8\text{--}1.9$ GeV	$E_\gamma = 1.9\text{--}2.0$ GeV	$E_\gamma = 2.0\text{--}2.1$ GeV
3.00 ... 2.95	0.000 ± 0.000 (0.000)			
2.95 ... 2.90	0.000 ± 0.000 (0.000)	0.000 ± 0.000 (0.000)	0.000 ± 0.000 (0.000)	0.008 ± 0.003 (0.003)
2.90 ... 2.85	0.000 ± 0.000 (0.000)	0.000 ± 0.000 (0.000)	0.003 ± 0.002 (0.002)	0.001 ± 0.010 (0.010)
2.85 ... 2.80	0.000 ± 0.000 (0.000)	0.000 ± 0.000 (0.000)	0.004 ± 0.002 (0.002)	0.010 ± 0.003 (0.003)
2.80 ... 2.75	0.000 ± 0.000 (0.000)	0.000 ± 0.000 (0.000)	0.003 ± 0.001 (0.001)	0.009 ± 0.007 (0.007)
2.75 ... 2.70	0.000 ± 0.000 (0.000)	0.000 ± 0.000 (0.000)	0.009 ± 0.005 (0.005)	0.016 ± 0.011 (0.011)
2.70 ... 2.65	0.000 ± 0.000 (0.000)	0.001 ± 0.001 (0.001)	0.003 ± 0.010 (0.010)	0.014 ± 0.013 (0.013)
2.65 ... 2.60	0.000 ± 0.000 (0.000)	0.002 ± 0.004 (0.004)	0.023 ± 0.007 (0.007)	0.036 ± 0.011 (0.011)
2.60 ... 2.55	0.000 ± 0.000 (0.000)	0.005 ± 0.004 (0.004)	0.028 ± 0.008 (0.008)	0.036 ± 0.019 (0.019)
2.55 ... 2.50	0.002 ± 0.002 (0.001)	0.007 ± 0.007 (0.007)	0.047 ± 0.010 (0.010)	0.042 ± 0.012 (0.012)
2.50 ... 2.45	0.003 ± 0.002 (0.002)	0.022 ± 0.004 (0.002)	0.046 ± 0.005 (0.004)	0.042 ± 0.028 (0.028)
2.45 ... 2.40	0.002 ± 0.001 (0.001)	0.033 ± 0.005 (0.005)	0.055 ± 0.011 (0.011)	0.056 ± 0.007 (0.007)
2.40 ... 2.35	0.006 ± 0.002 (0.002)	0.047 ± 0.009 (0.009)	0.071 ± 0.017 (0.017)	0.076 ± 0.025 (0.025)
2.35 ... 2.30	0.019 ± 0.006 (0.006)	0.051 ± 0.006 (0.006)	0.060 ± 0.007 (0.007)	0.062 ± 0.022 (0.022)
2.30 ... 2.25	0.032 ± 0.004 (0.003)	0.063 ± 0.005 (0.000)	0.076 ± 0.021 (0.021)	0.057 ± 0.037 (0.037)
2.25 ... 2.20	0.045 ± 0.005 (0.004)	0.080 ± 0.012 (0.012)	0.073 ± 0.013 (0.013)	0.077 ± 0.033 (0.033)
2.20 ... 2.15	0.059 ± 0.009 (0.009)	0.093 ± 0.008 (0.008)	0.085 ± 0.012 (0.012)	0.078 ± 0.026 (0.026)
2.15 ... 2.10	0.075 ± 0.009 (0.009)	0.099 ± 0.012 (0.012)	0.092 ± 0.011 (0.011)	0.086 ± 0.032 (0.032)
2.10 ... 2.05	0.074 ± 0.006 (0.006)	0.117 ± 0.013 (0.013)	0.104 ± 0.009 (0.009)	0.106 ± 0.034 (0.034)
2.05 ... 2.00	0.096 ± 0.006 (0.006)	0.108 ± 0.015 (0.015)	0.115 ± 0.006 (0.006)	0.108 ± 0.037 (0.037)
2.00 ... 1.95	0.095 ± 0.006 (0.004)	0.119 ± 0.021 (0.021)	0.135 ± 0.011 (0.011)	0.122 ± 0.026 (0.026)
1.95 ... 1.90	0.134 ± 0.008 (0.004)	0.152 ± 0.022 (0.022)	0.142 ± 0.019 (0.019)	0.131 ± 0.033 (0.033)
1.90 ... 1.85	0.123 ± 0.007 (0.003)	0.178 ± 0.010 (0.010)	0.156 ± 0.024 (0.024)	0.138 ± 0.049 (0.049)
1.85 ... 1.80	0.155 ± 0.007 (0.006)	0.176 ± 0.017 (0.017)	0.194 ± 0.023 (0.023)	0.154 ± 0.047 (0.047)
1.80 ... 1.75	0.176 ± 0.008 (0.007)	0.205 ± 0.028 (0.028)	0.203 ± 0.019 (0.019)	0.195 ± 0.059 (0.059)
1.75 ... 1.70	0.196 ± 0.011 (0.011)	0.223 ± 0.013 (0.013)	0.199 ± 0.033 (0.033)	0.197 ± 0.038 (0.038)
1.70 ... 1.65	0.249 ± 0.014 (0.014)	0.251 ± 0.014 (0.014)	0.220 ± 0.035 (0.035)	0.215 ± 0.045 (0.045)
1.65 ... 1.60	0.263 ± 0.009 (0.005)	0.262 ± 0.020 (0.020)	0.282 ± 0.017 (0.017)	0.208 ± 0.051 (0.051)
1.60 ... 1.55	0.319 ± 0.038 (0.038)	0.322 ± 0.024 (0.024)	0.301 ± 0.022 (0.022)	0.260 ± 0.037 (0.037)
1.55 ... 1.50	0.338 ± 0.028 (0.028)	0.319 ± 0.039 (0.039)	0.324 ± 0.022 (0.022)	0.261 ± 0.037 (0.037)
1.50 ... 1.45	0.362 ± 0.028 (0.028)	0.352 ± 0.046 (0.046)	0.324 ± 0.028 (0.028)	0.262 ± 0.032 (0.032)
1.45 ... 1.40	0.365 ± 0.032 (0.032)	0.399 ± 0.027 (0.027)	0.318 ± 0.030 (0.030)	0.274 ± 0.033 (0.033)
1.40 ... 1.35	0.440 ± 0.026 (0.026)	0.387 ± 0.013 (0.013)	0.341 ± 0.023 (0.023)	0.293 ± 0.031 (0.031)
1.35 ... 1.30	0.477 ± 0.012 (0.005)	0.402 ± 0.039 (0.039)	0.359 ± 0.022 (0.022)	0.306 ± 0.023 (0.023)
1.30 ... 1.25	0.500 ± 0.012 (0.004)	0.437 ± 0.014 (0.014)	0.374 ± 0.026 (0.026)	0.345 ± 0.018 (0.018)
1.25 ... 1.20	0.537 ± 0.028 (0.028)	0.446 ± 0.020 (0.020)	0.420 ± 0.022 (0.022)	0.357 ± 0.026 (0.026)
1.20 ... 1.15	0.509 ± 0.016 (0.016)	0.483 ± 0.020 (0.020)	0.417 ± 0.026 (0.026)	0.369 ± 0.021 (0.021)
1.15 ... 1.10	0.574 ± 0.012 (0.007)	0.509 ± 0.026 (0.026)	0.465 ± 0.016 (0.016)	0.391 ± 0.018 (0.018)
1.10 ... 1.05	0.559 ± 0.011 (0.009)	0.547 ± 0.043 (0.043)	0.471 ± 0.013 (0.013)	0.427 ± 0.015 (0.015)
1.05 ... 1.00	0.604 ± 0.022 (0.022)	0.562 ± 0.034 (0.034)	0.525 ± 0.014 (0.014)	0.449 ± 0.020 (0.020)
1.00 ... 0.95	0.639 ± 0.020 (0.020)	0.590 ± 0.033 (0.033)	0.519 ± 0.027 (0.027)	0.434 ± 0.010 (0.005)
0.95 ... 0.90	0.700 ± 0.027 (0.027)	0.612 ± 0.012 (0.011)	0.514 ± 0.022 (0.022)	0.437 ± 0.010 (0.003)
0.90 ... 0.85	0.691 ± 0.014 (0.014)	0.610 ± 0.032 (0.032)	0.517 ± 0.017 (0.017)	0.471 ± 0.011 (0.010)
0.85 ... 0.80	0.749 ± 0.024 (0.024)	0.628 ± 0.022 (0.022)	0.540 ± 0.025 (0.025)	0.460 ± 0.018 (0.018)
0.80 ... 0.75	0.753 ± 0.014 (0.014)	0.656 ± 0.015 (0.015)	0.563 ± 0.011 (0.008)	0.490 ± 0.011 (0.007)
0.75 ... 0.70	0.773 ± 0.017 (0.017)	0.664 ± 0.013 (0.013)	0.585 ± 0.012 (0.007)	0.528 ± 0.028 (0.028)
0.70 ... 0.65	0.795 ± 0.017 (0.017)	0.693 ± 0.035 (0.035)	0.588 ± 0.012 (0.008)	0.564 ± 0.012 (0.009)
0.65 ... 0.60	0.850 ± 0.021 (0.021)	0.721 ± 0.020 (0.020)	0.680 ± 0.012 (0.007)	0.613 ± 0.024 (0.024)
0.60 ... 0.55	0.916 ± 0.027 (0.027)	0.784 ± 0.020 (0.020)	0.735 ± 0.029 (0.029)	0.726 ± 0.050 (0.050)
0.55 ... 0.50	1.066 ± 0.026 (0.026)	0.936 ± 0.019 (0.019)	0.903 ± 0.017 (0.017)	0.786 ± 0.039 (0.039)
0.50 ... 0.45	1.212 ± 0.050 (0.050)	1.147 ± 0.017 (0.017)	1.104 ± 0.051 (0.051)	0.965 ± 0.016 (0.010)
0.45 ... 0.40	1.470 ± 0.027 (0.027)	1.392 ± 0.027 (0.027)	1.319 ± 0.047 (0.047)	1.270 ± 0.019 (0.016)
0.40 ... 0.35	1.858 ± 0.032 (0.032)	1.806 ± 0.024 (0.024)	1.681 ± 0.021 (0.016)	1.557 ± 0.020 (0.017)
0.35 ... 0.30	2.387 ± 0.043 (0.043)	2.234 ± 0.049 (0.049)	2.106 ± 0.044 (0.044)	1.883 ± 0.027 (0.027)
0.30 ... 0.25	3.021 ± 0.052 (0.052)	2.754 ± 0.047 (0.047)	2.595 ± 0.026 (0.006)	2.373 ± 0.036 (0.036)
0.25 ... 0.20	3.712 ± 0.090 (0.090)	3.417 ± 0.057 (0.057)	3.212 ± 0.087 (0.087)	2.949 ± 0.037 (0.037)
0.20 ... 0.15	4.338 ± 0.060 (0.060)	4.060 ± 0.057 (0.057)	3.853 ± 0.101 (0.101)	3.599 ± 0.109 (0.109)
0.15 ... 0.10	4.954 ± 0.080 (0.080)	4.640 ± 0.071 (0.071)	4.405 ± 0.099 (0.099)	3.994 ± 0.118 (0.118)
0.10 ... 0.05	4.726 ± 0.170 (0.170)	4.560 ± 0.148 (0.148)	4.172 ± 0.175 (0.175)	3.964 ± 0.193 (0.193)
0.05 ... 0.00	0.996 ± 0.095 (0.095)	1.049 ± 0.063 (0.063)	0.985 ± 0.094 (0.094)	0.945 ± 0.105 (0.105)

Table 9. Differential cross-section $d\sigma/dt_{\pi\pi}$ ($\mu\text{b}/\text{GeV}^2$) of the reaction $\gamma p \rightarrow p\pi^+\pi^-$.

$-t_{\pi\pi}$ (GeV 2)	$E_\gamma = 2.1\text{--}2.2$ GeV	$E_\gamma = 2.2\text{--}2.3$ GeV	$E_\gamma = 2.3\text{--}2.4$ GeV	$E_\gamma = 2.4\text{--}2.5$ GeV
3.70	3.65	0.000 ± 0.000 (0.000)	0.000 ± 0.000 (0.000)	0.000 ± 0.000 (0.000)
3.65	3.60	0.000 ± 0.000 (0.000)	0.000 ± 0.000 (0.000)	0.000 ± 0.000 (0.000)
3.60	3.55	0.000 ± 0.000 (0.000)	0.000 ± 0.000 (0.000)	0.000 ± 0.000 (0.000)
3.55	3.50	0.000 ± 0.000 (0.000)	0.000 ± 0.000 (0.000)	0.004 ± 0.003 (0.003)
3.50	3.45	0.000 ± 0.000 (0.000)	0.000 ± 0.000 (0.000)	0.002 ± 0.002 (0.001)
3.45	3.40	0.000 ± 0.000 (0.000)	0.000 ± 0.000 (0.000)	0.010 ± 0.005 (0.005)
3.40	3.35	0.000 ± 0.000 (0.000)	0.000 ± 0.000 (0.000)	0.004 ± 0.005 (0.005)
3.35	3.30	0.000 ± 0.000 (0.000)	0.001 ± 0.001 (0.001)	0.000 ± 0.007 (0.007)
3.30	3.25	0.000 ± 0.000 (0.000)	0.000 ± 0.002 (0.002)	0.004 ± 0.005 (0.005)
3.25	3.20	0.001 ± 0.001 (0.001)	0.002 ± 0.003 (0.003)	0.002 ± 0.012 (0.012)
3.20	3.15	0.003 ± 0.003 (0.002)	0.004 ± 0.004 (0.004)	0.020 ± 0.009 (0.009)
3.15	3.10	0.008 ± 0.005 (0.005)	0.003 ± 0.004 (0.004)	0.005 ± 0.021 (0.021)
3.10	3.05	0.001 ± 0.010 (0.010)	0.005 ± 0.012 (0.012)	0.021 ± 0.013 (0.013)
3.05	3.00	0.005 ± 0.002 (0.002)	0.017 ± 0.003 (0.003)	0.029 ± 0.007 (0.007)
3.00	2.95	0.005 ± 0.014 (0.014)	0.018 ± 0.012 (0.012)	0.023 ± 0.012 (0.012)
2.95	2.90	0.009 ± 0.041 (0.041)	0.018 ± 0.015 (0.015)	0.027 ± 0.015 (0.015)
2.90	2.85	0.015 ± 0.028 (0.028)	0.022 ± 0.010 (0.010)	0.017 ± 0.039 (0.039)
2.85	2.80	0.015 ± 0.017 (0.017)	0.022 ± 0.009 (0.009)	0.039 ± 0.018 (0.018)
2.80	2.75	0.023 ± 0.074 (0.074)	0.030 ± 0.016 (0.016)	0.041 ± 0.012 (0.012)
2.75	2.70	0.035 ± 0.020 (0.020)	0.030 ± 0.023 (0.023)	0.025 ± 0.030 (0.030)
2.70	2.65	0.032 ± 0.039 (0.039)	0.038 ± 0.012 (0.012)	0.043 ± 0.040 (0.040)
2.65	2.60	0.043 ± 0.028 (0.028)	0.041 ± 0.029 (0.029)	0.036 ± 0.028 (0.028)
2.60	2.55	0.048 ± 0.077 (0.077)	0.042 ± 0.025 (0.025)	0.028 ± 0.034 (0.034)
2.55	2.50	0.056 ± 0.041 (0.041)	0.046 ± 0.031 (0.031)	0.039 ± 0.046 (0.046)
2.50	2.45	0.050 ± 0.041 (0.041)	0.049 ± 0.024 (0.024)	0.046 ± 0.036 (0.036)
2.45	2.40	0.083 ± 0.045 (0.045)	0.057 ± 0.019 (0.019)	0.055 ± 0.026 (0.026)
2.40	2.35	0.043 ± 0.043 (0.043)	0.068 ± 0.022 (0.022)	0.064 ± 0.020 (0.020)
2.35	2.30	0.080 ± 0.027 (0.027)	0.059 ± 0.032 (0.032)	0.067 ± 0.017 (0.017)
2.30	2.25	0.080 ± 0.017 (0.017)	0.076 ± 0.017 (0.017)	0.077 ± 0.031 (0.031)
2.25	2.20	0.090 ± 0.025 (0.025)	0.083 ± 0.022 (0.022)	0.087 ± 0.016 (0.016)
2.20	2.15	0.093 ± 0.025 (0.025)	0.090 ± 0.033 (0.033)	0.079 ± 0.026 (0.026)
2.15	2.10	0.097 ± 0.031 (0.031)	0.096 ± 0.020 (0.020)	0.096 ± 0.025 (0.025)
2.10	2.05	0.122 ± 0.037 (0.037)	0.101 ± 0.019 (0.019)	0.103 ± 0.024 (0.024)
2.05	2.00	0.111 ± 0.035 (0.035)	0.124 ± 0.028 (0.028)	0.098 ± 0.026 (0.026)
2.00	1.95	0.143 ± 0.047 (0.047)	0.115 ± 0.037 (0.037)	0.104 ± 0.019 (0.019)
1.95	1.90	0.138 ± 0.031 (0.031)	0.119 ± 0.030 (0.030)	0.114 ± 0.018 (0.018)
1.90	1.85	0.169 ± 0.020 (0.020)	0.113 ± 0.043 (0.043)	0.122 ± 0.014 (0.014)
1.85	1.80	0.165 ± 0.055 (0.055)	0.146 ± 0.037 (0.037)	0.128 ± 0.032 (0.032)
1.80	1.75	0.163 ± 0.025 (0.025)	0.140 ± 0.039 (0.039)	0.137 ± 0.016 (0.016)
1.75	1.70	0.174 ± 0.031 (0.031)	0.164 ± 0.023 (0.023)	0.137 ± 0.020 (0.020)
1.70	1.65	0.179 ± 0.051 (0.051)	0.150 ± 0.029 (0.029)	0.148 ± 0.025 (0.025)
1.65	1.60	0.200 ± 0.032 (0.032)	0.175 ± 0.024 (0.024)	0.160 ± 0.021 (0.021)
1.60	1.55	0.208 ± 0.020 (0.020)	0.176 ± 0.016 (0.016)	0.170 ± 0.031 (0.031)
1.55	1.50	0.209 ± 0.027 (0.027)	0.177 ± 0.023 (0.023)	0.171 ± 0.028 (0.028)
1.50	1.45	0.225 ± 0.029 (0.029)	0.211 ± 0.013 (0.013)	0.177 ± 0.025 (0.025)
1.45	1.40	0.243 ± 0.028 (0.028)	0.217 ± 0.024 (0.024)	0.213 ± 0.038 (0.038)
1.40	1.35	0.273 ± 0.021 (0.021)	0.262 ± 0.024 (0.024)	0.187 ± 0.043 (0.043)
1.35	1.30	0.288 ± 0.015 (0.015)	0.274 ± 0.018 (0.018)	0.241 ± 0.027 (0.027)
1.30	1.25	0.313 ± 0.022 (0.022)	0.281 ± 0.030 (0.030)	0.248 ± 0.024 (0.024)
1.25	1.20	0.322 ± 0.037 (0.037)	0.304 ± 0.019 (0.019)	0.269 ± 0.024 (0.024)
1.20	1.15	0.369 ± 0.023 (0.023)	0.330 ± 0.025 (0.025)	0.265 ± 0.030 (0.030)
1.15	1.10	0.364 ± 0.020 (0.020)	0.333 ± 0.030 (0.030)	0.305 ± 0.031 (0.031)
1.10	1.05	0.398 ± 0.014 (0.014)	0.328 ± 0.029 (0.029)	0.307 ± 0.024 (0.024)
1.05	1.00	0.392 ± 0.030 (0.030)	0.363 ± 0.021 (0.021)	0.338 ± 0.036 (0.036)
1.00	0.95	0.405 ± 0.013 (0.013)	0.337 ± 0.014 (0.014)	0.320 ± 0.021 (0.021)
0.95	0.90	0.401 ± 0.030 (0.030)	0.341 ± 0.017 (0.017)	0.333 ± 0.010 (0.010)
0.90	0.85	0.408 ± 0.025 (0.025)	0.380 ± 0.010 (0.005)	0.346 ± 0.011 (0.011)
0.85	0.80	0.446 ± 0.018 (0.018)	0.390 ± 0.019 (0.019)	0.344 ± 0.010 (0.007)
0.80	0.75	0.465 ± 0.040 (0.040)	0.400 ± 0.015 (0.015)	0.344 ± 0.016 (0.016)
0.75	0.70	0.458 ± 0.011 (0.004)	0.436 ± 0.029 (0.029)	0.390 ± 0.011 (0.011)
0.70	0.65	0.489 ± 0.021 (0.021)	0.442 ± 0.031 (0.031)	0.420 ± 0.023 (0.023)
0.65	0.60	0.565 ± 0.019 (0.019)	0.527 ± 0.013 (0.013)	0.511 ± 0.012 (0.011)
0.60	0.55	0.659 ± 0.033 (0.033)	0.607 ± 0.024 (0.024)	0.576 ± 0.017 (0.017)
0.55	0.50	0.778 ± 0.026 (0.026)	0.745 ± 0.017 (0.017)	0.706 ± 0.056 (0.056)
0.50	0.45	0.924 ± 0.074 (0.074)	0.908 ± 0.017 (0.006)	0.860 ± 0.038 (0.038)
0.45	0.40	1.132 ± 0.057 (0.057)	1.069 ± 0.026 (0.026)	1.020 ± 0.033 (0.033)
0.40	0.35	1.367 ± 0.080 (0.080)	1.309 ± 0.059 (0.059)	1.235 ± 0.036 (0.036)
0.35	0.30	1.737 ± 0.078 (0.078)	1.577 ± 0.054 (0.054)	1.536 ± 0.043 (0.043)
0.30	0.25	2.222 ± 0.094 (0.094)	2.027 ± 0.047 (0.047)	1.916 ± 0.079 (0.079)
0.25	0.20	2.769 ± 0.129 (0.129)	2.524 ± 0.125 (0.125)	2.341 ± 0.051 (0.051)
0.20	0.15	3.294 ± 0.118 (0.118)	3.072 ± 0.149 (0.149)	2.859 ± 0.104 (0.104)
0.15	0.10	3.635 ± 0.184 (0.184)	3.412 ± 0.108 (0.108)	3.223 ± 0.092 (0.092)
0.10	0.05	3.652 ± 0.177 (0.177)	3.467 ± 0.152 (0.152)	3.285 ± 0.144 (0.144)
0.05	0.00	0.909 ± 0.088 (0.088)	0.862 ± 0.095 (0.095)	0.804 ± 0.047 (0.047)
				0.817 ± 0.109 (0.109)

Table 10. Differential cross-section $d\sigma/dt_{\pi\pi}$ ($\mu\text{b}/\text{GeV}^2$) of the reaction $\gamma p \rightarrow p\pi^+\pi^-$.

$-t_{\pi\pi}$ (GeV 2)	$E_\gamma = 2.5\text{--}2.6$ GeV
3.90	... 3.85 0.001 \pm 0.001 (0.001)
3.85	... 3.80 0.002 \pm 0.002 (0.001)
3.80	... 3.75 0.001 \pm 0.001 (0.001)
3.75	... 3.70 0.004 \pm 0.003 (0.003)
3.70	... 3.65 0.011 \pm 0.007 (0.007)
3.65	... 3.60 0.001 \pm 0.014 (0.014)
3.60	... 3.55 0.007 \pm 0.003 (0.000)
3.55	... 3.50 0.003 \pm 0.005 (0.005)
3.50	... 3.45 0.006 \pm 0.016 (0.016)
3.45	... 3.40 0.007 \pm 0.017 (0.017)
3.40	... 3.35 0.005 \pm 0.021 (0.021)
3.35	... 3.30 0.005 \pm 0.036 (0.036)
3.30	... 3.25 0.015 \pm 0.028 (0.028)
3.25	... 3.20 0.011 \pm 0.037 (0.037)
3.20	... 3.15 0.014 \pm 0.027 (0.027)
3.15	... 3.10 0.012 \pm 0.023 (0.023)
3.10	... 3.05 0.020 \pm 0.048 (0.048)
3.05	... 3.00 0.016 \pm 0.061 (0.061)
3.00	... 2.95 0.010 \pm 0.053 (0.053)
2.95	... 2.90 0.018 \pm 0.047 (0.047)
2.90	... 2.85 0.011 \pm 0.065 (0.065)
2.85	... 2.80 0.019 \pm 0.075 (0.075)
2.80	... 2.75 0.028 \pm 0.050 (0.050)
2.75	... 2.70 0.017 \pm 0.053 (0.053)
2.70	... 2.65 0.033 \pm 0.057 (0.057)
2.65	... 2.60 0.027 \pm 0.027 (0.027)
2.60	... 2.55 0.029 \pm 0.049 (0.049)
2.55	... 2.50 0.042 \pm 0.011 (0.011)
2.50	... 2.45 0.048 \pm 0.042 (0.042)
2.45	... 2.40 0.060 \pm 0.030 (0.030)
2.40	... 2.35 0.024 \pm 0.060 (0.060)
2.35	... 2.30 0.066 \pm 0.032 (0.032)
2.30	... 2.25 0.071 \pm 0.038 (0.038)
2.25	... 2.20 0.064 \pm 0.038 (0.038)
2.20	... 2.15 0.066 \pm 0.026 (0.026)
2.15	... 2.10 0.052 \pm 0.056 (0.056)
2.10	... 2.05 0.051 \pm 0.041 (0.041)
2.05	... 2.00 0.072 \pm 0.041 (0.041)
2.00	... 1.95 0.055 \pm 0.055 (0.055)
1.95	... 1.90 0.063 \pm 0.056 (0.056)
1.90	... 1.85 0.070 \pm 0.061 (0.061)
1.85	... 1.80 0.084 \pm 0.030 (0.030)
1.80	... 1.75 0.073 \pm 0.051 (0.051)
1.75	... 1.70 0.095 \pm 0.060 (0.060)
1.70	... 1.65 0.115 \pm 0.027 (0.027)
1.65	... 1.60 0.122 \pm 0.041 (0.041)
1.60	... 1.55 0.100 \pm 0.062 (0.062)
1.55	... 1.50 0.137 \pm 0.053 (0.053)
1.50	... 1.45 0.152 \pm 0.072 (0.072)
1.45	... 1.40 0.167 \pm 0.033 (0.033)
1.40	... 1.35 0.154 \pm 0.087 (0.087)
1.35	... 1.30 0.198 \pm 0.047 (0.047)
1.30	... 1.25 0.222 \pm 0.041 (0.041)
1.25	... 1.20 0.230 \pm 0.047 (0.047)
1.20	... 1.15 0.250 \pm 0.029 (0.029)
1.15	... 1.10 0.242 \pm 0.011 (0.002)
1.10	... 1.05 0.256 \pm 0.034 (0.034)
1.05	... 1.00 0.289 \pm 0.021 (0.021)
1.00	... 0.95 0.304 \pm 0.012 (0.006)
0.95	... 0.90 0.299 \pm 0.044 (0.044)
0.90	... 0.85 0.285 \pm 0.012 (0.004)
0.85	... 0.80 0.274 \pm 0.011 (0.004)
0.80	... 0.75 0.307 \pm 0.012 (0.005)
0.75	... 0.70 0.375 \pm 0.023 (0.023)
0.70	... 0.65 0.401 \pm 0.015 (0.001)
0.65	... 0.60 0.430 \pm 0.054 (0.054)
0.60	... 0.55 0.555 \pm 0.018 (0.004)
0.55	... 0.50 0.649 \pm 0.039 (0.039)
0.50	... 0.45 0.756 \pm 0.048 (0.048)
0.45	... 0.40 0.893 \pm 0.041 (0.041)
0.40	... 0.35 1.088 \pm 0.026 (0.022)
0.35	... 0.30 1.404 \pm 0.029 (0.014)
0.30	... 0.25 1.729 \pm 0.033 (0.031)
0.25	... 0.20 2.272 \pm 0.041 (0.041)
0.20	... 0.15 2.772 \pm 0.044 (0.044)
0.15	... 0.10 3.136 \pm 0.132 (0.132)
0.10	... 0.05 3.068 \pm 0.278 (0.278)
0.05	... 0.00 0.776 \pm 0.116 (0.116)

Table 11. Differential cross-section $d\sigma/dt_{p\pi}$ ($\mu\text{b}/\text{GeV}^2$) of the reaction $\gamma p \rightarrow p\pi^+\pi^-$.

$-t_{p\pi}$ (GeV^2)	$E_\gamma = 0.5\text{--}0.6 \text{ GeV}$	$E_\gamma = 0.6\text{--}0.7 \text{ GeV}$	$E_\gamma = 0.7\text{--}0.8 \text{ GeV}$	$E_\gamma = 0.8\text{--}0.9 \text{ GeV}$	
1.00 ... 0.95	0.000 ± 0.000 (0.000)	0.000 ± 0.000 (0.000)			
0.95 ... 0.90	0.000 ± 0.000 (0.000)	0.000 ± 0.000 (0.000)			
0.90 ... 0.85	0.000 ± 0.000 (0.000)	0.000 ± 0.000 (0.000)			
0.85 ... 0.80	0.000 ± 0.000 (0.000)	0.010 ± 0.004 (0.004)			
0.80 ... 0.75	0.000 ± 0.000 (0.000)	0.079 ± 0.013 (0.013)			
0.75 ... 0.70	0.000 ± 0.000 (0.000)	0.310 ± 0.025 (0.025)			
0.70 ... 0.65	0.000 ± 0.000 (0.000)	0.000 ± 0.000 (0.000)	0.000 ± 0.000 (0.000)	0.014 ± 0.005 (0.005)	0.726 ± 0.036 (0.036)
0.65 ... 0.60	0.000 ± 0.000 (0.000)	0.000 ± 0.000 (0.000)	0.000 ± 0.000 (0.000)	0.097 ± 0.012 (0.012)	1.487 ± 0.048 (0.048)
0.60 ... 0.55	0.000 ± 0.000 (0.000)	0.002 ± 0.002 (0.002)	0.463 ± 0.026 (0.026)	2.151 ± 0.057 (0.057)	
0.55 ... 0.50	0.000 ± 0.000 (0.000)	0.020 ± 0.005 (0.005)	1.476 ± 0.046 (0.046)	2.904 ± 0.065 (0.065)	
0.50 ... 0.45	0.000 ± 0.000 (0.000)	0.279 ± 0.018 (0.018)	2.823 ± 0.062 (0.062)	3.184 ± 0.069 (0.069)	
0.45 ... 0.40	0.002 ± 0.002 (0.002)	1.052 ± 0.036 (0.036)	3.972 ± 0.073 (0.073)	3.864 ± 0.083 (0.083)	
0.40 ... 0.35	0.152 ± 0.015 (0.015)	2.529 ± 0.056 (0.056)	4.788 ± 0.086 (0.086)	4.770 ± 0.100 (0.100)	
0.35 ... 0.30	0.739 ± 0.033 (0.033)	4.181 ± 0.078 (0.078)	5.058 ± 0.096 (0.096)	5.440 ± 0.104 (0.104)	
0.30 ... 0.25	1.836 ± 0.057 (0.057)	5.780 ± 0.104 (0.104)	6.295 ± 0.112 (0.112)	6.202 ± 0.108 (0.108)	
0.25 ... 0.20	3.613 ± 0.119 (0.096)	7.992 ± 0.131 (0.131)	7.889 ± 0.121 (0.121)	7.675 ± 0.116 (0.116)	
0.20 ... 0.15	7.028 ± 0.207 (0.150)	10.748 ± 0.140 (0.140)	9.220 ± 0.119 (0.119)	8.758 ± 0.119 (0.119)	
0.15 ... 0.10	10.988 ± 0.178 (0.157)	14.619 ± 0.145 (0.145)	11.550 ± 0.127 (0.127)	10.054 ± 0.126 (0.126)	
0.10 ... 0.05	17.940 ± 0.171 (0.171)	18.808 ± 0.157 (0.157)	13.736 ± 0.142 (0.142)	11.122 ± 0.134 (0.134)	
0.05 ... 0.00	6.080 ± 0.098 (0.098)	9.441 ± 0.116 (0.116)	8.054 ± 0.111 (0.111)	5.760 ± 0.099 (0.099)	
$-t_{p\pi}$ (GeV^2)	$E_\gamma = 0.9\text{--}1.0 \text{ GeV}$	$E_\gamma = 1.0\text{--}1.1 \text{ GeV}$	$E_\gamma = 1.1\text{--}1.2 \text{ GeV}$	$E_\gamma = 1.2\text{--}1.3 \text{ GeV}$	
1.55 ... 1.50	0.000 ± 0.000 (0.000)				
1.50 ... 1.45	0.000 ± 0.000 (0.000)	0.000 ± 0.000 (0.000)	0.000 ± 0.000 (0.000)	0.003 ± 0.001 (0.001)	
1.45 ... 1.40	0.000 ± 0.000 (0.000)	0.000 ± 0.000 (0.000)	0.000 ± 0.000 (0.000)	0.012 ± 0.002 (0.001)	
1.40 ... 1.35	0.000 ± 0.000 (0.000)	0.000 ± 0.000 (0.000)	0.000 ± 0.000 (0.000)	0.040 ± 0.003 (0.002)	
1.35 ... 1.30	0.000 ± 0.000 (0.000)	0.000 ± 0.000 (0.000)	0.002 ± 0.001 (0.000)	0.092 ± 0.007 (0.007)	
1.30 ... 1.25	0.000 ± 0.000 (0.000)	0.000 ± 0.000 (0.000)	0.014 ± 0.002 (0.002)	0.154 ± 0.009 (0.009)	
1.25 ... 1.20	0.000 ± 0.000 (0.000)	0.000 ± 0.000 (0.000)	0.045 ± 0.004 (0.004)	0.241 ± 0.006 (0.003)	
1.20 ... 1.15	0.000 ± 0.000 (0.000)	0.002 ± 0.001 (0.000)	0.108 ± 0.007 (0.007)	0.342 ± 0.008 (0.008)	
1.15 ... 1.10	0.000 ± 0.000 (0.000)	0.019 ± 0.002 (0.002)	0.231 ± 0.007 (0.007)	0.423 ± 0.017 (0.017)	
1.10 ... 1.05	0.000 ± 0.000 (0.000)	0.074 ± 0.004 (0.001)	0.405 ± 0.008 (0.008)	0.502 ± 0.012 (0.012)	
1.05 ... 1.00	0.001 ± 0.001 (0.001)	0.198 ± 0.016 (0.016)	0.574 ± 0.012 (0.012)	0.578 ± 0.016 (0.016)	
1.00 ... 0.95	0.015 ± 0.007 (0.007)	0.415 ± 0.025 (0.025)	0.728 ± 0.015 (0.015)	0.676 ± 0.021 (0.021)	
0.95 ... 0.90	0.062 ± 0.012 (0.012)	0.708 ± 0.032 (0.032)	0.876 ± 0.014 (0.014)	0.803 ± 0.043 (0.043)	
0.90 ... 0.85	0.172 ± 0.019 (0.019)	1.008 ± 0.048 (0.048)	1.009 ± 0.017 (0.017)	0.940 ± 0.059 (0.059)	
0.85 ... 0.80	0.431 ± 0.028 (0.028)	1.249 ± 0.059 (0.059)	1.223 ± 0.017 (0.017)	1.092 ± 0.050 (0.050)	
0.80 ... 0.75	0.818 ± 0.037 (0.037)	1.460 ± 0.043 (0.043)	1.442 ± 0.015 (0.015)	1.229 ± 0.036 (0.036)	
0.75 ... 0.70	1.332 ± 0.048 (0.048)	1.694 ± 0.066 (0.066)	1.712 ± 0.017 (0.015)	1.420 ± 0.046 (0.046)	
0.70 ... 0.65	1.570 ± 0.050 (0.050)	2.032 ± 0.064 (0.064)	1.929 ± 0.027 (0.027)	1.611 ± 0.052 (0.052)	
0.65 ... 0.60	1.994 ± 0.056 (0.056)	2.376 ± 0.052 (0.052)	2.160 ± 0.057 (0.057)	1.878 ± 0.040 (0.040)	
0.60 ... 0.55	2.545 ± 0.067 (0.067)	2.723 ± 0.096 (0.096)	2.391 ± 0.036 (0.036)	2.146 ± 0.107 (0.107)	
0.55 ... 0.50	2.950 ± 0.074 (0.074)	3.009 ± 0.146 (0.146)	2.794 ± 0.068 (0.068)	2.503 ± 0.098 (0.098)	
0.50 ... 0.45	3.353 ± 0.081 (0.081)	3.501 ± 0.163 (0.163)	3.198 ± 0.112 (0.112)	2.776 ± 0.122 (0.122)	
0.45 ... 0.40	4.108 ± 0.094 (0.094)	4.029 ± 0.244 (0.244)	3.490 ± 0.152 (0.152)	3.018 ± 0.188 (0.188)	
0.40 ... 0.35	4.838 ± 0.102 (0.102)	4.589 ± 0.244 (0.244)	3.804 ± 0.154 (0.154)	3.341 ± 0.191 (0.191)	
0.35 ... 0.30	5.743 ± 0.109 (0.109)	5.056 ± 0.267 (0.267)	4.179 ± 0.158 (0.158)	3.636 ± 0.182 (0.182)	
0.30 ... 0.25	6.262 ± 0.110 (0.110)	5.518 ± 0.289 (0.289)	4.480 ± 0.184 (0.184)	3.993 ± 0.161 (0.161)	
0.25 ... 0.20	7.013 ± 0.111 (0.111)	6.151 ± 0.222 (0.222)	5.003 ± 0.169 (0.169)	4.678 ± 0.182 (0.182)	
0.20 ... 0.15	8.150 ± 0.117 (0.117)	7.013 ± 0.209 (0.209)	5.438 ± 0.177 (0.177)	5.019 ± 0.209 (0.209)	
0.15 ... 0.10	9.381 ± 0.128 (0.128)	7.789 ± 0.163 (0.163)	5.564 ± 0.097 (0.097)	5.020 ± 0.166 (0.166)	
0.10 ... 0.05	9.837 ± 0.134 (0.134)	7.658 ± 0.178 (0.178)	5.541 ± 0.089 (0.089)	5.122 ± 0.197 (0.197)	
0.05 ... 0.00	4.684 ± 0.094 (0.094)	3.953 ± 0.130 (0.130)	3.010 ± 0.103 (0.103)	2.829 ± 0.108 (0.108)	

Table 12. Differential cross-section $d\sigma/dt_{p\pi}$ ($\mu\text{b}/\text{GeV}^2$) of the reaction $\gamma p \rightarrow p\pi^+\pi^-$.

$-t_{p\pi}$ (GeV^2)	$E_\gamma = 1.3\text{--}1.4$ GeV	$E_\gamma = 1.4\text{--}1.5$ GeV	$E_\gamma = 1.5\text{--}1.6$ GeV	$E_\gamma = 1.6\text{--}1.7$ GeV
2.30 ... 2.25	0.000 ± 0.000 (0.000)			
2.25 ... 2.20	0.000 ± 0.000 (0.000)			
2.20 ... 2.15	0.000 ± 0.000 (0.000)	0.000 ± 0.000 (0.000)	0.000 ± 0.000 (0.000)	0.001 ± 0.001 (0.000)
2.15 ... 2.10	0.000 ± 0.000 (0.000)	0.000 ± 0.000 (0.000)	0.000 ± 0.000 (0.000)	0.001 ± 0.001 (0.000)
2.10 ... 2.05	0.000 ± 0.000 (0.000)	0.000 ± 0.000 (0.000)	0.000 ± 0.000 (0.000)	0.012 ± 0.002 (0.001)
2.05 ... 2.00	0.000 ± 0.000 (0.000)	0.000 ± 0.000 (0.000)	0.001 ± 0.001 (0.000)	0.024 ± 0.003 (0.001)
2.00 ... 1.95	0.000 ± 0.000 (0.000)	0.000 ± 0.000 (0.000)	0.002 ± 0.001 (0.001)	0.047 ± 0.004 (0.004)
1.95 ... 1.90	0.000 ± 0.000 (0.000)	0.000 ± 0.000 (0.000)	0.012 ± 0.002 (0.001)	0.075 ± 0.004 (0.004)
1.90 ... 1.85	0.000 ± 0.000 (0.000)	0.000 ± 0.000 (0.000)	0.028 ± 0.005 (0.005)	0.088 ± 0.005 (0.004)
1.85 ... 1.80	0.000 ± 0.000 (0.000)	0.001 ± 0.001 (0.001)	0.055 ± 0.007 (0.007)	0.106 ± 0.006 (0.006)
1.80 ... 1.75	0.000 ± 0.000 (0.000)	0.004 ± 0.004 (0.004)	0.083 ± 0.005 (0.005)	0.120 ± 0.005 (0.004)
1.75 ... 1.70	0.000 ± 0.000 (0.000)	0.020 ± 0.002 (0.001)	0.107 ± 0.012 (0.012)	0.147 ± 0.006 (0.005)
1.70 ... 1.65	0.001 ± 0.001 (0.000)	0.053 ± 0.003 (0.001)	0.133 ± 0.013 (0.013)	0.147 ± 0.010 (0.010)
1.65 ... 1.60	0.004 ± 0.001 (0.001)	0.074 ± 0.014 (0.014)	0.147 ± 0.006 (0.003)	0.165 ± 0.010 (0.010)
1.60 ... 1.55	0.019 ± 0.002 (0.001)	0.115 ± 0.005 (0.005)	0.161 ± 0.008 (0.008)	0.207 ± 0.008 (0.008)
1.55 ... 1.50	0.045 ± 0.004 (0.004)	0.148 ± 0.007 (0.007)	0.197 ± 0.008 (0.008)	0.257 ± 0.008 (0.004)
1.50 ... 1.45	0.088 ± 0.008 (0.008)	0.174 ± 0.009 (0.009)	0.227 ± 0.007 (0.007)	0.278 ± 0.019 (0.019)
1.45 ... 1.40	0.133 ± 0.011 (0.011)	0.219 ± 0.017 (0.017)	0.272 ± 0.019 (0.019)	0.308 ± 0.017 (0.017)
1.40 ... 1.35	0.179 ± 0.006 (0.006)	0.246 ± 0.017 (0.017)	0.330 ± 0.009 (0.009)	0.330 ± 0.017 (0.017)
1.35 ... 1.30	0.245 ± 0.012 (0.012)	0.291 ± 0.018 (0.018)	0.374 ± 0.020 (0.020)	0.391 ± 0.018 (0.018)
1.30 ... 1.25	0.289 ± 0.007 (0.003)	0.368 ± 0.010 (0.010)	0.429 ± 0.026 (0.026)	0.429 ± 0.018 (0.018)
1.25 ... 1.20	0.351 ± 0.008 (0.008)	0.435 ± 0.010 (0.009)	0.485 ± 0.022 (0.022)	0.431 ± 0.010 (0.007)
1.20 ... 1.15	0.422 ± 0.024 (0.024)	0.517 ± 0.013 (0.013)	0.514 ± 0.018 (0.018)	0.459 ± 0.027 (0.027)
1.15 ... 1.10	0.492 ± 0.016 (0.016)	0.571 ± 0.016 (0.016)	0.562 ± 0.038 (0.038)	0.541 ± 0.011 (0.009)
1.10 ... 1.05	0.570 ± 0.028 (0.028)	0.656 ± 0.012 (0.003)	0.591 ± 0.026 (0.026)	0.621 ± 0.014 (0.014)
1.05 ... 1.00	0.654 ± 0.011 (0.009)	0.693 ± 0.012 (0.011)	0.663 ± 0.012 (0.006)	0.627 ± 0.020 (0.020)
1.00 ... 0.95	0.733 ± 0.023 (0.023)	0.793 ± 0.022 (0.022)	0.750 ± 0.013 (0.011)	0.705 ± 0.013 (0.004)
0.95 ... 0.90	0.819 ± 0.018 (0.018)	0.871 ± 0.020 (0.020)	0.836 ± 0.013 (0.009)	0.773 ± 0.015 (0.015)
0.90 ... 0.85	0.936 ± 0.013 (0.010)	0.952 ± 0.022 (0.022)	0.919 ± 0.014 (0.009)	0.844 ± 0.025 (0.025)
0.85 ... 0.80	1.073 ± 0.014 (0.007)	1.081 ± 0.018 (0.018)	0.990 ± 0.014 (0.003)	0.927 ± 0.061 (0.061)
0.80 ... 0.75	1.207 ± 0.052 (0.052)	1.175 ± 0.038 (0.038)	1.121 ± 0.015 (0.011)	1.055 ± 0.016 (0.013)
0.75 ... 0.70	1.337 ± 0.037 (0.037)	1.347 ± 0.025 (0.025)	1.257 ± 0.029 (0.029)	1.168 ± 0.016 (0.016)
0.70 ... 0.65	1.517 ± 0.037 (0.037)	1.522 ± 0.035 (0.035)	1.421 ± 0.021 (0.021)	1.287 ± 0.017 (0.008)
0.65 ... 0.60	1.773 ± 0.059 (0.059)	1.741 ± 0.053 (0.053)	1.614 ± 0.039 (0.039)	1.455 ± 0.026 (0.026)
0.60 ... 0.55	2.008 ± 0.056 (0.056)	1.926 ± 0.059 (0.059)	1.809 ± 0.037 (0.037)	1.633 ± 0.041 (0.041)
0.55 ... 0.50	2.306 ± 0.056 (0.056)	2.142 ± 0.038 (0.038)	1.978 ± 0.021 (0.021)	1.780 ± 0.045 (0.045)
0.50 ... 0.45	2.484 ± 0.091 (0.091)	2.361 ± 0.032 (0.032)	2.186 ± 0.037 (0.037)	1.962 ± 0.032 (0.032)
0.45 ... 0.40	2.827 ± 0.089 (0.089)	2.612 ± 0.024 (0.024)	2.388 ± 0.052 (0.052)	2.204 ± 0.064 (0.064)
0.40 ... 0.35	3.104 ± 0.126 (0.126)	2.820 ± 0.091 (0.091)	2.642 ± 0.022 (0.019)	2.507 ± 0.082 (0.082)
0.35 ... 0.30	3.338 ± 0.088 (0.088)	3.211 ± 0.066 (0.066)	3.037 ± 0.065 (0.065)	2.908 ± 0.074 (0.074)
0.30 ... 0.25	3.753 ± 0.096 (0.096)	3.584 ± 0.134 (0.134)	3.398 ± 0.058 (0.058)	3.164 ± 0.058 (0.058)
0.25 ... 0.20	4.236 ± 0.125 (0.125)	3.885 ± 0.102 (0.102)	3.567 ± 0.089 (0.089)	3.316 ± 0.052 (0.052)
0.20 ... 0.15	4.334 ± 0.137 (0.137)	3.929 ± 0.137 (0.137)	3.663 ± 0.101 (0.101)	3.358 ± 0.055 (0.055)
0.15 ... 0.10	4.410 ± 0.107 (0.107)	4.137 ± 0.129 (0.129)	3.809 ± 0.070 (0.070)	3.614 ± 0.038 (0.038)
0.10 ... 0.05	4.587 ± 0.161 (0.161)	4.337 ± 0.123 (0.123)	4.026 ± 0.052 (0.052)	3.745 ± 0.030 (0.028)
0.05 ... 0.00	2.611 ± 0.099 (0.099)	2.602 ± 0.116 (0.116)	2.422 ± 0.075 (0.075)	2.200 ± 0.047 (0.047)

Table 13. Differential cross-section $d\sigma/dt_{p\pi}$ ($\mu\text{b}/\text{GeV}^2$) of the reaction $\gamma p \rightarrow p\pi^+\pi^-$.

$-t_{p\pi}$ (GeV^2)	$E_\gamma = 1.7\text{--}1.8$ GeV	$E_\gamma = 1.8\text{--}1.9$ GeV	$E_\gamma = 1.9\text{--}2.0$ GeV	$E_\gamma = 2.0\text{--}2.1$ GeV
3.00 ... 2.95	0.000 ± 0.000 (0.000)			
2.95 ... 2.90	0.000 ± 0.000 (0.000)			
2.90 ... 2.85	0.000 ± 0.000 (0.000)	0.000 ± 0.000 (0.000)	0.000 ± 0.000 (0.000)	0.001 ± 0.001 (0.000)
2.85 ... 2.80	0.000 ± 0.000 (0.000)	0.000 ± 0.000 (0.000)	0.000 ± 0.000 (0.000)	0.001 ± 0.001 (0.000)
2.80 ... 2.75	0.000 ± 0.000 (0.000)	0.000 ± 0.000 (0.000)	0.000 ± 0.000 (0.000)	0.004 ± 0.001 (0.001)
2.75 ... 2.70	0.000 ± 0.000 (0.000)	0.000 ± 0.000 (0.000)	0.000 ± 0.000 (0.000)	0.006 ± 0.002 (0.001)
2.70 ... 2.65	0.000 ± 0.000 (0.000)	0.000 ± 0.000 (0.000)	0.001 ± 0.001 (0.001)	0.014 ± 0.003 (0.003)
2.65 ... 2.60	0.000 ± 0.000 (0.000)	0.000 ± 0.000 (0.000)	0.001 ± 0.001 (0.000)	0.022 ± 0.003 (0.003)
2.60 ... 2.55	0.000 ± 0.000 (0.000)	0.000 ± 0.000 (0.000)	0.008 ± 0.005 (0.005)	0.032 ± 0.003 (0.003)
2.55 ... 2.50	0.000 ± 0.000 (0.000)	0.000 ± 0.000 (0.000)	0.012 ± 0.005 (0.005)	0.035 ± 0.013 (0.013)
2.50 ... 2.45	0.000 ± 0.000 (0.000)	0.002 ± 0.001 (0.001)	0.028 ± 0.005 (0.005)	0.041 ± 0.005 (0.005)
2.45 ... 2.40	0.000 ± 0.000 (0.000)	0.006 ± 0.001 (0.001)	0.039 ± 0.004 (0.002)	0.058 ± 0.007 (0.007)
2.40 ... 2.35	0.000 ± 0.000 (0.000)	0.016 ± 0.003 (0.003)	0.050 ± 0.004 (0.004)	0.049 ± 0.013 (0.013)
2.35 ... 2.30	0.002 ± 0.001 (0.001)	0.029 ± 0.006 (0.006)	0.055 ± 0.008 (0.008)	0.051 ± 0.005 (0.005)
2.30 ... 2.25	0.005 ± 0.001 (0.001)	0.046 ± 0.009 (0.009)	0.061 ± 0.004 (0.004)	0.074 ± 0.012 (0.012)
2.25 ... 2.20	0.009 ± 0.002 (0.002)	0.056 ± 0.008 (0.008)	0.075 ± 0.009 (0.009)	0.087 ± 0.011 (0.011)
2.20 ... 2.15	0.027 ± 0.004 (0.004)	0.060 ± 0.005 (0.005)	0.083 ± 0.008 (0.008)	0.087 ± 0.007 (0.007)
2.15 ... 2.10	0.041 ± 0.004 (0.004)	0.094 ± 0.005 (0.003)	0.083 ± 0.007 (0.007)	0.097 ± 0.016 (0.016)
2.10 ... 2.05	0.058 ± 0.005 (0.005)	0.101 ± 0.005 (0.003)	0.104 ± 0.005 (0.004)	0.109 ± 0.019 (0.019)
2.05 ... 2.00	0.084 ± 0.005 (0.001)	0.111 ± 0.008 (0.008)	0.108 ± 0.010 (0.010)	0.110 ± 0.026 (0.026)
2.00 ... 1.95	0.094 ± 0.008 (0.008)	0.109 ± 0.006 (0.001)	0.134 ± 0.006 (0.005)	0.125 ± 0.013 (0.013)
1.95 ... 1.90	0.101 ± 0.008 (0.008)	0.128 ± 0.006 (0.003)	0.135 ± 0.015 (0.015)	0.136 ± 0.015 (0.015)
1.90 ... 1.85	0.120 ± 0.010 (0.010)	0.130 ± 0.006 (0.006)	0.131 ± 0.006 (0.003)	0.147 ± 0.022 (0.022)
1.85 ... 1.80	0.144 ± 0.014 (0.014)	0.130 ± 0.006 (0.005)	0.153 ± 0.018 (0.018)	0.148 ± 0.016 (0.016)
1.80 ... 1.75	0.135 ± 0.007 (0.007)	0.183 ± 0.018 (0.018)	0.176 ± 0.011 (0.011)	0.167 ± 0.011 (0.011)
1.75 ... 1.70	0.174 ± 0.012 (0.012)	0.188 ± 0.009 (0.009)	0.191 ± 0.009 (0.009)	0.176 ± 0.009 (0.009)
1.70 ... 1.65	0.192 ± 0.012 (0.012)	0.201 ± 0.007 (0.007)	0.203 ± 0.015 (0.015)	0.187 ± 0.018 (0.018)
1.65 ... 1.60	0.205 ± 0.028 (0.028)	0.207 ± 0.014 (0.014)	0.210 ± 0.008 (0.008)	0.206 ± 0.015 (0.015)
1.60 ... 1.55	0.230 ± 0.019 (0.019)	0.243 ± 0.017 (0.017)	0.224 ± 0.017 (0.017)	0.211 ± 0.023 (0.023)
1.55 ... 1.50	0.245 ± 0.008 (0.003)	0.248 ± 0.009 (0.009)	0.254 ± 0.024 (0.024)	0.212 ± 0.020 (0.020)
1.50 ... 1.45	0.296 ± 0.013 (0.013)	0.275 ± 0.016 (0.016)	0.247 ± 0.024 (0.024)	0.251 ± 0.012 (0.012)
1.45 ... 1.40	0.300 ± 0.014 (0.014)	0.303 ± 0.013 (0.013)	0.276 ± 0.011 (0.011)	0.253 ± 0.030 (0.030)
1.40 ... 1.35	0.324 ± 0.021 (0.021)	0.336 ± 0.025 (0.025)	0.281 ± 0.011 (0.011)	0.249 ± 0.022 (0.022)
1.35 ... 1.30	0.348 ± 0.035 (0.035)	0.320 ± 0.010 (0.010)	0.301 ± 0.021 (0.021)	0.271 ± 0.028 (0.028)
1.30 ... 1.25	0.370 ± 0.022 (0.022)	0.347 ± 0.022 (0.022)	0.341 ± 0.018 (0.018)	0.298 ± 0.016 (0.016)
1.25 ... 1.20	0.399 ± 0.010 (0.006)	0.369 ± 0.026 (0.026)	0.360 ± 0.031 (0.031)	0.298 ± 0.028 (0.028)
1.20 ... 1.15	0.439 ± 0.010 (0.008)	0.408 ± 0.027 (0.027)	0.379 ± 0.030 (0.030)	0.337 ± 0.025 (0.025)
1.15 ... 1.10	0.431 ± 0.012 (0.012)	0.442 ± 0.028 (0.028)	0.384 ± 0.026 (0.026)	0.354 ± 0.018 (0.018)
1.10 ... 1.05	0.481 ± 0.016 (0.016)	0.470 ± 0.039 (0.039)	0.412 ± 0.019 (0.019)	0.392 ± 0.011 (0.011)
1.05 ... 1.00	0.552 ± 0.015 (0.015)	0.497 ± 0.025 (0.025)	0.475 ± 0.016 (0.016)	0.405 ± 0.014 (0.014)
1.00 ... 0.95	0.593 ± 0.012 (0.002)	0.524 ± 0.021 (0.021)	0.519 ± 0.012 (0.006)	0.462 ± 0.011 (0.011)
0.95 ... 0.90	0.653 ± 0.026 (0.026)	0.607 ± 0.012 (0.009)	0.541 ± 0.038 (0.038)	0.459 ± 0.023 (0.023)
0.90 ... 0.85	0.722 ± 0.013 (0.006)	0.682 ± 0.020 (0.020)	0.613 ± 0.027 (0.027)	0.519 ± 0.019 (0.019)
0.85 ... 0.80	0.840 ± 0.014 (0.007)	0.726 ± 0.021 (0.021)	0.686 ± 0.013 (0.011)	0.592 ± 0.027 (0.027)
0.80 ... 0.75	0.924 ± 0.015 (0.003)	0.869 ± 0.015 (0.015)	0.760 ± 0.023 (0.023)	0.662 ± 0.018 (0.018)
0.75 ... 0.70	1.058 ± 0.016 (0.010)	0.960 ± 0.015 (0.007)	0.862 ± 0.014 (0.009)	0.753 ± 0.028 (0.028)
0.70 ... 0.65	1.206 ± 0.034 (0.034)	1.069 ± 0.016 (0.016)	0.932 ± 0.029 (0.029)	0.865 ± 0.025 (0.025)
0.65 ... 0.60	1.376 ± 0.017 (0.017)	1.196 ± 0.026 (0.026)	1.073 ± 0.029 (0.029)	0.997 ± 0.015 (0.005)
0.60 ... 0.55	1.523 ± 0.018 (0.018)	1.390 ± 0.017 (0.007)	1.230 ± 0.017 (0.014)	1.104 ± 0.025 (0.025)
0.55 ... 0.50	1.655 ± 0.052 (0.052)	1.539 ± 0.018 (0.006)	1.414 ± 0.050 (0.050)	1.315 ± 0.018 (0.014)
0.50 ... 0.45	1.842 ± 0.046 (0.046)	1.729 ± 0.024 (0.024)	1.666 ± 0.042 (0.042)	1.508 ± 0.039 (0.039)
0.45 ... 0.40	2.135 ± 0.026 (0.026)	2.038 ± 0.021 (0.013)	1.939 ± 0.068 (0.068)	1.792 ± 0.037 (0.037)
0.40 ... 0.35	2.519 ± 0.050 (0.050)	2.380 ± 0.029 (0.029)	2.247 ± 0.110 (0.110)	2.038 ± 0.062 (0.062)
0.35 ... 0.30	2.838 ± 0.032 (0.032)	2.642 ± 0.094 (0.094)	2.466 ± 0.041 (0.041)	2.288 ± 0.092 (0.092)
0.30 ... 0.25	3.064 ± 0.092 (0.092)	2.827 ± 0.076 (0.076)	2.646 ± 0.090 (0.090)	2.464 ± 0.108 (0.108)
0.25 ... 0.20	3.180 ± 0.054 (0.054)	2.955 ± 0.027 (0.010)	2.743 ± 0.039 (0.039)	2.559 ± 0.114 (0.114)
0.20 ... 0.15	3.252 ± 0.055 (0.055)	3.044 ± 0.028 (0.025)	2.859 ± 0.046 (0.046)	2.735 ± 0.099 (0.099)
0.15 ... 0.10	3.439 ± 0.063 (0.063)	3.316 ± 0.076 (0.076)	3.052 ± 0.057 (0.057)	2.815 ± 0.073 (0.073)
0.10 ... 0.05	3.449 ± 0.062 (0.062)	3.229 ± 0.079 (0.079)	2.990 ± 0.048 (0.048)	2.784 ± 0.114 (0.114)
0.05 ... 0.00	1.981 ± 0.068 (0.068)	1.774 ± 0.022 (0.021)	1.591 ± 0.037 (0.037)	1.423 ± 0.077 (0.077)

Table 14. Differential cross-section $d\sigma/dt_{p\pi}$ ($\mu\text{b}/\text{GeV}^2$) of the reaction $\gamma p \rightarrow p\pi^+\pi^-$.

$-t_{p\pi}$ (GeV 2)	$E_\gamma = 2.1\text{--}2.2$ GeV	$E_\gamma = 2.2\text{--}2.3$ GeV	$E_\gamma = 2.3\text{--}2.4$ GeV	$E_\gamma = 2.4\text{--}2.5$ GeV
3.65	3.60	0.000 ± 0.000 (0.000)	0.000 ± 0.000 (0.000)	0.000 ± 0.000 (0.000)
3.60	3.55	0.000 ± 0.000 (0.000)	0.000 ± 0.000 (0.000)	0.001 ± 0.001 (0.001)
3.55	3.50	0.000 ± 0.000 (0.000)	0.000 ± 0.000 (0.000)	0.000 ± 0.000 (0.000)
3.50	3.45	0.000 ± 0.000 (0.000)	0.000 ± 0.000 (0.000)	0.000 ± 0.000 (0.000)
3.45	3.40	0.000 ± 0.000 (0.000)	0.000 ± 0.000 (0.000)	0.002 ± 0.002 (0.002)
3.40	3.35	0.000 ± 0.000 (0.000)	0.000 ± 0.000 (0.000)	0.006 ± 0.004 (0.004)
3.35	3.30	0.000 ± 0.000 (0.000)	0.000 ± 0.000 (0.000)	0.008 ± 0.003 (0.003)
3.30	3.25	0.000 ± 0.000 (0.000)	0.000 ± 0.000 (0.000)	0.010 ± 0.005 (0.005)
3.25	3.20	0.000 ± 0.000 (0.000)	0.001 ± 0.001 (0.001)	0.007 ± 0.007 (0.007)
3.20	3.15	0.000 ± 0.000 (0.000)	0.002 ± 0.001 (0.001)	0.012 ± 0.003 (0.003)
3.15	3.10	0.000 ± 0.000 (0.000)	0.004 ± 0.002 (0.002)	0.020 ± 0.004 (0.004)
3.10	3.05	0.000 ± 0.000 (0.000)	0.002 ± 0.003 (0.003)	0.025 ± 0.004 (0.004)
3.05	3.00	0.001 ± 0.001 (0.001)	0.006 ± 0.002 (0.001)	0.030 ± 0.004 (0.002)
3.00	2.95	0.001 ± 0.001 (0.001)	0.011 ± 0.002 (0.002)	0.032 ± 0.006 (0.006)
2.95	2.90	0.004 ± 0.001 (0.001)	0.015 ± 0.003 (0.002)	0.024 ± 0.004 (0.004)
2.90	2.85	0.007 ± 0.002 (0.001)	0.026 ± 0.003 (0.001)	0.028 ± 0.003 (0.003)
2.85	2.80	0.014 ± 0.002 (0.002)	0.023 ± 0.003 (0.002)	0.039 ± 0.004 (0.002)
2.80	2.75	0.017 ± 0.003 (0.003)	0.031 ± 0.007 (0.007)	0.043 ± 0.004 (0.004)
2.75	2.70	0.023 ± 0.004 (0.004)	0.034 ± 0.004 (0.004)	0.049 ± 0.005 (0.005)
2.70	2.65	0.031 ± 0.003 (0.002)	0.042 ± 0.009 (0.009)	0.040 ± 0.009 (0.009)
2.65	2.60	0.044 ± 0.004 (0.002)	0.047 ± 0.006 (0.006)	0.041 ± 0.023 (0.023)
2.60	2.55	0.041 ± 0.004 (0.003)	0.063 ± 0.011 (0.011)	0.060 ± 0.005 (0.005)
2.55	2.50	0.053 ± 0.005 (0.005)	0.062 ± 0.008 (0.008)	0.062 ± 0.008 (0.008)
2.50	2.45	0.063 ± 0.005 (0.005)	0.064 ± 0.013 (0.013)	0.066 ± 0.027 (0.027)
2.45	2.40	0.068 ± 0.009 (0.009)	0.069 ± 0.010 (0.010)	0.076 ± 0.025 (0.025)
2.40	2.35	0.069 ± 0.005 (0.002)	0.080 ± 0.007 (0.007)	0.094 ± 0.015 (0.015)
2.35	2.30	0.076 ± 0.007 (0.007)	0.074 ± 0.007 (0.007)	0.082 ± 0.010 (0.010)
2.30	2.25	0.070 ± 0.016 (0.016)	0.101 ± 0.014 (0.014)	0.081 ± 0.016 (0.016)
2.25	2.20	0.089 ± 0.013 (0.013)	0.102 ± 0.010 (0.010)	0.102 ± 0.015 (0.015)
2.20	2.15	0.100 ± 0.009 (0.009)	0.102 ± 0.018 (0.018)	0.104 ± 0.013 (0.013)
2.15	2.10	0.124 ± 0.019 (0.019)	0.106 ± 0.008 (0.008)	0.097 ± 0.024 (0.024)
2.10	2.05	0.146 ± 0.020 (0.020)	0.104 ± 0.017 (0.017)	0.103 ± 0.017 (0.017)
2.05	2.00	0.156 ± 0.016 (0.016)	0.124 ± 0.010 (0.010)	0.104 ± 0.024 (0.024)
2.00	1.95	0.155 ± 0.068 (0.068)	0.124 ± 0.013 (0.013)	0.123 ± 0.023 (0.023)
1.95	1.90	0.144 ± 0.044 (0.044)	0.119 ± 0.018 (0.018)	0.124 ± 0.019 (0.019)
1.90	1.85	0.150 ± 0.029 (0.029)	0.137 ± 0.020 (0.020)	0.127 ± 0.022 (0.022)
1.85	1.80	0.150 ± 0.062 (0.062)	0.154 ± 0.016 (0.016)	0.120 ± 0.007 (0.007)
1.80	1.75	0.178 ± 0.026 (0.026)	0.164 ± 0.012 (0.012)	0.145 ± 0.027 (0.027)
1.75	1.70	0.169 ± 0.007 (0.007)	0.145 ± 0.017 (0.017)	0.156 ± 0.010 (0.010)
1.70	1.65	0.190 ± 0.038 (0.038)	0.165 ± 0.017 (0.017)	0.152 ± 0.030 (0.030)
1.65	1.60	0.172 ± 0.021 (0.021)	0.182 ± 0.009 (0.009)	0.165 ± 0.015 (0.015)
1.60	1.55	0.198 ± 0.026 (0.026)	0.178 ± 0.021 (0.021)	0.161 ± 0.024 (0.024)
1.55	1.50	0.182 ± 0.017 (0.017)	0.198 ± 0.015 (0.015)	0.179 ± 0.021 (0.021)
1.50	1.45	0.208 ± 0.024 (0.024)	0.193 ± 0.020 (0.020)	0.207 ± 0.012 (0.012)
1.45	1.40	0.233 ± 0.030 (0.030)	0.204 ± 0.013 (0.013)	0.193 ± 0.018 (0.018)
1.40	1.35	0.243 ± 0.012 (0.012)	0.214 ± 0.030 (0.030)	0.198 ± 0.008 (0.005)
1.35	1.30	0.260 ± 0.031 (0.031)	0.238 ± 0.014 (0.014)	0.198 ± 0.030 (0.030)
1.30	1.25	0.284 ± 0.013 (0.013)	0.248 ± 0.019 (0.019)	0.203 ± 0.023 (0.023)
1.25	1.20	0.299 ± 0.045 (0.045)	0.247 ± 0.024 (0.024)	0.214 ± 0.024 (0.024)
1.20	1.15	0.296 ± 0.029 (0.029)	0.260 ± 0.024 (0.024)	0.241 ± 0.039 (0.039)
1.15	1.10	0.313 ± 0.046 (0.046)	0.265 ± 0.027 (0.027)	0.274 ± 0.021 (0.021)
1.10	1.05	0.339 ± 0.036 (0.036)	0.298 ± 0.032 (0.032)	0.258 ± 0.017 (0.017)
1.05	1.00	0.365 ± 0.019 (0.019)	0.332 ± 0.025 (0.025)	0.313 ± 0.019 (0.019)
1.00	0.95	0.421 ± 0.011 (0.007)	0.350 ± 0.033 (0.033)	0.323 ± 0.029 (0.029)
0.95	0.90	0.459 ± 0.027 (0.027)	0.387 ± 0.023 (0.023)	0.354 ± 0.011 (0.011)
0.90	0.85	0.494 ± 0.012 (0.008)	0.446 ± 0.011 (0.008)	0.375 ± 0.015 (0.015)
0.85	0.80	0.542 ± 0.029 (0.029)	0.463 ± 0.016 (0.016)	0.435 ± 0.012 (0.012)
0.80	0.75	0.598 ± 0.012 (0.011)	0.534 ± 0.012 (0.009)	0.480 ± 0.016 (0.016)
0.75	0.70	0.681 ± 0.041 (0.041)	0.599 ± 0.013 (0.013)	0.556 ± 0.012 (0.006)
0.70	0.65	0.800 ± 0.018 (0.018)	0.717 ± 0.014 (0.012)	0.653 ± 0.029 (0.029)
0.65	0.60	0.897 ± 0.035 (0.035)	0.832 ± 0.015 (0.011)	0.758 ± 0.016 (0.016)
0.60	0.55	1.081 ± 0.034 (0.034)	1.013 ± 0.021 (0.021)	0.910 ± 0.019 (0.019)
0.55	0.50	1.259 ± 0.022 (0.022)	1.165 ± 0.026 (0.026)	1.118 ± 0.029 (0.029)
0.50	0.45	1.462 ± 0.067 (0.067)	1.378 ± 0.061 (0.061)	1.267 ± 0.028 (0.028)
0.45	0.40	1.668 ± 0.039 (0.039)	1.560 ± 0.057 (0.057)	1.493 ± 0.048 (0.048)
0.40	0.35	1.936 ± 0.107 (0.107)	1.748 ± 0.054 (0.054)	1.656 ± 0.052 (0.052)
0.35	0.30	2.068 ± 0.098 (0.098)	1.897 ± 0.084 (0.084)	1.782 ± 0.085 (0.085)
0.30	0.25	2.180 ± 0.112 (0.112)	1.996 ± 0.082 (0.082)	1.852 ± 0.081 (0.081)
0.25	0.20	2.281 ± 0.136 (0.136)	2.179 ± 0.099 (0.099)	1.990 ± 0.054 (0.054)
0.20	0.15	2.502 ± 0.122 (0.122)	2.292 ± 0.082 (0.082)	2.186 ± 0.047 (0.047)
0.15	0.10	2.644 ± 0.107 (0.107)	2.437 ± 0.101 (0.101)	2.301 ± 0.079 (0.079)
0.10	0.05	2.528 ± 0.088 (0.088)	2.370 ± 0.058 (0.058)	2.269 ± 0.059 (0.059)
0.05	0.00	1.280 ± 0.070 (0.070)	1.185 ± 0.059 (0.059)	1.192 ± 0.090 (0.090)

Table 15. Differential cross-section $d\sigma/dt_{p\pi}$ ($\mu\text{b}/\text{GeV}^2$) of the reaction $\gamma p \rightarrow p\pi^+\pi^-$.

$-t_{p\pi}$ (GeV 2)	$E_\gamma = 2.5\text{--}2.6$ GeV
3.75	3.70 0.000 ± 0.000 (0.000)
3.70	3.65 0.002 ± 0.002 (0.001)
3.65	3.60 0.002 ± 0.001 (0.000)
3.60	3.55 0.001 ± 0.001 (0.001)
3.55	3.50 0.004 ± 0.002 (0.000)
3.50	3.45 0.005 ± 0.002 (0.001)
3.45	3.40 0.007 ± 0.006 (0.006)
3.40	3.35 0.014 ± 0.003 (0.003)
3.35	3.30 0.025 ± 0.005 (0.003)
3.30	3.25 0.019 ± 0.007 (0.007)
3.25	3.20 0.026 ± 0.005 (0.000)
3.20	3.15 0.018 ± 0.004 (0.002)
3.15	3.10 0.026 ± 0.010 (0.010)
3.10	3.05 0.033 ± 0.007 (0.007)
3.05	3.00 0.033 ± 0.005 (0.003)
3.00	2.95 0.045 ± 0.006 (0.004)
2.95	2.90 0.030 ± 0.019 (0.019)
2.90	2.85 0.026 ± 0.016 (0.016)
2.85	2.80 0.037 ± 0.018 (0.018)
2.80	2.75 0.037 ± 0.035 (0.035)
2.75	2.70 0.070 ± 0.024 (0.024)
2.70	2.65 0.034 ± 0.049 (0.049)
2.65	2.60 0.024 ± 0.038 (0.038)
2.60	2.55 0.050 ± 0.039 (0.039)
2.55	2.50 0.054 ± 0.034 (0.034)
2.50	2.45 0.033 ± 0.037 (0.037)
2.45	2.40 0.042 ± 0.031 (0.031)
2.40	2.35 0.063 ± 0.036 (0.036)
2.35	2.30 0.074 ± 0.022 (0.022)
2.30	2.25 0.080 ± 0.020 (0.020)
2.25	2.20 0.084 ± 0.020 (0.020)
2.20	2.15 0.082 ± 0.041 (0.041)
2.15	2.10 0.075 ± 0.021 (0.021)
2.10	2.05 0.095 ± 0.032 (0.032)
2.05	2.00 0.097 ± 0.023 (0.023)
2.00	1.95 0.100 ± 0.041 (0.041)
1.95	1.90 0.093 ± 0.025 (0.025)
1.90	1.85 0.095 ± 0.026 (0.026)
1.85	1.80 0.105 ± 0.015 (0.015)
1.80	1.75 0.106 ± 0.018 (0.018)
1.75	1.70 0.135 ± 0.019 (0.019)
1.70	1.65 0.130 ± 0.024 (0.024)
1.65	1.60 0.131 ± 0.056 (0.056)
1.60	1.55 0.146 ± 0.035 (0.035)
1.55	1.50 0.158 ± 0.009 (0.004)
1.50	1.45 0.203 ± 0.022 (0.022)
1.45	1.40 0.153 ± 0.030 (0.030)
1.40	1.35 0.157 ± 0.034 (0.034)
1.35	1.30 0.145 ± 0.047 (0.047)
1.30	1.25 0.155 ± 0.046 (0.046)
1.25	1.20 0.194 ± 0.032 (0.032)
1.20	1.15 0.190 ± 0.055 (0.055)
1.15	1.10 0.196 ± 0.056 (0.056)
1.10	1.05 0.248 ± 0.055 (0.055)
1.05	1.00 0.245 ± 0.017 (0.017)
1.00	0.95 0.273 ± 0.025 (0.025)
0.95	0.90 0.339 ± 0.013 (0.012)
0.90	0.85 0.345 ± 0.013 (0.008)
0.85	0.80 0.424 ± 0.024 (0.024)
0.80	0.75 0.432 ± 0.014 (0.010)
0.75	0.70 0.507 ± 0.054 (0.054)
0.70	0.65 0.624 ± 0.044 (0.044)
0.65	0.60 0.735 ± 0.062 (0.062)
0.60	0.55 0.885 ± 0.068 (0.068)
0.55	0.50 1.004 ± 0.041 (0.041)
0.50	0.45 1.219 ± 0.053 (0.053)
0.45	0.40 1.366 ± 0.096 (0.096)
0.40	0.35 1.465 ± 0.078 (0.078)
0.35	0.30 1.578 ± 0.070 (0.070)
0.30	0.25 1.750 ± 0.033 (0.015)
0.25	0.20 1.783 ± 0.169 (0.169)
0.20	0.15 2.052 ± 0.037 (0.019)
0.15	0.10 2.172 ± 0.086 (0.086)
0.10	0.05 2.197 ± 0.152 (0.152)
0.05	0.00 1.113 ± 0.075 (0.075)

Appendix D. Total cross-sections for ρ and Δ production

Table 16. Total cross-section of the reaction $\gamma p \rightarrow p\rho^0$ analyzed with different methods.

E_γ (GeV)	Söding	Ross-Stodolsky	Breit-Wigner
1.00 ... 1.10	3.89 ± 2.66 (2.66)	11.84 ± 4.47 (4.47)	6.14 ± 2.10 (2.10)
1.10 ... 1.20	10.51 ± 2.19 (2.19)	13.32 ± 3.07 (3.07)	12.01 ± 1.45 (1.45)
1.20 ... 1.30	14.74 ± 1.47 (1.47)	18.51 ± 2.34 (2.34)	16.13 ± 1.37 (1.37)
1.30 ... 1.40	16.92 ± 1.40 (1.40)	25.41 ± 2.46 (2.46)	18.27 ± 1.75 (1.75)
1.40 ... 1.50	18.27 ± 1.00 (1.00)	27.17 ± 1.68 (1.68)	18.73 ± 1.50 (1.50)
1.50 ... 1.60	21.06 ± 0.98 (0.98)	29.38 ± 1.12 (1.12)	21.90 ± 1.62 (1.62)
1.60 ... 1.70	21.97 ± 0.88 (0.88)	27.71 ± 1.02 (1.02)	22.69 ± 1.55 (1.55)
1.70 ... 1.80	22.87 ± 0.79 (0.79)	27.13 ± 0.83 (0.83)	24.12 ± 1.38 (1.38)
1.80 ... 1.90	22.11 ± 0.74 (0.74)	25.10 ± 0.77 (0.77)	23.36 ± 1.27 (1.27)
1.90 ... 2.00	21.37 ± 0.67 (0.67)	23.47 ± 0.66 (0.66)	22.30 ± 1.17 (1.17)
2.00 ... 2.10	20.41 ± 0.66 (0.57)	21.76 ± 0.76 (0.56)	21.19 ± 0.99 (0.99)
2.10 ... 2.20	19.01 ± 1.28 (0.61)	19.79 ± 1.17 (0.57)	19.81 ± 1.10 (0.92)
2.20 ... 2.30	18.39 ± 0.80 (0.54)	18.80 ± 0.72 (0.52)	19.01 ± 0.80 (0.80)
2.30 ... 2.40	17.20 ± 0.52 (0.52)	17.41 ± 0.55 (0.49)	17.89 ± 0.72 (0.72)
2.40 ... 2.50	16.86 ± 0.87 (0.59)	16.89 ± 0.84 (0.56)	17.31 ± 0.76 (0.73)
2.50 ... 2.60	17.15 ± 0.69 (0.69)	16.86 ± 0.64 (0.64)	17.43 ± 0.85 (0.85)

Table 17. Total cross-section of the reaction $\gamma p \rightarrow \Delta^{++}\pi^-$. For the separation from the ρ^0 production final state the Söding model was used.

E_γ (GeV)	σ (μb)
0.50 ... 0.55	31.35 ± (1.37)
0.55 ... 0.60	53.80 ± (1.98)
0.60 ... 0.65	63.59 ± (2.23)
0.65 ... 0.70	62.05 ± (2.88)
0.70 ... 0.75	63.85 ± (2.33)
0.75 ... 0.80	59.92 ± (2.37)
0.80 ... 0.85	59.76 ± (2.56)
0.85 ... 0.90	64.82 ± (2.10)
0.90 ... 0.95	64.13 ± (1.86)
0.95 ... 1.00	55.23 ± (1.92)
1.00 ... 1.10	39.12 ± 1.24 (0.75)
1.10 ... 1.20	29.80 ± 0.74 (0.61)
1.20 ... 1.30	22.98 ± 0.78 (0.63)
1.30 ... 1.40	20.63 ± 0.66 (0.49)
1.40 ... 1.50	17.47 ± 0.68 (0.29)
1.50 ... 1.60	16.61 ± 0.89 (0.29)
1.60 ... 1.70	13.86 ± 0.27 (0.25)
1.70 ... 1.80	11.73 ± 0.52 (0.22)
1.80 ... 1.90	10.11 ± 0.34 (0.20)
1.90 ... 2.00	8.72 ± 0.49 (0.18)
2.00 ... 2.10	7.44 ± 0.32 (0.15)
2.10 ... 2.20	6.90 ± 0.47 (0.16)
2.20 ... 2.30	5.82 ± 0.68 (0.13)
2.30 ... 2.40	5.45 ± 0.13 (0.13)
2.40 ... 2.50	5.19 ± 0.27 (0.14)
2.50 ... 2.60	4.78 ± 0.29 (0.16)

Table 18. Total cross-section of the reaction $\gamma p \rightarrow \Delta^0\pi^+$. For the separation from the ρ^0 production final state the Söding model was used.

E_γ (GeV)	σ (μb)
0.50 ... 0.55	0.21 ± (1.10)
0.55 ... 0.60	4.03 ± (2.50)
0.60 ... 0.65	1.95 ± (2.12)
0.65 ... 0.70	3.15 ± (3.10)
0.70 ... 0.75	2.52 ± (6.02)
0.75 ... 0.80	1.17 ± (4.03)
0.80 ... 0.85	1.17 ± (2.05)
0.85 ... 0.90	4.16 ± (1.37)
0.90 ... 0.95	6.90 ± (1.86)
0.95 ... 1.00	7.67 ± (1.44)
1.00 ... 1.10	9.28 ± 0.69 (0.57)
1.10 ... 1.20	7.67 ± 0.58 (0.46)
1.20 ... 1.30	4.83 ± 0.58 (0.35)
1.30 ... 1.40	2.90 ± 0.42 (0.42)
1.40 ... 1.50	2.92 ± 0.34 (0.25)
1.50 ... 1.60	3.20 ± 0.32 (0.24)
1.60 ... 1.70	2.61 ± 0.30 (0.21)
1.70 ... 1.80	2.51 ± 0.18 (0.18)
1.80 ... 1.90	2.10 ± 0.27 (0.17)
1.90 ... 2.00	1.56 ± 0.14 (0.14)
2.00 ... 2.10	1.34 ± 0.22 (0.12)
2.10 ... 2.20	1.41 ± 0.24 (0.13)
2.20 ... 2.30	0.99 ± 0.64 (0.11)
2.30 ... 2.40	0.80 ± 0.19 (0.10)
2.40 ... 2.50	1.04 ± 0.32 (0.11)
2.50 ... 2.60	0.80 ± 0.65 (0.13)

Appendix E. Comparison of differential cross-sections of $\gamma p \rightarrow p\rho^0$ analyzed with different methods

Table 19. Differential cross-section $d\sigma/dt$ ($\mu\text{b}/\text{GeV}^2$) of the reaction $\gamma p \rightarrow p\rho^0$.

$-t_\rho$ (GeV^2)			$1.4 \leq E_\gamma$ (GeV) < 1.6		
			Söding	Ross-Stodolsky	Breit-Wigner
0.06	...	0.10	83.44 ± 3.54 (3.54)	133.94 ± 4.33 (4.33)	78.52 ± 2.95 (2.95)
0.10	...	0.20	61.26 ± 1.06 (1.06)	78.33 ± 0.88 (0.88)	61.18 ± 1.91 (1.91)
0.20	...	0.30	35.07 ± 0.95 (0.95)	40.04 ± 1.57 (1.57)	33.03 ± 1.22 (1.22)
0.30	...	0.40	14.31 ± 0.54 (0.44)	15.65 ± 0.59 (0.34)	13.46 ± 0.62 (0.30)
0.40	...	0.50	8.78 ± 0.67 (0.67)	8.85 ± 0.78 (0.78)	8.08 ± 0.63 (0.63)
0.50	...	0.70	7.86 ± 0.38 (0.31)	7.84 ± 0.31 (0.31)	7.36 ± 0.35 (0.35)
0.70	...	0.90	6.80 ± 0.43 (0.43)	8.04 ± 0.31 (0.07)	6.68 ± 0.41 (0.41)
0.90	...	1.10	5.98 ± 0.29 (0.29)	8.00 ± 0.32 (0.19)	6.23 ± 0.30 (0.27)
1.10	...	1.35	4.80 ± 0.68 (0.68)	8.30 ± 1.61 (1.61)	5.08 ± 0.42 (0.42)
$-t_\rho$ (GeV^2)			$1.6 \leq E_\gamma$ (GeV) < 1.8		
			Söding	Ross-Stodolsky	Breit-Wigner
0.05	...	0.10	76.83 ± 4.82 (4.82)	100.00 ± 4.48 (4.48)	86.59 ± 4.38 (4.38)
0.10	...	0.20	65.78 ± 0.76 (0.51)	75.01 ± 0.92 (0.92)	70.94 ± 1.85 (1.85)
0.20	...	0.30	39.26 ± 0.73 (0.73)	42.56 ± 1.04 (1.04)	41.64 ± 1.30 (1.30)
0.30	...	0.40	18.09 ± 0.56 (0.56)	19.32 ± 0.51 (0.51)	18.53 ± 0.70 (0.70)
0.40	...	0.50	9.48 ± 0.32 (0.19)	10.79 ± 0.36 (0.36)	9.96 ± 0.35 (0.34)
0.50	...	0.70	5.87 ± 0.29 (0.29)	6.31 ± 0.39 (0.39)	5.81 ± 0.41 (0.41)
0.70	...	0.90	5.72 ± 0.32 (0.31)	5.01 ± 0.21 (0.11)	5.09 ± 0.22 (0.18)
0.90	...	1.10	5.12 ± 0.40 (0.11)	4.56 ± 0.23 (0.11)	4.54 ± 0.22 (0.05)
1.10	...	1.50	4.43 ± 0.40 (0.40)	4.78 ± 0.32 (0.32)	4.58 ± 0.29 (0.29)
$-t_\rho$ (GeV^2)			$1.8 \leq E_\gamma$ (GeV) < 2.0		
			Söding	Ross-Stodolsky	Breit-Wigner
0.05	...	0.10	82.34 ± 3.29 (3.29)	93.56 ± 3.34 (3.34)	88.20 ± 3.46 (3.46)
0.10	...	0.20	65.78 ± 1.25 (1.25)	69.76 ± 1.58 (1.58)	68.43 ± 1.79 (1.79)
0.20	...	0.30	38.40 ± 0.81 (0.81)	39.99 ± 0.94 (0.94)	39.61 ± 0.93 (0.93)
0.30	...	0.40	20.10 ± 0.47 (0.47)	20.53 ± 0.76 (0.76)	20.41 ± 0.79 (0.79)
0.40	...	0.50	10.80 ± 0.47 (0.47)	11.41 ± 0.60 (0.60)	11.43 ± 0.69 (0.69)
0.50	...	0.70	5.62 ± 0.43 (0.43)	5.68 ± 0.43 (0.43)	5.77 ± 0.39 (0.39)
0.70	...	0.90	4.28 ± 0.48 (0.48)	4.02 ± 0.19 (0.19)	4.12 ± 0.18 (0.11)
0.90	...	1.10	4.72 ± 0.71 (0.71)	3.91 ± 0.23 (0.23)	3.98 ± 0.19 (0.19)
1.10	...	1.50	3.49 ± 0.29 (0.29)	3.00 ± 0.15 (0.12)	3.07 ± 0.15 (0.15)
$-t_\rho$ (GeV^2)			$2.0 \leq E_\gamma$ (GeV) < 2.2		
			Söding	Ross-Stodolsky	Breit-Wigner
0.05	...	0.10	73.68 ± 3.31 (3.31)	80.03 ± 3.75 (3.75)	77.57 ± 3.56 (3.56)
0.10	...	0.20	58.27 ± 2.31 (2.31)	60.46 ± 2.58 (2.58)	60.07 ± 2.55 (2.55)
0.20	...	0.30	35.69 ± 1.65 (1.65)	36.19 ± 1.66 (1.66)	36.02 ± 1.73 (1.73)
0.30	...	0.40	18.92 ± 1.00 (1.00)	18.70 ± 1.04 (1.04)	18.99 ± 1.17 (1.17)
0.40	...	0.50	10.90 ± 1.71 (1.71)	10.65 ± 1.75 (1.75)	11.25 ± 1.99 (1.99)
0.50	...	0.70	4.94 ± 0.19 (0.14)	4.86 ± 0.11 (0.08)	4.91 ± 0.19 (0.08)
0.70	...	0.90	3.30 ± 0.35 (0.35)	2.95 ± 0.11 (0.11)	3.38 ± 0.36 (0.36)
0.90	...	1.10	4.01 ± 0.62 (0.62)	2.99 ± 0.24 (0.24)	3.42 ± 0.35 (0.35)
1.10	...	1.50	2.86 ± 0.53 (0.53)	2.11 ± 0.09 (0.09)	2.37 ± 0.23 (0.23)
$-t_\rho$ (GeV^2)			$2.2 \leq E_\gamma$ (GeV) < 2.4		
			Söding	Ross-Stodolsky	Breit-Wigner
0.05	...	0.10	63.43 ± 3.17 (3.17)	68.13 ± 3.04 (3.04)	66.40 ± 2.98 (2.98)
0.10	...	0.20	52.60 ± 1.96 (1.96)	53.78 ± 2.14 (2.14)	52.90 ± 1.99 (1.99)
0.20	...	0.30	32.93 ± 1.19 (1.19)	32.78 ± 1.19 (1.19)	33.07 ± 1.11 (1.11)
0.30	...	0.40	17.47 ± 0.70 (0.70)	17.08 ± 0.70 (0.70)	17.40 ± 0.67 (0.67)
0.40	...	0.50	10.01 ± 0.31 (0.18)	9.87 ± 0.22 (0.19)	10.18 ± 0.35 (0.06)
0.50	...	0.70	5.02 ± 0.20 (0.11)	4.65 ± 0.20 (0.20)	5.03 ± 0.23 (0.18)
0.70	...	0.90	3.02 ± 0.27 (0.27)	2.52 ± 0.20 (0.20)	3.24 ± 0.23 (0.23)
0.90	...	1.10	2.73 ± 0.21 (0.21)	2.29 ± 0.11 (0.11)	3.41 ± 0.37 (0.37)
1.10	...	1.50	2.48 ± 0.44 (0.44)	1.60 ± 0.08 (0.04)	2.38 ± 0.15 (0.15)
$-t_\rho$ (GeV^2)			$2.4 \leq E_\gamma$ (GeV) < 2.6		
			Söding	Ross-Stodolsky	Breit-Wigner
0.05	...	0.10	51.05 ± 6.83 (6.83)	55.05 ± 6.88 (6.88)	52.63 ± 6.73 (6.73)
0.10	...	0.20	47.82 ± 3.16 (3.16)	49.09 ± 3.16 (3.16)	47.80 ± 2.73 (2.73)
0.20	...	0.30	30.47 ± 1.82 (1.82)	30.05 ± 1.45 (1.45)	30.23 ± 1.55 (1.55)
0.30	...	0.40	16.28 ± 0.77 (0.77)	15.76 ± 0.71 (0.71)	15.96 ± 0.78 (0.78)
0.40	...	0.50	9.51 ± 0.86 (0.86)	9.09 ± 0.77 (0.77)	9.75 ± 0.95 (0.95)
0.50	...	0.70	4.93 ± 0.25 (0.16)	4.62 ± 0.16 (0.16)	5.43 ± 0.26 (0.19)
0.70	...	0.90	2.77 ± 0.27 (0.20)	2.22 ± 0.24 (0.24)	2.84 ± 0.18 (0.11)
0.90	...	1.10	3.24 ± 0.18 (0.14)	2.03 ± 0.22 (0.22)	2.37 ± 0.41 (0.41)
1.10	...	1.50	2.72 ± 0.27 (0.27)	1.62 ± 0.18 (0.18)	2.22 ± 0.42 (0.42)

Appendix F. Differential cross-sections of $\gamma p \rightarrow \Delta^{++} \pi^-$

Table 20. Differential cross-section $d\sigma/dt_{\Delta^{++}}$ ($\mu\text{b}/\text{GeV}^2$) of the reaction $\gamma p \rightarrow \Delta^{++} \pi^-$.

$-t_{\pi\pi}$ (GeV 2)	$E_\gamma = 1.1\text{--}1.4$ GeV	$E_\gamma = 1.4\text{--}1.8$ GeV	$E_\gamma = 1.8\text{--}2.2$ GeV	$E_\gamma = 2.2\text{--}2.6$ GeV
0.00 ... 0.10	76.348 \pm 3.750 (3.750)	48.037 \pm 6.768 (2.861)	24.878 \pm 0.933 (0.933)	14.295 \pm 0.591 (0.591)
0.10 ... 0.20	51.354 \pm 1.754 (1.668)	24.509 \pm 0.928 (0.928)	15.751 \pm 0.808 (0.745)	9.751 \pm 0.534 (0.534)
0.20 ... 0.30	36.317 \pm 1.780 (1.780)	14.588 \pm 0.616 (0.616)	10.213 \pm 0.531 (0.486)	8.009 \pm 0.356 (0.356)
0.30 ... 0.40	23.623 \pm 1.286 (1.255)	8.434 \pm 0.701 (0.451)	6.619 \pm 0.367 (0.367)	5.221 \pm 0.277 (0.277)
0.40 ... 0.50	19.795 \pm 1.783 (1.367)	5.832 \pm 0.459 (0.396)	3.968 \pm 0.457 (0.255)	3.704 \pm 0.198 (0.198)
0.50 ... 0.70	15.799 \pm 1.044 (1.044)	8.173 \pm 0.531 (0.381)	2.229 \pm 0.188 (0.147)	2.200 \pm 0.118 (0.118)
0.70 ... 0.90	8.968 \pm 0.921 (0.921)	7.804 \pm 0.645 (0.387)	2.402 \pm 0.174 (0.140)	0.520 \pm 0.070 (0.070)
0.90 ... 1.10	5.871 \pm 0.568 (0.568)	4.288 \pm 0.359 (0.359)	2.692 \pm 0.154 (0.154)	0.546 \pm 0.062 (0.062)
1.10 ... 1.50		2.160 \pm 0.265 (0.265)	1.525 \pm 0.328 (0.169)	0.781 \pm 0.063 (0.063)

Appendix G. Decay spin density matrix elements for the ρ decay in $\gamma p \rightarrow p\rho \rightarrow p\pi^+\pi^-$

Table 21. Density matrix elements of ρ^0 decay in the helicity system of reaction $\gamma p \rightarrow p\rho^0$.

$-t_\rho$ (GeV 2)	1.4 $\leq E_\gamma$ (GeV) < 1.8		
	ρ^{00}	ρ^{1-1}	ρ^{10}
0.05 ... 0.10	-0.042 \pm 0.014 (0.014)	0.022 \pm 0.043 (0.043)	-0.073 \pm 0.022 (0.022)
0.10 ... 0.15	0.064 \pm 0.040 (0.040)	0.064 \pm 0.043 (0.043)	-0.048 \pm 0.025 (0.025)
0.15 ... 0.20	0.130 \pm 0.045 (0.045)	0.064 \pm 0.042 (0.042)	-0.024 \pm 0.027 (0.027)
0.20 ... 0.25	0.157 \pm 0.053 (0.053)	0.044 \pm 0.049 (0.049)	-0.012 \pm 0.034 (0.034)
0.25 ... 0.30	0.174 \pm 0.065 (0.065)	0.027 \pm 0.061 (0.061)	0.006 \pm 0.045 (0.045)
0.30 ... 0.40	0.208 \pm 0.071 (0.071)	0.049 \pm 0.065 (0.065)	-0.021 \pm 0.048 (0.048)
0.40 ... 0.50	0.303 \pm 0.103 (0.103)	0.042 \pm 0.090 (0.090)	-0.009 \pm 0.070 (0.070)
0.50 ... 1.00	0.491 \pm 0.201 (0.048)	0.017 \pm 0.038 (0.038)	0.176 \pm 0.073 (0.030)
$-t_\rho$ (GeV 2)	1.8 $\leq E_\gamma$ (GeV) < 2.2		
	ρ^{00}	ρ^{1-1}	ρ^{10}
0.05 ... 0.10	-0.023 \pm 0.027 (0.027)	0.031 \pm 0.032 (0.032)	-0.073 \pm 0.010 (0.010)
0.10 ... 0.15	0.072 \pm 0.028 (0.028)	0.098 \pm 0.032 (0.032)	-0.069 \pm 0.018 (0.018)
0.15 ... 0.20	0.102 \pm 0.034 (0.034)	0.107 \pm 0.036 (0.036)	-0.053 \pm 0.021 (0.021)
0.20 ... 0.25	0.095 \pm 0.040 (0.040)	0.112 \pm 0.042 (0.042)	-0.036 \pm 0.025 (0.025)
0.25 ... 0.30	0.103 \pm 0.046 (0.046)	0.099 \pm 0.050 (0.050)	-0.018 \pm 0.031 (0.031)
0.30 ... 0.40	0.125 \pm 0.044 (0.044)	0.084 \pm 0.050 (0.050)	0.000 \pm 0.030 (0.030)
0.40 ... 0.50	0.113 \pm 0.072 (0.072)	0.117 \pm 0.072 (0.072)	-0.018 \pm 0.046 (0.046)
0.50 ... 1.00	0.213 \pm 0.066 (0.066)	0.295 \pm 0.059 (0.059)	-0.011 \pm 0.042 (0.042)
1.00 ... 1.90	0.312 \pm 0.074 (0.074)	0.148 \pm 0.061 (0.061)	-0.005 \pm 0.045 (0.045)
$-t_\rho$ (GeV 2)	2.2 $\leq E_\gamma$ (GeV) < 2.6		
	ρ^{00}	ρ^{1-1}	ρ^{10}
0.05 ... 0.10	0.003 \pm 0.059 (0.059)	0.054 \pm 0.039 (0.039)	-0.067 \pm 0.011 (0.011)
0.10 ... 0.15	0.070 \pm 0.037 (0.037)	0.075 \pm 0.043 (0.043)	-0.073 \pm 0.023 (0.023)
0.15 ... 0.20	0.089 \pm 0.043 (0.043)	0.095 \pm 0.048 (0.048)	-0.058 \pm 0.027 (0.027)
0.20 ... 0.25	0.102 \pm 0.050 (0.050)	0.091 \pm 0.054 (0.054)	-0.057 \pm 0.031 (0.031)
0.25 ... 0.30	0.100 \pm 0.060 (0.060)	0.094 \pm 0.064 (0.064)	-0.037 \pm 0.038 (0.038)
0.30 ... 0.40	0.084 \pm 0.053 (0.053)	0.075 \pm 0.059 (0.059)	-0.009 \pm 0.036 (0.036)
0.40 ... 0.50	0.083 \pm 0.073 (0.073)	0.097 \pm 0.081 (0.081)	0.003 \pm 0.049 (0.049)
0.50 ... 1.00	0.128 \pm 0.073 (0.073)	0.295 \pm 0.070 (0.070)	-0.009 \pm 0.048 (0.048)
1.00 ... 2.60	0.206 \pm 0.104 (0.104)	0.283 \pm 0.090 (0.090)	0.061 \pm 0.064 (0.064)

Table 22. Density matrix elements of ρ^0 decay in the Gottfried-Jackson system of reaction $\gamma p \rightarrow p \rho^0$.

$-t_\rho$ (GeV 2)			1.4 $\leq E_\gamma$ (GeV) < 1.8		
			ρ^{00}	ρ^{1-1}	ρ^{10}
0.05	...	0.10	-0.001 ± 0.046 (0.046)	0.047 ± 0.073 (0.073)	0.120 ± 0.034 (0.034)
0.10	...	0.15	0.184 ± 0.045 (0.045)	0.122 ± 0.040 (0.040)	0.108 ± 0.024 (0.024)
0.15	...	0.20	0.309 ± 0.048 (0.048)	0.148 ± 0.038 (0.038)	0.087 ± 0.027 (0.027)
0.20	...	0.25	0.370 ± 0.057 (0.057)	0.141 ± 0.043 (0.043)	0.057 ± 0.033 (0.033)
0.25	...	0.30	0.401 ± 0.072 (0.072)	0.132 ± 0.052 (0.052)	0.013 ± 0.044 (0.044)
0.30	...	0.40	0.336 ± 0.076 (0.076)	0.107 ± 0.057 (0.057)	0.006 ± 0.050 (0.050)
0.40	...	0.50	0.273 ± 0.108 (0.108)	0.026 ± 0.085 (0.085)	0.002 ± 0.072 (0.072)
0.50	...	1.00	0.123 ± 0.054 (0.047)	-0.167 ± 0.070 (0.040)	0.085 ± 0.035 (0.030)
$-t_\rho$ (GeV 2)			1.8 $\leq E_\gamma$ (GeV) < 2.2		
			ρ^{00}	ρ^{1-1}	ρ^{10}
0.05	...	0.10	0.089 ± 0.030 (0.030)	0.080 ± 0.033 (0.033)	0.156 ± 0.013 (0.013)
0.10	...	0.15	0.198 ± 0.032 (0.032)	0.158 ± 0.029 (0.029)	0.123 ± 0.017 (0.017)
0.15	...	0.20	0.286 ± 0.039 (0.039)	0.193 ± 0.031 (0.031)	0.103 ± 0.020 (0.020)
0.20	...	0.25	0.337 ± 0.047 (0.047)	0.223 ± 0.034 (0.034)	0.076 ± 0.024 (0.024)
0.25	...	0.30	0.377 ± 0.055 (0.055)	0.225 ± 0.039 (0.039)	0.042 ± 0.031 (0.031)
0.30	...	0.40	0.385 ± 0.051 (0.051)	0.198 ± 0.037 (0.037)	0.014 ± 0.027 (0.027)
0.40	...	0.50	0.314 ± 0.081 (0.081)	0.209 ± 0.061 (0.061)	-0.012 ± 0.048 (0.048)
0.50	...	1.00	0.145 ± 0.070 (0.070)	0.256 ± 0.060 (0.060)	0.069 ± 0.040 (0.040)
1.00	...	1.90	0.266 ± 0.077 (0.077)	0.123 ± 0.060 (0.060)	0.012 ± 0.044 (0.044)
$-t_\rho$ (GeV 2)			2.2 $\leq E_\gamma$ (GeV) < 2.6		
			ρ^{00}	ρ^{1-1}	ρ^{10}
0.05	...	0.10	0.115 ± 0.027 (0.027)	0.112 ± 0.035 (0.035)	0.155 ± 0.014 (0.014)
0.10	...	0.15	0.226 ± 0.044 (0.044)	0.149 ± 0.038 (0.038)	0.138 ± 0.021 (0.021)
0.15	...	0.20	0.297 ± 0.053 (0.053)	0.192 ± 0.040 (0.040)	0.117 ± 0.024 (0.024)
0.20	...	0.25	0.341 ± 0.060 (0.060)	0.202 ± 0.044 (0.044)	0.097 ± 0.029 (0.029)
0.25	...	0.30	0.366 ± 0.071 (0.071)	0.219 ± 0.051 (0.051)	0.065 ± 0.037 (0.037)
0.30	...	0.40	0.407 ± 0.064 (0.064)	0.225 ± 0.045 (0.045)	0.011 ± 0.036 (0.036)
0.40	...	0.50	0.354 ± 0.085 (0.085)	0.213 ± 0.067 (0.067)	-0.048 ± 0.053 (0.053)
0.50	...	1.00	0.100 ± 0.080 (0.080)	0.277 ± 0.068 (0.068)	-0.011 ± 0.046 (0.046)
1.00	...	2.60	0.097 ± 0.118 (0.106)	0.229 ± 0.090 (0.090)	0.070 ± 0.060 (0.060)